Reconfigurable Antennas for Adaptive MIMO Communication Systems

A Thesis

Submitted to the Faculty

of

Drexel University

by

Daniele Piazza

in partial fulfillment of the

requirements for the degree

of

Doctor of Philosophy

June 2009

Dedications

To my family: thanks for your love and support during my studies

Acknowledgments

I would like to express my sincere thanks to Prof. Kapil R. Dandekar for his invaluable and unique guidance during my studies and for his support in preparing this thesis.

I would like to thank Prof. Michele D'Amico who gave me the opportunity to continue my research studies at Politecnico di Milano.

I am very grateful to all my colleagues and friends from the Drexel Wireless System Laboratory for their continuos collaboration on common research topics.

Special thanks to my parents and my brother that have always been close to me and supported me with their continuos help, their patience and their love during my studies and my research.

A big thank to my girlfriend Anita for supporting and encouraging me during these years and a special thank to all my friends that have been close to me in these years.

Table of Contents

List of Tables

List of Figures

Abstract

Reconfigurable Antennas for Adaptive MIMO Communication Systems

Daniele Piazza

Advisor: Kapil R. Dandekar, Ph.D.

The requirements for the next generation wireless systems seek to provide reliable high data rate at low cost. Unfortunately the current wireless communication infrastructure is not fully equipped to offer this unprecedented quality of service. Major obstacles include: limited bandwidth availability, limited transmit power, and signal strength fluctuations which are intrinsic to the multivariate wireless channel. Multiple Input Multiple Output (MIMO) antenna systems have emerged as one of the most significant technical breakthrough in modern wireless communications able to satisfy these stringent requirements. However the necessity of assuring a high data rate in a large variety of environments while reducing the antenna array space occupation on portable devices requires an improvement in current MIMO technology. To overcome these limitations, we propose in this thesis, the use of reconfigurable antennas that adaptively change, through RF switches, their radiation properties and frequency of operation according to wireless channel characteristics.

The key idea of this work is to show that reconfigurable antennas, through their capability to dynamically change their electrical and radiation properties, can be used to change the propagation characteristics of the wireless channel existing between the transmitting

and receiving antennas. The proposed MIMO system breaks from the conventional wisdom that the wireless propagation channel cannot be changed intentionally by the transceivers in the link.

Three different novel classes of electrically multi element reconfigurable antennas are proposed as suitable candidates for reconfigurable MIMO systems: *i*) a reconfigurable printed dipole antenna array that exploits inter element mutual coupling to achieve pattern reconfigurability, *ii*) circular patches capable of exciting higher order modes to achieve pattern and polarization diversity, and *iii*) a metamaterial leaky wave array that can be reconfigured in pattern to achieve unprecedented degrees of pattern reconfigurability.

To effectively use such antennas with actual communication systems, a low power consumption method for selecting the array configuration is proposed. This technique exploits the close relationship between the environment that surrounds the antenna array and the antenna radiation characteristics in order to select optimal array radiation patterns without the need for intense channel sensing or excessive training. A complete reconfigurable antenna system composed of mutli-element reconfigurable antennas and a control unit capable of efficiently driving the antennas is proposed to deliver unprecedented system performance.

Analytical models of the proposed system are used to fully characterize the functionality and performance of the technology. A complete evaluation of the proposed system is conducted through electromagnetic simulations and field measurements collected with a channel sounder specifically designed to measure the performance of multi element antenna systems. It is demonstrated that the novel multi element reconfigurable antenna system is

capable of providing *i*) increased data rate compared to common non reconfigurable antennas in single link communications as well as in multi-link ad hoc networks, *ii*) reduced space occupation by the antenna on the communication device exploiting the principles of pattern and polarization diversity, *iii*) reduced number of radio-frequency chains needed at the receiver/transmitter and *iv*) reduced amount of transmit power for achieving performance comparable to that of standard non reconfigurable antenna systems.

Chapter 1: Introduction

The recent growth in demand for wireless services, coupled with the limited spectrum available for these services, has spawned new efforts to increase the spectral efficiency of wireless links. In traditional communications systems, increased efficiency can only be obtained either by *i*) increasing the transmit signal power (which is limited by regulatory agencies), *ii*) applying increasingly sophisticated error control coding strategies, or *iii*) increasing the bandwidth allocated to a specific user. Recent research [1–4], however, has shown that in multipath propagation environments, the spatial characteristics of the propagation channel can be exploited to increase spectral efficiency through the use of multiple antennas at the transmitting and receiving nodes. Such multiple-input multiple-output (MIMO) technology figures prominently on the list of recent technical advances with a chance of resolving the bottleneck of traffic capacity in future Internet-intensive wireless networks. Perhaps even more surprising is that just a few years after its invention the technology seems poised to penetrate large-scale standards-driven commercial wireless products and networks such as broadband wireless access systems, wireless local area networks (WLAN), fourth-generation (4G) networks and beyond.

MIMO systems can be defined simply. Given an arbitrary wireless communication system, we consider a link for which the transmitting end as well as the receiving end is equipped with multiple antenna elements. Such a system is illustrated in Fig.1.1. The idea

behind MIMO is that the signals on the receive (RX) antennas, which are the results of signals form the transmit (TX) antennas that travel through complex multipath environments are combined in such a way that the quality (bit-error rate or BER) or the data rate (bits/sec) of the communication for each MIMO user will be improved relative to Single Input Single Output (SISO) systems. Such an advantage can be used to increase link and network quality of service.

A key feature of MIMO systems is the ability to turn multipath propagation, traditionally a pitfall of wireless transmission, into a benefit for the user. MIMO effectively takes advantage of random fading [1, 2] and when available, multipath delay spread [3, 4] for multiplying transfer rates. The prospect of many orders of magnitude improvement in wireless communication performance at no cost of extra spectrum (only hardware and complexity are added) is largely responsible for the success of MIMO as a topic for new research. This has prompted progress in areas as diverse as channel modeling, information theory and coding, signal processing, antenna design and multi antenna-aware cellular design, fixed or mobile.

This dissertation focuses on MIMO antenna array design for user terminals. In particular the benefits of MIMO communication are enhanced through a combination of novel adaptive antenna array structures and algorithms that drive the antenna elements for adaptation to the changing multivariate channel. The antenna arrays and their driving algorithms directly affect the multipath wireless channel and they can be appropriately designed for improved system performance. The key idea of this work, as illustrated in Fig.1.2, is to

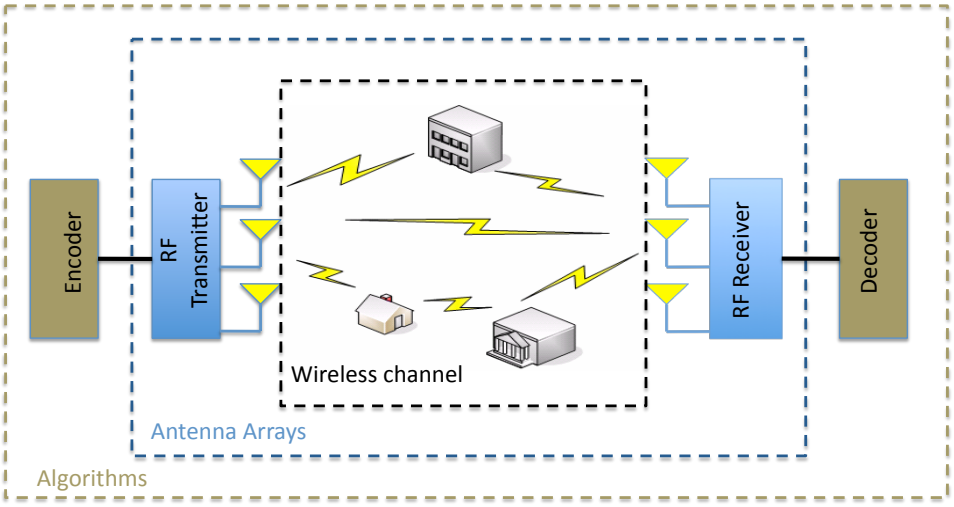

Figure 1.1: MIMO system and its layers.

show that reconfigurable antennas, through their capability to dynamically change their electrical and radiation properties, can be used to change the propagation characteristics of the wireless channel existing between the transmitting and receiving antennas and therefore notably improve the link quality with respect to standard non reconfigurable MIMO systems. The proposed MIMO system breaks then with the common belief that in a wireless communication system the propagation channel cannot be changed intentionally.

1.1 Antennas for MIMO systems

Two general conditions need to be fulfilled in an antenna design for MIMO system to achieve high performance. In particular, the antenna system must be capable of: *i*) providing a high degree of diversity, and *ii*) receiving high Signal to Noise Ratios (SNR). Moreover if the antenna array is meant to be used on portable devices, a further requirement is to have

compact design comparable in size to a single element antenna.

To achieve the highest diversity in MIMO communication systems generally requires spacing the antennas far apart (typically at multiples of the wavelength) [1, 5] yet small user terminals such as notebook computers or cell phones necessitate placing the antennas close together. A solution to this problem is to employ antennas with different polarizations and radiation patterns [6–8]. By choosing the patterns and polarizations of the antennas carefully, it is possible to achieve good performance by orienting the antennas such that they have minimal overlap between their patterns. This makes polarization/pattern diversity attractive in the design of small user terminals for MIMO communication systems. Several antenna solutions have been proposed in the literature exploiting this concept and the benefits of polarization/pattern diversity have been demonstrated through analysis and measurements in [6–11].

Another technique proposed to increase the diversity level of the system is to have the transmitting and receiving node equipped with several antennas and to select the subset of antennas that provide the highest diversity at the transmitting and receiving node [12, 13]. Switching circuitry, linked with the transceiver chains, is used to select the group of antennas that guarantee the optimal system diversity for a given channel state information. Such antenna selection techniques have been widely investigated [12–15] and it has been demonstrated to be effective in improving the diversity and performance of a MIMO communication system. A drawback of this technology is the presence of several antennas, often spaced far apart, most of which are not employed at any given time to transmit and receive

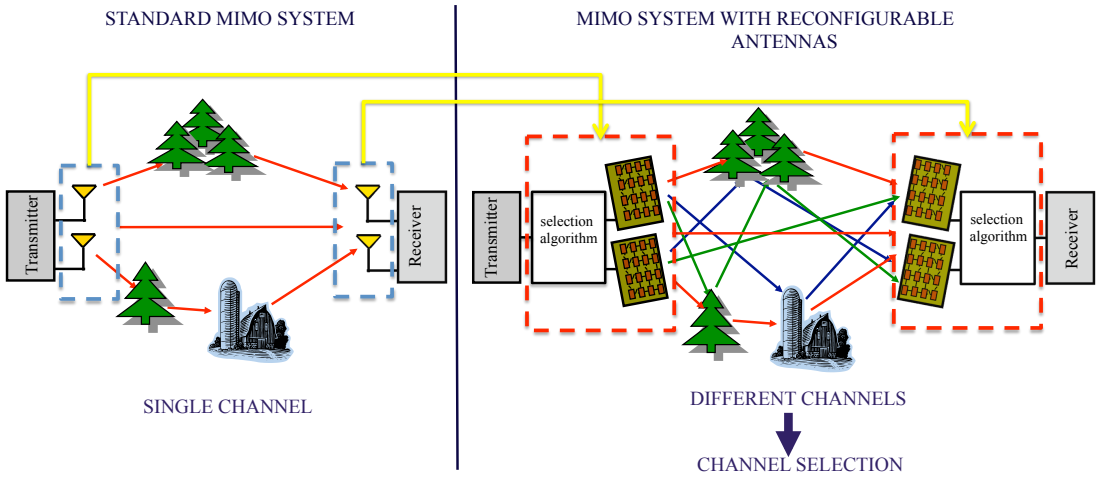

Figure 1.2: Comparison between a standard MIMO system and a MIMO system equipped with reconfigurable antennas.

data. As commonly described, antenna selection is an impractical solution for portable devices where space is a critical constraint.

To enhance the level of received SNR it is necessary to have the transmitter efficiently send all the power in direction of the receiver, with the receiver being capable of collecting most of the impinging power. Beamforming arrays have been proposed to address this problem [16–20]. Different antennas are fed with the same signal and phase shifting is performed at the input of each array element to steer the array radiation beam in different directions over the solid angle [16–18]. An optimal alignment for maximum received SNR can be achieved by steering the radiation beam at the receiver and at the transmitter [16, 17, 19, 20]. While this technique allows for an increase in SNR at the receiver, it does not provide any degree of diversity since an array is used as a single antenna (i.e. the information on each array element is the same).

Another technique recently proposed to enhance the level of received SNR in single input single output (SISO) systems consists of using electronically reconfigurable antennas [21–41]. These antennas are capable of dynamically changing their radiation properties by means of RF switches used to vary the current distribution on the antenna structure. Radiation pattern shape, polarization state and frequency of operation can be tuned to accommodate the operating requirements. By dynamically varying the shape of the radiation pattern, it is possible to improve the level of received signal power similar to a beamforming array. By changing the antenna polarization, the transmit and receive polarization states can be adaptively aligned for maximum received SNR. Many designs capable of changing the radiation pattern shape [21–36] or the polarization state [37–41] have been proposed. These designs have drawn a lot of interest due to their transformative behavior and compactness that can be exploited in several applications.

1.2 Innovative aspects of this thesis

The necessity of assuring a high data rate in a large variety of environments while reducing the antenna array space occupation on portable devices requires improving current MIMO antenna technology. The work presented in this thesis addresses this need and a novel class of reconfigurable antenna arrays that combines the strengths of the techniques proposed in Section 1.1 is presented. The novelty of having a compact array solution composed of reconfigurable antenna elements is addressed for the first time in this thesis. Reconfigurable antenna structures that dramatically increase the MIMO diversity system level, while being

able to improve the SNR at the receiver and being compact in size are presented. The designs proposed in this thesis are based on three different microstrip antenna types: *i*) printed dipoles, *ii*) circular patches, and *iii*) leaky wave antennas. The potential of using innovative metamaterial structures to achieve high reconfigurability in MIMO systems is also investigated in this thesis through a novel leaky wave antenna design. Reconfigurability is achieved by means of actuators including PIN diodes and varactor diodes, whose actuation time is in the order of nanoseconds, an order of magnitude faster than current micro electro mechanical system (MEMS) switches. Such actuation speed allows for variation of antenna characteristics within a data packet time frame, in order to instantly adapt the wireless channel characteristics for enhanced communication performance on a per data frame basis. However, despite their switching speed and high reliability, current PIN diodes introduce losses that affect the overall array radiation efficiency and power consumption. Next generation switches (e.g. MEMS switches with increased switching speed and reliability) will help diminishing the losses and further improve the benefit achievable with reconfigurable antennas in MIMO systems.

The benefits and costs of implementation and operation of reconfigurable antennas are unclear from a system perspective. System and operating environment complexity makes it difficult to identify a particular antenna functionality that will automatically result in greater throughput, higher link reliability, or lower bit error rates. A system performance evaluation of the proposed new class of reconfigurable antennas for MIMO system is presented for the first time in this thesis. The benefit achievable with the proposed antennas

are determined using electromagnetic simulation tools and field measurements. The analysis conducted in this thesis investigates the benefit offered by each proposed antenna structure in terms of achievable channel capacity and bit error rate (BER). In particular, channel capacity is selected as performance metric because it allows to study the antenna array performance in a communication link independently from the system modulation and the adopted coding technique. This work also provide insights on the design characteristics of reconfigurable antennas for MIMO systems, considering the effect of parameters like radiation efficiency, diversity and input impedance matching on the system performance. Quantitive studies that consider the system-level performance of antenna reconfigurability for MIMO are conducted for single link communication system and for next generation ad hoc wireless networks. In single link communication the reconfigurable antenna is used only to optimize the wireless channel between the transmitting and receiving node, while in ad hoc networks the adaptive system has the twofold role of maximizing the single link data rate while mitigating co-channel interference.

Having multiple array configurations that can be used to change the propagation characteristics allow for an improvement in overall system performance, but also raises the need for efficient selection schemes to be used for effectively selecting the optimal array configuration. Estimating the channel response for each antenna configuration at the transmitter and at the receiver, prior to selecting the array configuration, has been demonstrated to be power consuming and detrimental to the performance of the reconfigurable MIMO system [42]. The negative effect of exhaustive channel estimation on the performance of the

communication system increases proportionally with the number of antenna configurations, reaching the point where the losses caused by imperfect channel estimation may be higher than the capacity gain offered by recongurable antennas [42]. The development of efficient selection schemes for MIMO reconfigurable antennas is addressed for the first time in this thesis. A selection scheme that can be used to drive a class of multi element pattern reconfigurable antennas is proposed. This configuration selection algorithm is demonstrated and validated through electromagnetic simulations when applied to novel multi element reconfigurable circular patch antennas.

The main contributions presented in this dissertation can be summarized as follows:

1. Design of novel multi element reconfigurable antennas for MIMO communication systems. This item includes:

    - A novel reconfigurable printed dipole array (RPDA) that exploits the mutual coupling between two closely spaced reconfigurable dipoles to achieve variable degrees of pattern diversity. This contribution appears in [43, 44].
    - Reconfigurable circular patch antennas (RCPAs) that can be dynamically tuned in pattern and polarization and that comprise of a single antenna structure acting as a two element array. This contribution appears in [45–47].
    - A two port reconfigurable leaky wave antenna, built using a tunable metamaterial structure, that is capable of generating an ideal infinite number of array configurations. This contribution appears in [48].

2. System level performance evaluation of multi element reconfigurable antenna for MIMO systems. This item includes:

    - Measured and simulated analysis of the performance achievable using all the proposed antenna structures in single link MIMO communication systems. This contribution appears in [43, 44, 46, 47, 49, 50].
    - Measured and simulated analysis of the performance achievable using some of the proposed antenna structures in next generation MIMO ad hoc networks. This contribution appears in [51, 52].
    - Novel definition of spatial correlation coefficient to be used in cluster channel models for evaluation of multi element reconfigurable antennas. This contribution appears in [44]
    - Insights on the design characteristics of reconfigurable antennas for MIMO systems, considering the effect of parameters like radiation efficiency, diversity and input impedance matching on the system performance. This contribution appears in [49, 50, 52, 53].

3. Selection schemes for multi element reconfigurable antennas. This item includes:

    - A novel selection scheme to be used with a class of pattern reconfigurable antennas that allows to select the array configuration at the receiver without switching between all its configurations. This contribution appears in [53, 54].
    - A demonstration of the proposed selection algorithm when employed with RCPAs

in a clustered channel model. This contribution appears in [53, 55, 56].

The proposed solutions and techniques may be directly applicable to future MIMO wireless systems that are currently in the process of being standardized by IEEE 802.11n, IEEE 802.16e and 3GPP standard bodies.

1.3 Thesis outline

The dissertation is organized as follows:

In Chapter 2 the concepts of spatial, polarization and pattern diversity, fundamental in designing antennas for MIMO systems, are introduced and a review of the state of the art of reconfigurable antenna is provided. Different techniques that can be used to achieve pattern and polarization reconfigurability are introduced and their benefit and drawbacks are discussed.

In Chapter 3 an overview of MIMO systems is presented and the critical impact of the array design on the communication link performance is discussed. The concept of antenna element correlation is introduced and a novel definition of spatial correlation that includes the effects of antenna mismatch and radiation efficiency is proposed for studying multi element reconfigurable antennas.

In Chapter 4 a reconfigurable printed dipole array that exploits inter element mutual coupling to achieve pattern reconfigurability is introduced. The PIN diode-based reconfigurable antenna solution is first motivated through a capacity analysis of the antenna in a clustered MIMO channel model. Next, the widespread applicability of the proposed

technique is demonstrated, relative to conventional half wavelength printed dipoles, using computational electromagnetic simulation in an outdoor and indoor environment and field measurements in an indoor laboratory environment.

In Chapter 5 two novel reconfigurable multi element antennas that are capable of achieving high level of pattern reconfigurability and pattern diversity are presented: a circular patch antenna with two different antenna configurations exploiting only pattern diversity and a circular patch antenna with three different antenna configurations exploiting both pattern and polarization diversity. The benefits offered by each state (i.e., excited radiation pattern and polarization) of these antennas are investigated both in Line of Sight (LOS) and Non Line of Sight (NLOS) scenarios. The radiation efficiency and the level of pattern and polarization diversity of each configuration are investigated to explain the performance offered by this class of antennas in MIMO systems.

In Chapter 6 a method that allows multi element reconfigurable antennas to select the antenna configuration at the receiver without any extra power consumption and modifications to the data frame of a conventional, non reconfigurable MIMO system is presented. The selection scheme is conceived for selecting the array configuration without the need for switching between all the different array configurations. An evaluation of the performance achievable with the proposed algorithm are investigated in a MIMO clustered channel model using pattern reconfigurable circular patch antennas.

In Chapter 7 a novel leaky wave array built using metamaterial microstrip structures is presented. Composite right left handed (CRLH) metamaterials are proposed as a suit-

able solution for achieving high radiation pattern reconfigurability without sacrifying gain, impedance matching, or compactness. Field measurements collected in Line of Sight (LOS) and Non Line of Sight (NLOS) scenarios are used to determine the system achievable channel capacity and to quantify the level of power saving achievable for a fixed transmission rate with such antenna compared to a reference non reconfigurable antenna system. Analysis conducted in realistic clustered channel models are then used to provide a complete understanding of the achievable performance of this antenna structure in different environments.

In Chapter 8 the benefits achievable with reconfigurable antennas in MIMO ad-hoc networks are quantified, while also investigating antenna configuration selection schemes to be used by each network node. The analysis is conducted using two different types of multi element reconfigurable antennas. Ray tracing electromagnetic simulations and field channel measurements are employed to determine the capacity gain achievable with these antennas with respect to standard non reconfigurable antenna systems.

Chapter 9 provides a summary of this work. The main contributions of this work to the area of MIMO systems are illustrated. Future directions are proposed in designing antenna solutions and novel adaptive algorithms that exploit the benefits of having multi element reconfigurable antennas in next generation communication systems.

Chapter 2: Antenna diversity and reconfigurability

There are three main antenna diversity techniques commonly employed in MIMO array design for providing high decorrelation between the transmitted and received signals: space, polarization and pattern diversity. This chapter introduces the concepts of these three different diversity techniques exploited for designing multi element reconfigurable antennas. The chapter provides also an overview of the state of the art of pattern and polarization reconfigurable antennas. Different techniques that can be used to achieve pattern and polarization reconfigurability are introduced and their benefit and drawbacks are discussed.

2.1 Spatial, polarization and pattern diversity

To provide decorrelation between the different sub-channels of the MIMO link, three well know diversity techniques are used: *i*) spatial diversity, *ii*) polarization diversity, *iii*) pattern diversity. These techniques have been applied first in single input single output (SISO), single input multiple output (SIMO) and multiple input single output (MISO) communication systems and lately have become very attractive for MIMO systems. All multi element reconfigurable antennas presented in this thesis combine these diversity techniques in order to achieve high performance when employed in MIMO systems. The design described in Chapter 4 exploits spatial and pattern diversity, the array presented in Chapter 5 combine pattern and polarization diversity, while the antenna solution proposed in Chapter 7 takes

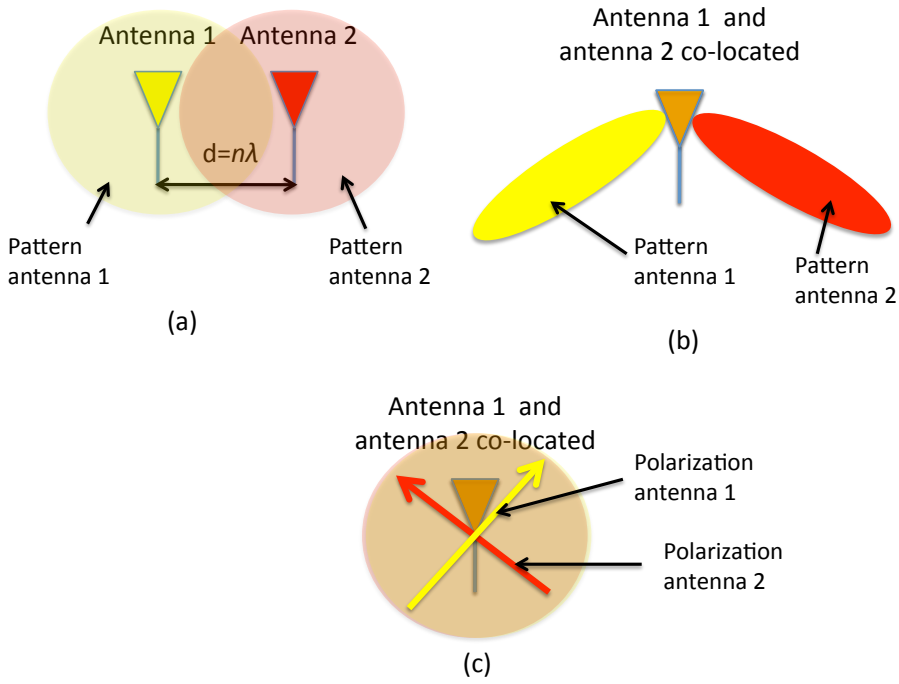

Figure 2.1: Three antenna diversity techniques: (a) spatial diversity, (b) pattern diversity, and (c) polarization diversity.

advantage of pattern diversity.

2.1.1 Spatial diversity

The simplest and most common form of diversity in wireless communications is spatial diversity [5, 57] (see Fig.2.1(a)). By having antennas at two separate points in space, the phase delay between them can allow the fading signal in the second antenna to be decorrelated from the first antenna. In order to achieve sufficient decorrelation, the antennas must have a minimum spacing depending upon the surrounding environment and in particular upon the width of the multipath angle of arrival. It has been shown in [57] that a spacing

greater than 3 λ, where λ is the wavelength, is required in an urban area to have complete decorrelation, while in an indoor environment with rich scattering, a minimum spacing of 0.5 λ is necessary [5]. For spacing less than 0.5 λ spatial diversity can be still employed at the mobile terminal, but it gives little benefit compared to larger spacing. At such distances, typical in handheld devices, there is a greater contribution of other forms of antenna diversity, mainly polarization diversity and pattern diversity.

2.1.2 Polarization diversity

Polarization diversity [6, 6, 9, 58] achieves decorrelation between the different sub-channels through an array of elements that excite different polarizations of the electric or magnetic field (see Fig.2.1(b)). The benefits of polarization diversity include the ability to locate the antennas in the same place, unlike spatial diversity. The impact of polarization diversity on sub-channel decorrelation and channel capacity in MIMO systems have been studied through simulation and measurements mainly employing dual polarized antennas [6, 58]. It has been shown that by employing a dual polarized system of co-located antennas it is possible to achieve the same channel capacity achieved through spatial diversity in indoor environment [6].

While previously it was thought that only two different polarizations (vertical and horizontal) could be used to decorrelate the communication sub-channels, lately it has been demonstrated how it is possible to use all three electric field components and all three magnetic fields components to drastically increase the capacity of a MIMO communication link [9]. The design of novel antennas that can propagate waves to cause independent

fluctuations in all six electric and magnetic field components has recently attracted lot of attention [9].

2.1.3 Pattern diversity

Pattern diversity [8, 59–61] exploits the difference in radiation pattern between the array elements to decorrelate the sub-channels of the communication link (see Fig.2.1(c)). This technique helps to achieve independent fading by transmitting/receiving different signal paths at each antenna. In the ideal case each array element has a radiation pattern that points in a direction different from all the others in order to capture signals that are uncorrelated from those collected at the other elements.

Developing antenna systems employing pattern diversity is a natural solution for systems where the array size is a constraint (i.e., antenna placement in notebook computers or mobile phones). It is in fact possible to co-locate the array elements and achieve the same link quality offered by a system employing spatial diversity.

Several studies have been conducted on pattern diversity in MIMO systems. In particular the benefits of pattern diversity have been shown through practical measurements with array designs employing switched parasitic antennas [59], dipoles with 90 degree hybrid [60] and multimode antennas [8, 61].

2.2 Reconfigurable antennas

The changing behavior of the wireless channel causes fluctuations in the level of received signal power. In order to limit the effect of the varying wireless channel on system performance a possible solution is to adopt reconfigurable antenna systems capable of adaptively tuning their radiation characteristics in response to the multivariate channel. Radiation pattern shape, polarization state and frequency of operation can be tuned to accommodate the operating requirements. Different solutions employing different techniques for reconfiguring the radiation characteristic have been proposed. In this Section we summarize the main techniques that can be employed to achieve pattern and polarization reconfigurability. Some of these techniques are exploited in this work for designing multi element antennas reconfigurable in pattern and polarization.

2.2.1 Polarization reconfigurable antennas

To achieve polarization reconfigurability, the antenna structure, material properties, and/or feed configuration have to change in ways that alter the way current flows on the antenna. The polarization state of an antenna can be changed between different kinds of linear polarization, between right- and left-handed circular polarizations [37, 39, 62, 63], or between linear and circular polarizations [38–40]. The main difficulty of this kind of reconfigurability is that this must be accomplished without significant changes in impedance or frequency characteristics. Two major mechanisms can be employed to achieve polarization modifcations: *i*) RF switches and *ii*) material changes.

Switches

Switches (either solide state or RF-MEMS) are the most common actuators employed to deliver reconfigurable polarization characteristics. One example of such a polarization-agile antenna is the patch antenna with switchable slots, or PASS antenna [62, 63]. The PASS antenna consists of a microstrip antenna with one or more slots cut out of the copper patch. A switch placed in the center of the slot is used to control the current distribution on the patch. When the switch is open, currents flow around the slot while when the switch is closed, the current can follow the shorter path created by the closed switch. Polarization reconfigurability is achieved by including two orthogonal slots on the surface of the patch. Alternate activation of the switches yields either right- or left-hand circular polarization. Other patch antenna geometries have been proposed to achieve polarization reconfiguration using switches. In [37] switches are used in the feed excitation slots to change the sense of the circular polarization. In [38] switches were used to connect and disconnect the corners of a rectangular patch to achieve different polarizations. A similar approach is also used in the multi element antenna design of Chapter 5 to achieve linear to circular polarization reconfiguration. A main difference in the application of this technique to the design of Chapter 5 is that the polarization reconfigurability is achieved exciting higher order modes in a circular patch antenna and that only two switches are used to change simultaneously the polarization of two array elements.

Slot antennas similar to the one in [39] can be used to achieve polarization reconfigurability. A slot-ring antenna can be reconfigured between linear and circular polarization or

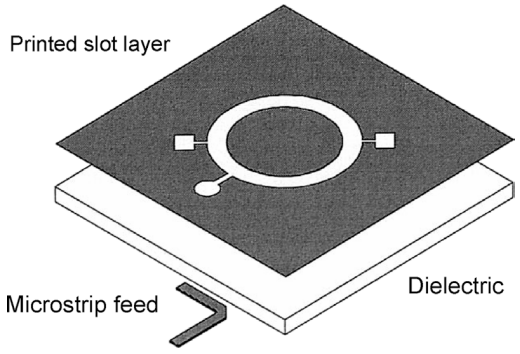

Figure 2.2: Basic topology of a microstrip-fed circularly polarized slot ring [39].

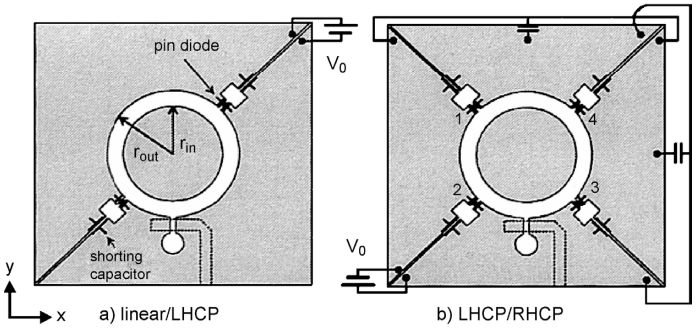

Figure 2.3: Polarization reconfigurable ring antenna that allows switching between (a) linear and circular polarization or (b) right-hand and left-hand circular polarization [39].

between two circular polarizations by means of PIN diodes [39]. The antenna basic topology is shown in Fig 2.2 and Fig.2.3 [39] illustrates the specific diode positions and biasing configurations for two different designs [39]. For the design of Fig.2.3(a), forward biasing the diodes delivers linear polarization, whereas reverse biasing the diodes results in circular polarization [39]. The design in Fig.2.3(b) includes two additional perturbation segments to allow switching from left- to right-handed circular polarizations [39].

MEMS actuators can also be used to achieve polarization reconfigurability. In the design

of [40], the MEMS actuator is located within a simple microstrip patch antenna excited in the corner to support two orthogonal modes. The actuator consists of a moveable metal strip suspended over a metal stub. When the strip is suspended above the stub, the antenna has a circularly polarized radiation pattern [40]. By lowering the metal strip dual linear polarization is achieved.

Material changes

Rainville and Harackiewicz [41] proposed a microstrip antenna that can be reconfigured in polarization magnetic biasing a ferrite film. Applying a static bias to a bulck ferrite substrate of a microstrip antenna the frequency of the cross-polarized field can be tuned to create different elliptical polarizations. Optimization of feed point and ferrite film properties could result in purely circular and linear polarizations as well [41].

2.2.2 Pattern reconfigurable antennas

The arrangement of currents on an antenna structure determines the spatial distribution of radiation from the structure. To develop antennas with specific reconfigurable radiation patterns, a designer must determine what kinds of source current distributions, including both magnitude and phase information, are necessary. Once the kind of current distribution has been defined, the baseline antenna design can be selected and then altered to achieve the desired source current distribution. Three different mechanisms can be employed to achieve pattern modifcations: *i*) RF switches, *ii*) material changes, and *iii*) structural changes.

Switches

Switches (solide states or RF-MEMS) can be used to change the current path on microstrip antennas and thus modify the shape of the radiation pattern. For example, reconfigurable radiation patterns can be achieved with slot-based radiators. In [21], an annular slot antenna is used as both a frequency- and pattern-reconfigurable device. Frequency reconfigurability for this antenna is supported through PIN diode switches that control input matching circuitry. Pattern reconfigurability is achieved through PIN diodes placed around the slot that can be activated and deactivated to create nulls in the radiation pattern [21].

A common effective technique to change radiation patterns for a fixed frequency of operation is the use of switched parasitic elements. Tuning of antenna radiation patterns in this manner relies on the mutual coupling between a driven antenna element and closely spaced parasitic elements. Changing the mutual coupling between the active and the parasitic elements results in changes of the effective source currents on both the driven and parasitic elements. Relative leads or lags in the induced current on the parasitic elements result in reflector or director behavior.

In [22] a parasitic dipole array is proposed. Fig.2.4 [22] shows the driven dipole element surrounded by parasitic dipoles loaded with tunable reactances. Variations in the loading reactance of each parasitic element changes the apparent magnitude and phase of the signal on each array element, resulting in a directive beam in a desired direction. A number of reconfigurable parasitic arrays have been proposed and studied, using both switched and reactively loaded elements, which provide a wide variety of functionality [23–26]. Note that

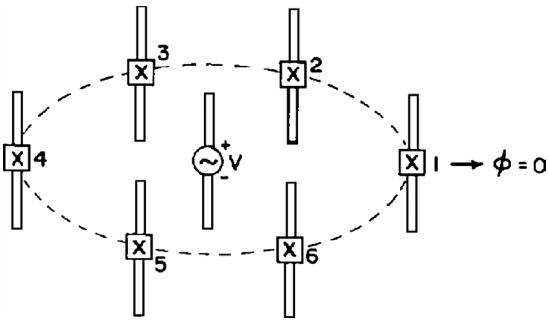

Figure 2.4: Reactively loaded parasitic dipoles for pattern reconfigurability [22].

although it is easier to achieve changes in beam steering with a parasitic array, the coupling between the driven element and the loaded parasitic elements can still affect the input impedance and the radiation efficiency of the antenna [25].

Microstrip-based reconfigurable antennas can also use switched or tuned parasitic elements. One example is that developed in [27]. The antenna is composed of a single dipole-like active element with two spaced parasitic elements positioned parallel to the driven element (see Fig.2.5 [27]). Parasitic element lengths are changed with electronic switches or varactors, which, in turn, alter the level of mutual coupling between the driven and parasitic elements. Tilts in the main beam in one plane can then be switched [27] as the lengths of the parasitic elements are changed. Another example that employs switched parasitic elements to achieve pattern reconfigurability is the printed spiral antenna presented in [28]. The antenna has two switched connections: one that shorts the end of the spiral to ground and one that opens a small gap in the spiral arm. When the two switches are activated the antenna becomes, in essence, an open microstrip line with a parasitic arm and a 45^o tilt

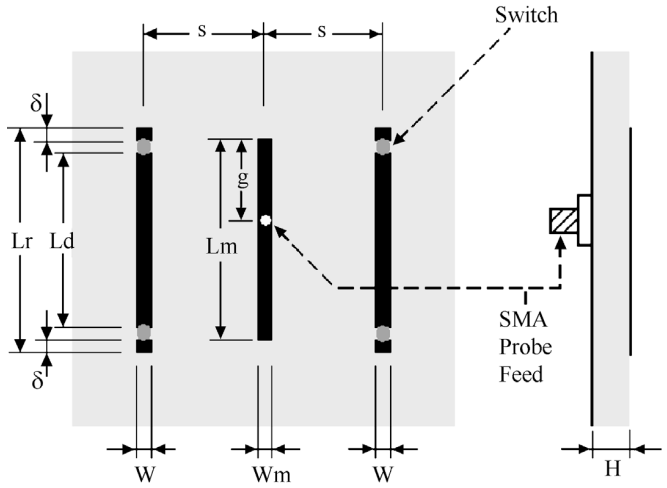

Figure 2.5: Microstrip switched parasitic element antenna [27].

from broadside in radiation pattern is achieved. Opening the switches results in a spiral like radiation pattern steered at broadside [28].

An approach similar to the switched parasitic elements technique is employed for the design of the multi element antenna proposed in Chapter 4. However, differently from the common switched parasitic elements technique, in the design of Chapter 4 all parasitic elements are removed and only active elements are employed in favor of a compact design.

Material changes

Ferrites, ferroelectric and variable dielectric materials can be used to reconfigure radiation patterns. Changing the material characteristics allow to change the resonant current distribution on the microstrip antenna, which then result in radiation pattern changes. Alternatively they can be used to alter propagation speeds in traveling/leaky-wave radiators

that result in beam steering.

Several researchers have investigated the use of the tunability of ferrite materials to produce steerable radiation patterns [29]. In [29], a circular microstrip patch antenna is designed with a tunable ferrite superstrate to provide beam tilting with respect to the broadside direction when the ferrite was biased with a permanent magnet. Such technique introduces however higher losses in the radiated field than a switch based pattern reconfigurable antenna.

In [30], the permittivity of a ferroelectric superstrate is tuned to achieve beam steering with a two-dimensional grid array of resonant slot antennas. Shown in Fig.2.6 [30], the structure consists of a nonmagnetic substrate and a tunable ferroelectric superstrate, which is then covered with a conducting plate that supports a two-dimensional array of radiating slots. When fed with an RF signal from below, changes to the applied bias between the conducting plate and the ground plane tune the permittivity of the ferroelectric and the beam direction of the structure changes [30]. However the practicality of achieving required bias voltages for ferroelectric tuning in this kind of parallel plate tuning configuration is an issue. Other reconfigurable leaky-wave antennas that include tunable ferroelectric materials in planar configurations have also been reported [31, 32].

Structural changes

A reconfigurable leaky-wave antenna using mechanical tuning has been proposed in [33]. In this case, a horizontally polarized antenna is used to couple energy into leaky transverse electric waves on a tunable impedance surface. The radiated beam from the surface can be

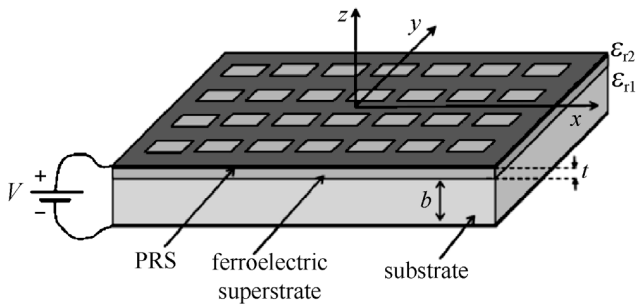

Figure 2.6: Ferroelectric reconfigurable leaky wave antenna [30].

steered in elevation over a range of 45^o by changing the apparent capacitance of the surface through mechanically shifting the top capacitive plane. The antenna and the surface are shown in Fig.2.7 [33]. An electronically tuned version of this antenna that uses varactors can produce reconfigurable backward as well as forward leaky-wave beams [34].

A different approach uses MEMS actuator to reconfigure the radiation pattern for a fixed frequency of operation [35]. The antenna, shown in Fig.2.8 [35] is composed of a planar V structure with a coplanar feed. Micromachined rotational hinges fixed to the substrate material hold the ends of each of the V arms in place. MEMS actuators move the arms laterally to alter the radiated main beam direction and/or beam shape [35].

2.2.3 Compound reconfigurable antennas

The ultimate class of reconfigurable antennas is the one composed of antennas that allow for simultaneous changes to radiation characteristics (radiation pattern and polarization state) and the frequency of operation. Recently, few groups have achieved this kind of reconfigurability, referred to here as here termed compound reconfigurability. A common proposed

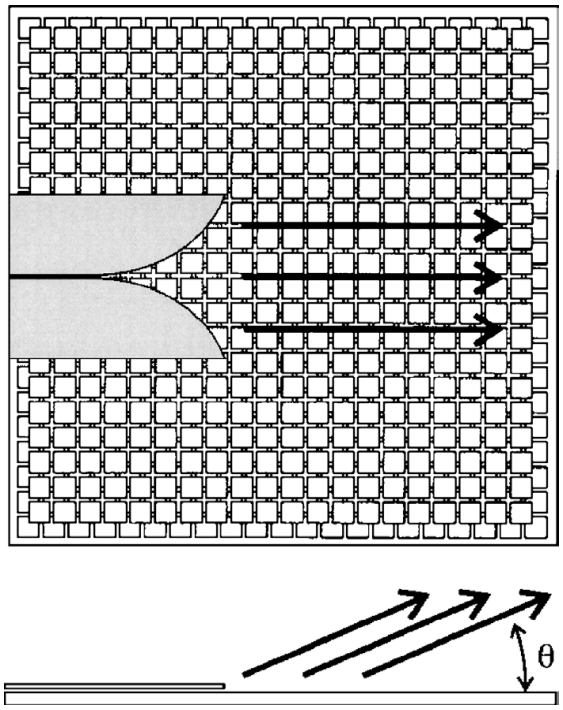

Figure 2.7: A horizontally polarized antenna couples energy into leaky modes on the tunable impedance surface. The waves propagate across the surface and radiate at an angle governed by the surface resonance frequency with respect to the excitation frequency. By tuning the surface resonance frequency, the beam is steered in the elevation plane [33].

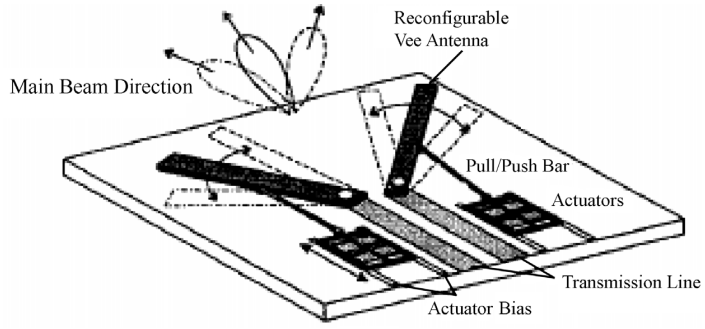

Figure 2.8: MEMS reconfigurable Vee antenna [35].

solution to achieve this type of reconfigurability is to employ pixel-based approaches that allows the antenna aperture to be divided into small parts and use this granularity to control the current or field distributions in the aperture. For most desired aperture functions, how the aperture should be configured or fed is not immediately apparent, so computational algorithms have been applied to arrive at suitable and sometimes optimal designs.

An example of a compound reconfigurable aperture uses switches (based in solid-state, MEMS, or other technologies) to connect and disconnect small subwavelength conductive pads to create any desired microstrip antenna topology [64]. The number of switches required for such an aperture can easily number into the thousands and high losses are experienced. A conceptual representation of the aperture is shown in Fig.2.9 [64]. The high number of switching configurations require for these topologies the development of techniques to efficiently selecting the proper configuration that synthesize the desired radiation pattern, polarization, and frequency of operation. In this case [64], the switching configuration is selected using a genetic algorithm used in concert with a finite-difference time-domain full-wave electromagnetic simulator. After each iteration of the genetic algorithm, the full-wave simulator is used to predict the performance of the resulting structure, and then the genetic algorithm makes more refinements to the design to achieve the specified performance goals.

Another version of a pixel-based reconfigurable antenna is proposed in [64]. In this case, semiconductor plasmas are used to form antenna structures [65]. High-conductivity plasma islands are formed and controlled by DC-injected currents into high-resistivity silicon-based

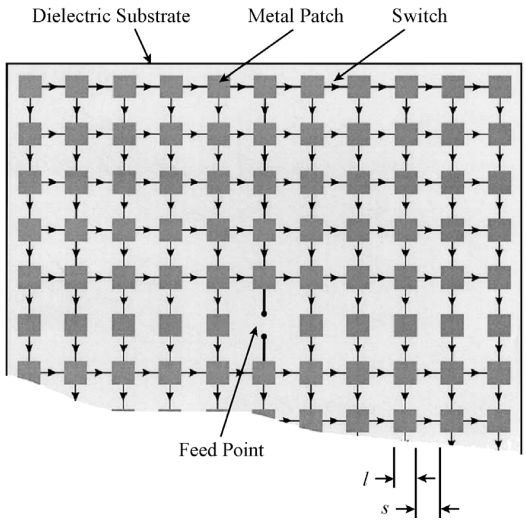

Figure 2.9: Conceptual drawing of a multifunctional aperture antenna based on switched links between small metallic patches [64].

diode structures. Fig.2.10 shows a detailed description of the proposed structure, including the plasma injection driver [65]. The implementation of such technology is just as complex as that of the previous example that uses many discrete switches. However this approach is more attractive for its ability to reduce its electromagnetic observability [65].

Although this flexible approach can deliver a range of structures with new and unexpected performance, it also has some limitations. In general, the presence of a high number of switching systems (based in solid-state, MEMS, or other technologies) introduces high losses and notably decreases the antenna radiation efficiency. Also, conductive pad density and switch capacitance may also degrade high frequency operation. Although the large number of switches between pads provides for graceful degradation of operation with switch failure, the bias network complexity for individually addressable switches may pre-

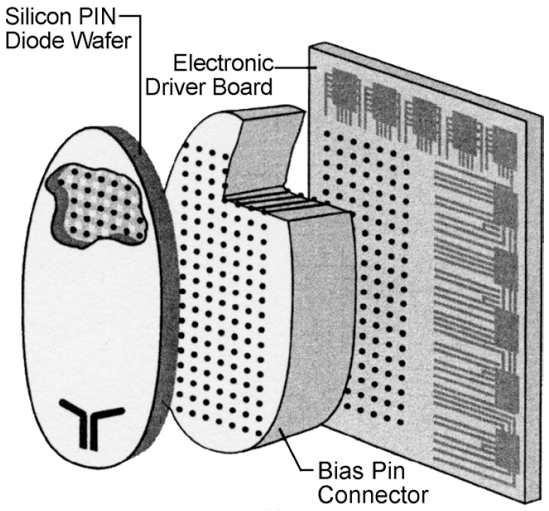

Figure 2.10: Controllable plasma grid structure for a reconfigurable aperture [65].

clude practical use until the switches and bias networks can be directly integrated into the structure during fabrication.

2.3 Summary

While all the reconfigurable antennas proposed so far in the literature have been developed for SISO communication systems, in this thesis we will propose novel reconfigurable antenna structures that are specifically developed to provide high performance when used in MIMO systems. Such structures aim at combining the concepts of pattern and polarization diversity described in Section 2.1 with the capabilities of reconfigurable antennas. The reconfigurable behavior of the multi element antennas proposed in this thesis find inspirations from some of the techniques described in this chapter revisited to achieve optimal performance when

used in MIMO communications. In particular, the multi element antenna proposed in Chapter 4 takes advantage of the switched parasitic elements technique with the main difference that all parasitic elements are removed and only active elements are employed in favor of a compact design. The design of Chapter 5 uses perturbation segments as in [38] to achieve linear to circular polarization reconfiguration, with the main difference that this same technique is applied to a different geometry and it is used in an array to simultaneously change the polarization of two antenna elements.

All the multi element reconfigurable array presented in this work employ a switch based reconfigurability which is preferred over a material or structural change approach because of its ease of implementation, its lower power consumption, and its low cost.

Finally we remark that in contrast to most of the reconfigurable antenna systems proposed in the literature, in this thesis the performance achievable with the proposed design are investigated in real MIMO communication systems by means of field measurements and electromagnetic simulations.

Chapter 3: MIMO channel models and antenna correlation

Channel models are one essential component in systems analysis in that they enable performance prediction and comparison of different systems designs in realistic propagation environments. This chapter describes a general MIMO system and provides an overview of the channel models used in this thesis, together with field measurements, to study the behavior of multi element reconfigurable antennas in MIMO communications. The concept of antenna element correlation is introduced and a novel definition of spatial correlation that includes the effects of antenna mismatch and radiation efficiency is proposed for studying multi element reconfigurable antennas.

3.1 MIMO system

A MIMO communication channel is created when there are antenna arrays at both the transmitter and receiver. Through the use of sophisticated signal processing techniques, MIMO communication can offer high link capacity, enhanced resistance to interference, and link robustness or reductions in fading thanks to diversity.

A general model of a MIMO communication system is represented in Fig.3.1. For simplicity, the channel is assumed time invariant over the interval of a transmission block. The figure is divided into *i*) signal processing and coding (bottom) and *ii*) the channel (top). In this system, a set of independent data streams Q represented by the symbol

vector $\mathbf{b}^n$ (n is a time index) are encoded into N_t discrete-time complex baseband streams $\mathbf{x}^n$ at the transmitter. The coding can distribute the input symbols over the N_t outputs (space) and/or over samples (time). The pulse-shaping block converts the discrete-time samples into continuous-time baseband waveforms $\mathbf{x}(f)$ (f is the frequency) and feeds them to the N_t channel inputs (RF chains and antennas). The channel $\mathbf{H}(f)$ combines the input signals to obtain the N_r element output (receive) waveform vector $\mathbf{y}(f)$. The matched filter then produces the discrete-time baseband sample stream $\mathbf{y}^n$, and the space/time decoder generates estimates of the Q transmitted streams $\mathbf{b}^n$. For linear channel elements, the MIMO channel input-output relationship can be written as

$$\mathbf{y}(f) = \mathbf{H}(f)\mathbf{x}(f) + \mathbf{n}(f) \tag{3.1}$$

where $\mathbf{y} \in C^{N_r \times 1}$ is the signal vector at the receiver array, $\mathbf{x} \in C^{N_t \times 1}$ is the signal vector at the transmit antenna array, $\mathbf{n} \in C^{N_r \times 1}$ is the complex additive white Gaussian noise (AWGN) vector and $\mathbf{H} \in C^{N_r \times N_t}$ is the channel transfer matrix.

Since the transmit vector is projected onto $\mathbf{H}(f)$ in 3.1, the number of independent data streams (Q) that can be supported must be at most equal to the rank of $\mathbf{H}(f)$. More generally, the properties of $\mathbf{H}(f)$, such as the distribution of its singular values [1], determine the performance potential for the MIMO system. Factors such as antenna impedance matching [18], array size and configuration [18], element pattern and polarization properties [18], mutual coupling [18], and multipath propagation characteristics [18] influence these properties. Therefore, poor design of system components or incorrect assumptions about the

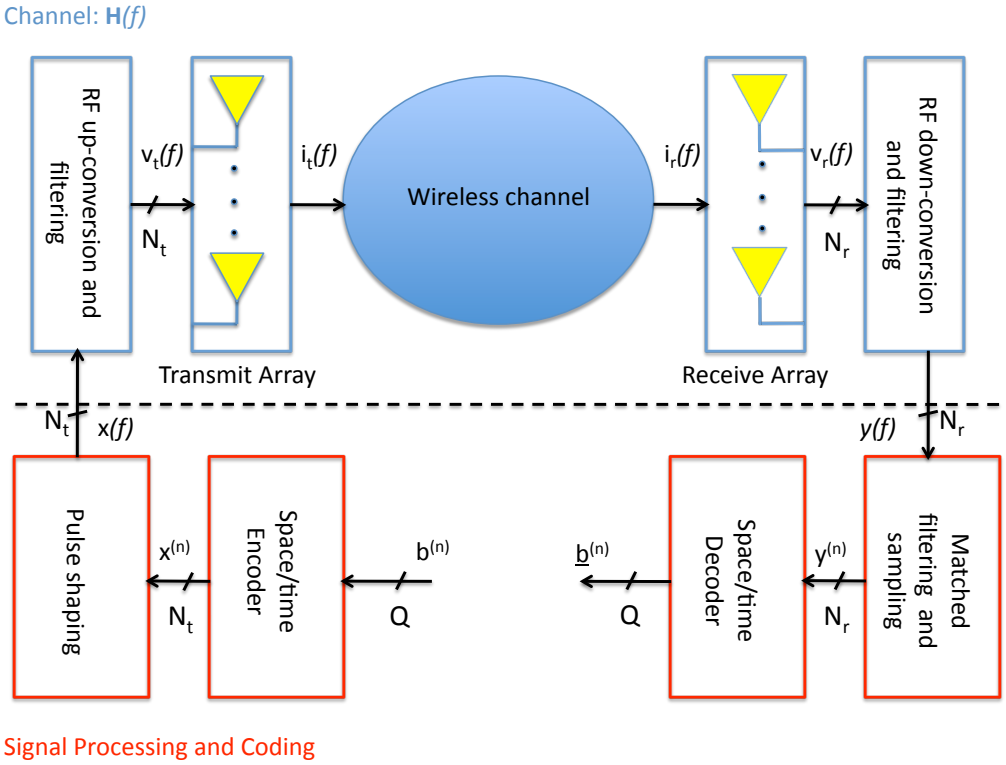

Figure 3.1: Block diagram of a generic MIMO system.

channel could lead to drastic reduction in system performance.

When not specified in the following discussion the frequency dependance, f, is dropped and narrowband communication is considered. This approach is justified when the channel response is constant over the system bandwidth (flat fading) [66] or when signals are divided into narrowband frequency bins and processed independently [66]. This mode highlights the effect of the spatial dimension, a unique factor of MIMO communications, and ignores the complexity of the wide-band channel response.

3.2 MIMO channel modeling

The MIMO channel generally includes the propagation environment, the physical transmit and receive arrays, and the system front-end electronics. Changes to any of these subsystems can have a dramatic impact on the system capacity. The goal of this work is to examine the influence of the antenna. We will assume the same propagation model for all of the work outlined in this dissertation.

Spatially correlated MIMO channels are typically derived under certain assumptions about the scattering in the propagation environment. One popular correlation model, called the clustered channel model [67], assumes that groups of scatterers are modeled as clusters located around the transmit and receive antenna arrays. Clustered channel models have been validated through measurements [68, 69] and variations have been adopted in different standards such as the IEEE 802.11n Technical Group (TG) [67] , for wireless local area networks (WLANs), and the 3GPP Technical Specification Group (TSG) [70], for third generation cellular systems.

Using this method, a mean angle of arrival (AOA) or departure (AOD) is associated with each cluster and the AOAs/AODs of the sub-paths within the same cluster are assumed to be distributed according to a certain probability density function (pdf). The pdf of the AOAs/AODs is chosen to fit the empirically derived angular distribution of the AOAs/AODs, or power angular spectrum (PAS), of the channel. The size of a cluster is measured by the cluster angular spread (AS) defined as the standard deviation of the PAS.

We denote the PAS with $P(\Omega)$, where $\Omega = (\phi, \theta)$ is the solid angle, ϕ is the azimuth

and θ is the elevation. Note that the PAS over the θ angles is generally assumed to be independent from the ϕ angles [71], and we can then write $P(\Omega) = P_\phi(\Omega)P_\theta(\Omega)$, where P_ϕ and P_θ are the angular power densities of the ϕ and θ components of the incident field, respectively. For the sake of simplicity it is generally assumed $P_\phi(\Omega) = P_\theta(\Omega) = P'(\Omega)$, which is equivalent to say that the channel is characterized by a unitary cross-polarization-discrimination ($XPD = 0\,dB$) as defined in [72,73]. Thus $P(\Omega) = P_\phi(\Omega) + P_\theta(\Omega) = 2P'(\Omega)$. Moreover, although the AOAs/AODs are physically distributed over the three dimensional space, it has been proven through channel measurements that most of the energy is localized over the azimuth directions [71]. Therefore $P(\Omega) = 2P'(\Omega) = Q(\Omega) * \delta(\phi - \phi_c)\delta(\theta - \pi/2)$, where $*$ denotes the convolution operator, ϕ_c is the mean AOA of the cluster and $Q(\Omega)$ is the PAS pdf.

A graphical representation of the clustered channel model is given in Fig.3.2 for the two dimensional space. Multiple scatterers around the receive array are modeled as clusters. We use the angle ϕ_c to denote the mean AOA of one cluster. Within the same cluster, each propagation path is characterized by an angle of arrival ϕ_0 and is generated according to a certain PAS. Depending on the system bandwidth, the excess delay across different paths may not be resolvable. In this case, multiple AOAs are defined with an offset ϕ_i relative to the mean AOA of the propagation path (ϕ_c). In typical channel models for indoor environments [67], the propagation paths within the same clusters are generated with the same mean AOA as the cluster and we assume $\phi_0 = \phi_c$. Several distributions have been proposed to approximate the empirically observed PAS. Through recent measurement

campaigns in indoor [74–77] and outdoor [78, 79] environments, it has been shown that the PAS pdf is accurately modeled by the truncated Laplacian distribution. This pdf has also been adopted to model the PAS by the IEEE 802.11n standard channel model [67] for WLANs and it will be employed through this thesis to analyze the benefit achievable with reconfigurable antennas in MIMO systems.

For spatially correlated MIMO channels the channel matrix $\mathbf{H}$ in (3.1) is defined as [8]

$$\mathbf{H} = \sqrt{\frac{K}{K+1}}\mathbf{H}_{los} + \sqrt{\frac{1}{K+1}}\mathbf{H}_{nlos} \tag{3.2}$$

where K is the Ricean K-factor, and $\mathbf{H}_{los}$ and $\mathbf{H}_{nlos}$ are the line of sight (LOS) and the nonline-of-sight (NLOS) components, respectively. We assume the LOS component of the channel to be rank one and we generate it as [67, 80]

$$\mathbf{H}_{los} = \mathbf{a}_r(\Omega_r) \cdot \mathbf{a}_t^{\dagger}(\Omega_t) \tag{3.3}$$

where $\mathbf{a}_t(\Omega_t)$ and $\mathbf{a}_r(\Omega_r)$ are the transmit and receive array responses, respectively, while Ω_t and Ω_r are the angles of departure/arrival corresponding to the LOS component at the transmitter and receiver sides, respectively.

There are two popular approaches to simulate NLOS components based on methods derived from single-input multiple-output (SIMO) channel models (see [81] and the references therein). The first one is a deterministic approach [82, 83], which generates the MIMO channel matrix based on a geometrical description of the propagation environment (i.e.,

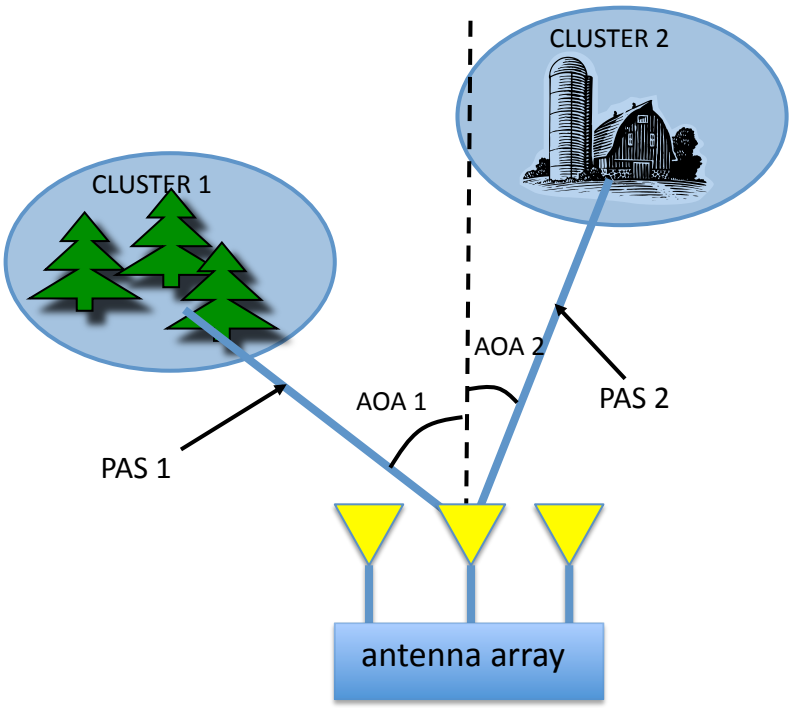

Figure 3.2: Geometry of the model representing clusters and propagation paths.

ray-tracing techniques). The second one is a stochastic method [84, 85], where the spatial correlation across MIMO channels is reproduced by a suitable choice of transmit and receive spatial correlation matrices. Deterministic models are used to predict the performance of MIMO communication systems in realistic propagation environments, since they describe accurately the spatial characteristics of wireless links. Stochastic models (ex. the Kronecker model [84]) are defined using a reduced set of channel parameters (i.e., angle spread, mean angle of arrival/departure) and are suitable for theoretical analysis of correlated MIMO channels.

3.2.1 Deterministic channel model

In deterministic channel models (i.e. ray tracing techniques) the entries of the MIMO channel matrix are expressed as a function of the channel spatial parameters. The matrix $\mathbf{H}_{nlos}$ is given by [82, 83]

$$\mathbf{H}_{nlos} = \frac{1}{\sqrt{N}} \sum_{i=1}^{N} \mathbf{V}_i \psi_i \mathbf{a}_r(\Omega_r) \mathbf{a}_t^{\dagger}(\Omega_t) \tag{3.4}$$

where N is the number of rays, $\mathbf{V}$ is a unitary matrix describing the polarization characteristics of the waves and ψ_i is the complex Rayleigh channel coefficient of the i-th ray. $\mathbf{a}_t(\Omega_t)$ and $\mathbf{a}_r(\Omega_r)$ are the transmit and receive array responses. The distributions on which the complex path gain and AOD/AOA are drawn are determined by the type of physical environment between the transmit and receive nodes. According to this model the channel covariance matrix is defined as

$$\mathbf{R}_H = E[vec(\mathbf{H}_{nlos}) vec(\mathbf{H}_{nlos}^{\dagger})] \tag{3.5}$$

3.2.2 Stochastic channel model

We use the Kronecker model to describe the stochastic evolution of channel matrix $\mathbf{H}_{nlos}$ [84, 85], as

$$\mathbf{H}_{nlos} = \mathbf{R}_r^{1/2} \mathbf{H}_w \mathbf{R}_t^{1/2} \tag{3.6}$$

where $\mathbf{R}_t$ and $\mathbf{R}_r$ denote respectively the transmit and receive spatial correlation matrices which express the correlation of the receive/transmit signals across the array elements. $\mathbf{H}_w \in C^{N_r \times N_t}$ is a matrix of complex Gaussian fading coefficients with independently distributed entries. The channel covariance matrix of the stochastic model in (3.6) is given by the Kronecker product of the transmit and receive correlation matrices as

$$\mathbf{R}_H = \mathbf{R}_t \otimes \mathbf{R}_r \tag{3.7}$$

Note that the Kronecker model in Eq. (3.6) assumes separability between transmit and receive spatial correlation. This model has been adopted by the IEEE 802.11n channel model standard [67] and it is used in this dissertation to study the benefit achievable with reconfigurable antenna systems in MIMO communications.

The (l,m) entry of the matrices $\mathbf{R}_t$ and $\mathbf{R}_r$, corresponding to the spatial correlation between the l-th and m-th array elements, is defined as [86]

$$r_{l,m} = \frac{\int_{4\pi} P(\Omega)\mathbf{E}_l(\Omega)\mathbf{E}_m^*(\Omega)d\Omega}{\int_{4\pi} P(\Omega)|\mathbf{E}_{iso}(\Omega)|^2 d\Omega} \tag{3.8}$$

where $\mathbf{E}_l(\Omega)$ and $\mathbf{E}_m(\Omega)$ are the far-field radiation patterns of the l-th and array m-th elements respectively and $\mathbf{E}_{iso}(\Omega)$ is the far-field radiation pattern of ideal isotropic radiators. Moreover, it is assumed that:

$$\int_{4\pi} P(\Omega)d\Omega = \int_{4\pi} |\mathbf{E}_l(\Omega)|^2 d\Omega = \int_{4\pi} |\mathbf{E}_{iso}(\Omega)|^2 d\Omega = 1 \tag{3.9}$$

where the first term of the equality is the condition for $P(\Omega)$ to be a pdf.

Note that the spatial correlation is normalized with respect to the antenna gain of ideal isotropic radiators such that the spatial correlation of different radiation patterns can be directly compared. In this case however the envelope of Eq. (3.8) is not guaranteed to be lower than one. To have an envelope correlation coefficient lower than one that can be used for direct estimation of the level of radiation pattern decorrelation, a conventional definition of normalization factor [72, 87] needs to be selected such as:

$$r_{l,m} = \frac{\int_{4\pi} P(\Omega)\mathbf{E}_l(\Omega)\mathbf{E}_m^*(\Omega)d\Omega}{[\int_{4\pi} P(\Omega)|\mathbf{E}_l(\Omega)|^2 d\Omega \int_{4\pi} P(\Omega)|\mathbf{E}_m(\Omega)|^2 d\Omega]^{1/2}} \tag{3.10}$$

For the case of antennas with variable characteristics, as the reconfigurable arrays treated in this thesis, however, it is desirable to allow for a direct comparison between the different array configurations when evaluating the system performance (e.g. determination of the channel capacity achievable with each array configuration). In this case it is then necessary to employ a spatial correlation coefficient with a common normalization factor. Also note that when using a common normalization factor with multi element reconfigurable antennas the condition in Eq. (3.9) is not guaranteed because the power radiated by the isotropic radiator and the l^{th} and m^{th} elements of the MIMO arrays are not equal for all the array configurations. Each antenna configuration has in fact different levels of radiated power given equal input power. This difference in radiated power occurs because of the different input impedance and efficiency of each array configuration.

In order to model the effects of antenna radiation efficiency and input impedance, the

definition in (3.8) has been revised [44]:

$$r_{l,m} = \sqrt{(1-|S_{11_l}|^2)\eta_l(1-|S_{11_m}|^2)\eta_m}\frac{\int_{4\pi} P(\Omega)\mathbf{E}_l(\Omega)\mathbf{E}_m^*(\Omega)d\Omega}{\int_{4\pi} P(\Omega)|\mathbf{E}_{iso}(\Omega)|^2 d\Omega} \tag{3.11}$$

where S_{11_l} and S_{11_m} are the voltage reflection coefficients at the l^{th} and m^{th} antenna input ports and η_l and η_m describe the percentage of power lost due to ohmic and dielectric losses in the respective antennas. Note that in this definition of spatial correlation coefficient the radiation pattern of an array element is defined for a unit driving current and all other elements in the array terminated in a matched load.

We observe that the spatial correlation in (3.11) is a function of the channel characteristics through $P(\Omega)$, and antenna array parameters such as polarization, radiation pattern through $\mathbf{E}(\Omega)$. Then, Eq. (3.11) suggests that the array parameters can be tuned as a function of the channel parameter to reduce the spatial correlation, resulting generally in improved system performance. This dependence is exploited by the novel adaptive antenna systems proposed in this work.

3.3 Summary

The two different types of MIMO channel models described in this chapter are used in this work, together with field measurements, to study the behavior of multi element reconfigurable antennas in next generation wireless communications. The deterministic model allows to precisely determine the performance achievable with a particular antenna system in a specific environment, including all main wireless propagation phenomena, without the

need of collecting field measurements. On the other hand the stochastic approach is a simpler approach, ideal for fast statistical analysis of reconfigurable multi element antenna systems behavior in different channel scenarios. The correlation coefficient defined in Eq. (3.11) is used throughout all next chapters as key parameter to relate the main array characteristics to the achievable system performance based on statistical channel parameters (e.g. angle spread and number of clusters).

Chapter 4: Reconfigurable printed dipole array

In this chapter a new reconfigurable antenna array for MIMO communication systems that improves link capacity in closely spaced antenna arrays is presented. The antenna system consists of an array of two printed dipoles separated by a distance of a quarter wavelength. Each of the dipoles can be reconfigured in length using PIN diode switches. The switch configuration can be modified in a manner adaptive to changes in the environment. The configuration of switches effects the mutual coupling between the array elements, and subsequently, the radiation pattern of each antenna, leading to different degrees of pattern diversity which can be used to improve link capacity. The PIN diode-based reconfigurable antenna solution is first motivated through a capacity analysis of the antenna in a clustered MIMO channel model. Next, the widespread applicability of the proposed technique is demonstrated, relative to conventional half wavelength printed dipoles, using computational electromagnetic simulation in an outdoor and indoor environment and field measurements in an indoor laboratory environment.

4.1 Design motivation

Achieving the highest performance in MIMO communication systems generally requires spacing the antennas far apart (typically at multiples of the wavelength) [1] yet small user terminals such as notebook computers or cell phones necessitate placing the antennas close

together. Placing the antenna close together causes high mutual coupling effect between the array antenna elements. It is well know that coupling has two relevant effects: *i*) modification of the impedance presented at the element terminals, and *ii*) modification of the pattern of the elements [18]. If the system is designed under the assumption that the antenna will present standard (e.g., 50Ω) impedance, then the impedance modification will certainly degrade the aggregate radiation efficiency of the array, which in turn will degrade the link performance for a given transmit power. Also for compact array design the high proximity of the array elements can down-grade significantly the diversity between the received/transmitted signals, causing lower achievable bit rate over the communication link [1,5]. We propose a novel adaptive antenna design that takes advantage of inter element mutual coupling, generally considered a pitfall in MIMO communications, to achieve pattern reconfigurability and increase the MIMO system diversity. Actively changing the mutual coupling existing between two close array elements it is possible to control each array element radiation pattern for a fixed frequency of operation.

4.2 Reconfigurable printed dipole array design

The proposed antenna solution has been realized using an array of two microstrip dipoles [88], the geometry of which is shown in Fig.4.1 and Fig.4.2. A quarter-wavelength microstrip balun acts as a unbalanced-to-balanced transformer from the feed coaxial line to the two printed dipole strips [18]. The ground plane of the microstrip line and the dipole strips are in the same plane. As indicated in this figure, the presence of a via-hole permits feed point

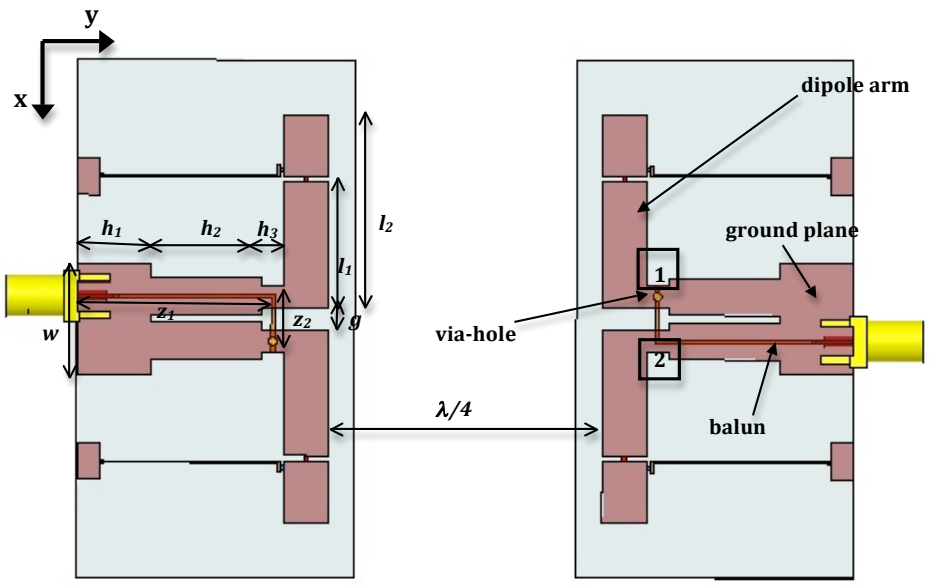

Figure 4.1: Reconfigurable printed dipole array (RPDA) design

2 of a printed dipole strip to be shifted in phase by 180° with respect to the feed point 1 of the other printed dipole strip. This occurs because of the 180° phase difference between the top strip and the ground plane of the microstrip line.

The lengths of the dipole-arm strip, and therefore the geometry of the antenna, can be changed using two PIN diode switches, which guarantee an isolation of $18\,dB$ and low insertion loss ($0.2\,dB$) at the frequency of 2.5 GHz. In this way, it is possible to define two configurations for the antenna, one when both of the switches are turned on ("long" configuration) and another when they are turned off ("short" configuration). In order to drive the switches, a direct bias voltage of $1.7\,V$ is supplied to the diode with two thin traces, the presence of which, as analyzed through electromagnetic simulations, does not corrupt the radiation characteristics of the antenna. A surface mounted capacitor of $47\,pF$ is placed

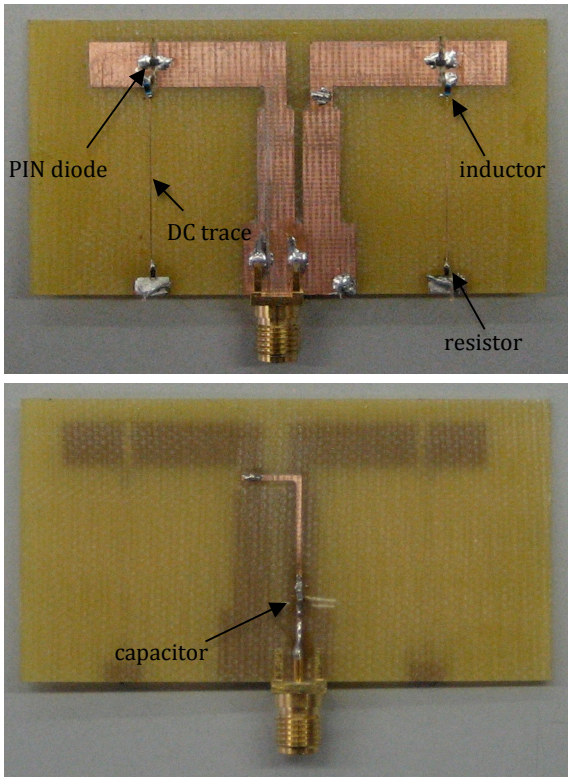

Figure 4.2: Antenna structure: top and bottom view

on the balun to block the DC current from flowing back to the RF input, an inductor of $400\,nH$ is used to block the RF from flowing in the DC supply trace, and a resistor of $100\,\Omega$ is mounted to limit the voltage across the diode as shown in Fig.4.2. The structural parameters of such reconfigurable printed dipole array (RPDA) are listed in Table 4.1.

The antenna structure has been analyzed and simulated using the finite difference time domain (FDTD) method through Ansoft HFSS. The behavior of the switch has been modeled using a lumped element circuits with the same scattering parameters of the PIN diodes in their ON and OFF states. The scattering parameters of the PIN diode have been mea-

Table 4.1: List of structural parameters of the reconfigurable printed dipole array (RPDA).

PCB substrate	thickness	$1.5\,mm$
	ϵ_r	4.4
	$tan\,\delta$	0.02
dipole arm	l_1	$19\,mm$
	l_2	$28\,mm$
	g_2	$3\,mm$
microstrip balun	z_1	$29\,mm$
	z_2	$9\,mm$
via-hole	radius	$0.4\,mm$
ground plane	h_1	$10\,mm$
	h_2	$16\,mm$
	h_3	$3\,mm$
	w	$15\,mm$

sured and its electrical equivalent circuit extracted to simulate its behavior in HFSS with lumped elements.

The close proximity of the two printed dipoles has been selected such that there is a strong mutual coupling between the two dipoles, but such that the mutual coupling is not too high to dramatically deteriorate the array radiation efficiency. This coupling is effectively used to have different radiation patterns for each array's geometry. In particular because of the vicinity of the two reconfigurable dipoles, varying the length of one of the dipoles, effects the input impedance and the current distribution of the other dipole, changing its radiation properties [18]. Fig.4.3 shows the coupling level between the different possible configurations of antenna geometry in an array (both "short", both "long", first antenna "short" and second "long", first antenna "long" and second "short"). It can be noted that the mutual coupling is different for each configuration of the array. Fig.4.4 shows the input impedance of one of the two dipoles for each array configuration. It can be noted

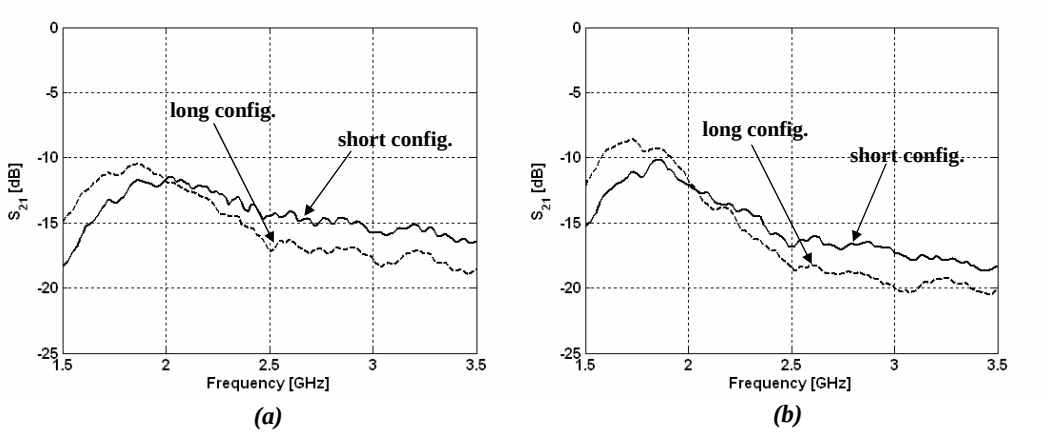

Figure 4.3: The measured S_{21} for the "long" and "short" antenna configuration in a 2 element array with inter-element separation of $\lambda/4$ when (a) the other antenna is in the "short" configuration, and (b) the other antenna is in the "long" configuration.

that the reconfigurable dipole is characterized by an input impedance that is different for each array's configuration. These differences in input impedance are due to the different lengths of the dipole and the different level of mutual coupling of each configuration. A difference in input impedance is in fact observed not only when the "active" dipole length is changed from "short" to "long" but also when the "parasitic" dipole length is changed from "short" to "long" leaving the "active" dipole length unchanged.

The strong mutual coupling effects between the two antennas influence also the radiation properties of the array's elements. Fig.4.5 shows the simulated radiation pattern of a single element half wavelength printed dipole.

The radiation pattern is greatly modified when the antenna is used in a two element

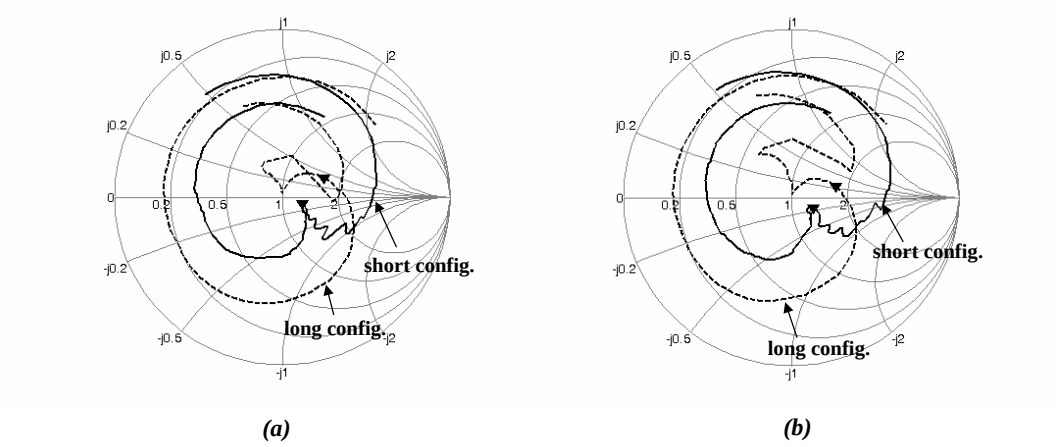

Figure 4.4: The measured antenna input impedance for the "long" and "short" antenna configuration in a 2 element array with inter-element separation of $\lambda/4$ for frequencies from $1.5\,GHz$ to $3.5\,GHz$ when (a) the other antenna is in the "short" configuration, and (b) the other antenna is in the "long" configuration. A marker selects the frequency of $2.484\,GHz$

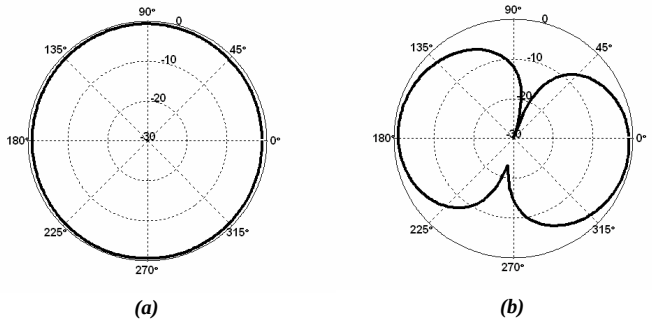

Figure 4.5: Simulated radiation pattern (in dBi) in the elevation plane (a) and in the azimuth plane (b) of the printed dipole in the "short" configuration for an operation frequency of $2.484\,GHz$.

array with inter element separation of $\lambda/4$. For the different possible configurations of antenna geometry in an array (both "short", both "long", first antenna "short" and second "long", first antenna "long" and second "short") the simulated and measured radiation patterns of the two elements are reported in Fig.4.6 and Fig.4.7 in the azimuth plane. The radiation pattern of each dipole configuration is obtained leaving the other dipole of the array closed on a 50 Ω load. The radiation pattern, which is linearly polarized, changes from one configuration to another. The plots shows that the difference between configurations is in the direction of the main beam and in the shape of the secondary lobe. In particular we observe a titling angle of $5° - 10°$ between the main lobes of the different configurations.

Table 4.2: Spatial correlation between patterns generated at two different ports of the RPDA.

$short - short$	$long - short$	$short - long$	$long - long$
0.43	0.28	0.28	0.31

Table 4.3: Spatial correlation between patterns generated at the same port of the RPDA.

	$E_{1,s-s}$	$E_{1,s-l}$	$E_{1,l-s}$	$E_{1,l-l}$
$E_{1,s-s}$	1	0.87	0.94	0.9
$E_{1,s-l}$	0.87	1	0.9	0.93
$E_{1,l-s}$	0.94	0.9	1	0.93
$E_{1,s-l}$	0.9	0.93	0.93	1

The level of diversity between the patterns generated at the two ports of the array, as well as between the patterns generated at the same port for different configurations of the array, is estimated through the spatial correlation coefficient value [89] [90]. Assuming a rich scattering environment ($P(\Omega)$ is uniformly distributed), the spatial correlation coefficient,

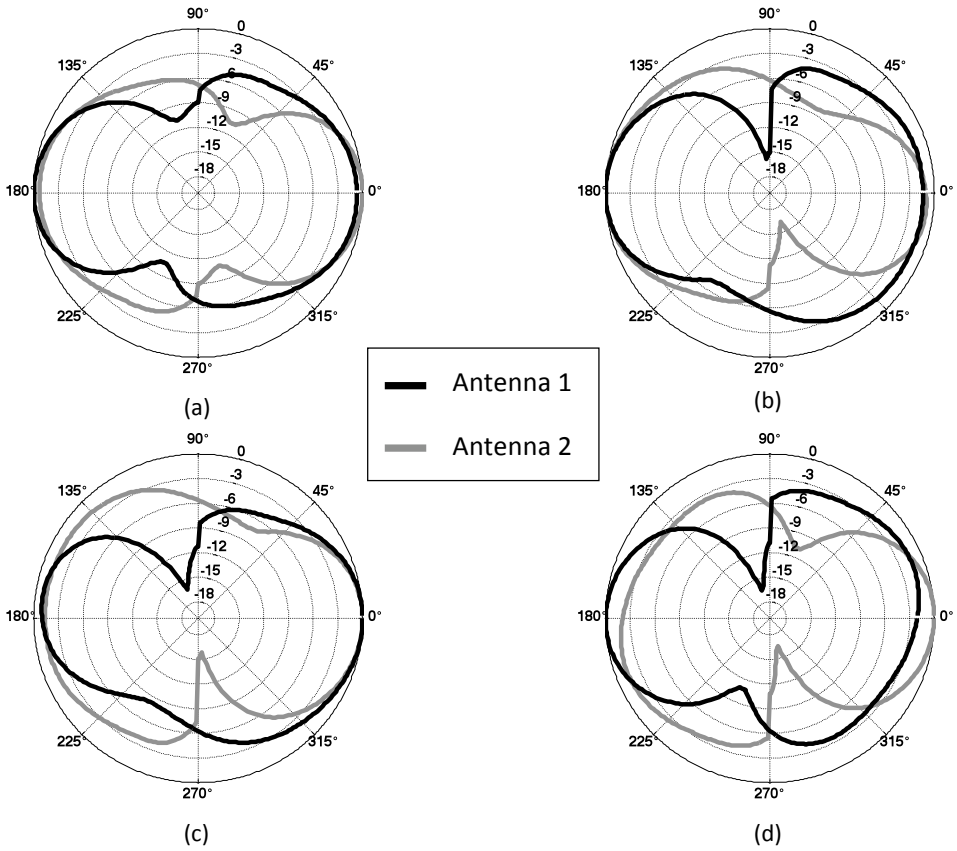

Figure 4.6: Measured radiation pattern (in dBi) in the azimuth plane of the RPDA for an operation frequency of $2.484\,GHz$:(a) antenna 1, "short", antenna 2, "short"; (b) antenna 1, "long", antenna 2, "short"; (c) antenna 1, "short", antenna 2,"long";(d) antenna 1, "long", antenna 2, "long".

$r_{j,k,l,m}$, is defined according to Eq. (3.10) as:

$$r_{j,k,l,m} = \frac{\int_{4\pi} \mathbf{E}_{j,k}(\Omega)\mathbf{E}^*_{l,m}(\Omega)d\Omega}{[\int_{4\pi} |\mathbf{E}_{j,k}(\Omega)|^2 d\Omega \int_{4\pi} |\mathbf{E}_{l,m}(\Omega)|^2 d\Omega]^{1/2}} \tag{4.1}$$

where j and l define the array port and k and m the antenna configuration at the port j and l respectively. $\mathbf{E}_{j,k}(\Omega)$ is the radiation pattern of the configuration k at port j over the solid angle $\Omega = (\phi, \theta)$ and $\langle * \rangle$ is the transpose operator. Table 4.2 reports the values of cor-

relation between the azimuthal patterns generated at the two ports of the array, while Table 4.3 reports the values of correlation between the azimuthal patterns generated at the same port for all the array configurations. It can be noted from Table 4.2 that the correlation values between radiation patterns at the two ports of the array are small enough for all the configurations (≤ 0.7) to provide significant diversity gain [89]. Table 4.3 shows then that the level of diversity between the different configurations is not very high ($r_{1,k,1,m} > 0.8$).

The measured radiation efficiency for each array configuration is reported in Table 4.4. We note an imbalance in the radiation efficiency for the different configurations: "short-short" is the most efficient one while "long-long" is the least efficient antenna configuration. We note that differences in radiation efficiencies exist because of losses introduced by PIN diode switches and losses introduced by different levels of inter element mutual coupling. This information is useful for estimating the performance achievable with the antenna design. The higher the radiation efficiency, the higher the received signal power for a fixed transmitted power and the higher is the achievable channel capacity.

Table 4.4: Measured radiation efficiency of the RPDA.

	$Antenna1$	$Antenna2$
$short - short$	84%	84%
$short - long$	77%	48%
$long - short$	48%	77%
$long - long$	52%	52%

The simulated as well as the measured values of the return loss of the antenna in the two configurations are shown in Fig.4.8. The return loss for the antenna is determined when the

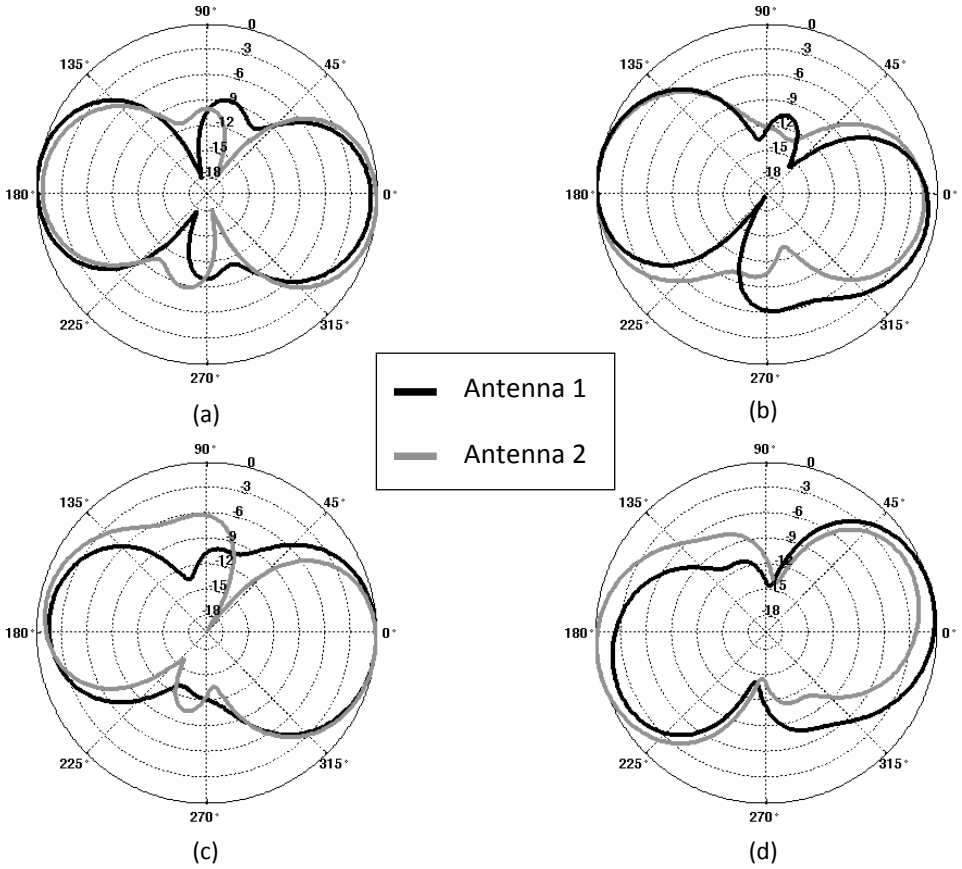

Figure 4.7: Simulated radiation pattern (in dBi) in the azimuth plane of the RPDA for an operation frequency of $2.484\,GHz$:(a) antenna 1, "short", antenna 2, "short"; (b) antenna 1, "long", antenna 2, "short"; (c) antenna 1, "short", antenna 2,"long";(d) antenna 1, "long", antenna 2, "long".

antenna is placed in a two element array with inter-element spacing of $\lambda/4$ so that the effects of mutual coupling can be incorporated into the antenna input impedance. The system has been designed to work in the frequency band between $2.4\,GHz$ and $2.484\,GHz$ typical of an 802.11-like MIMO-aware WLAN and Fig.4.8 shows that the antenna configurations are matched at the frequency band of interest (for a target S_{11} of $-10\,dB$). Fig.4.9 shows the measured $VSWR$ for all array configurations, from which it is evident that each antenna

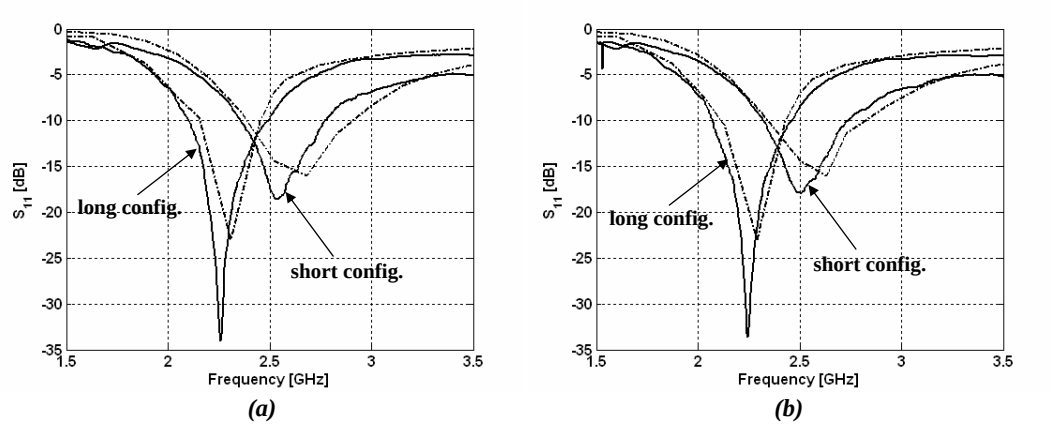

Figure 4.8: The measured reflection coefficient for the "long" and "short" antenna configuration in a 2 element array with inter-element separation of $\lambda/4$ when (a) the other antenna is in the "short" configuration, and (b) the other antenna is in the "long" configuration. The respective simulated curves are also shown dashed.

configuration is impedance matched over the bandwidth of interest.

The proper choice of the receiver and transmitter array switch configurations (i.e. the length of each antenna) is the one which decreases MIMO spatial channel correlation and maximizes channel capacity for a particular multipath environment. For example, the optimal choice could be determined by switching through all the possible length configurations at transmitter and receiver whenever the capacity experienced by the link falls below a predefined threshold.

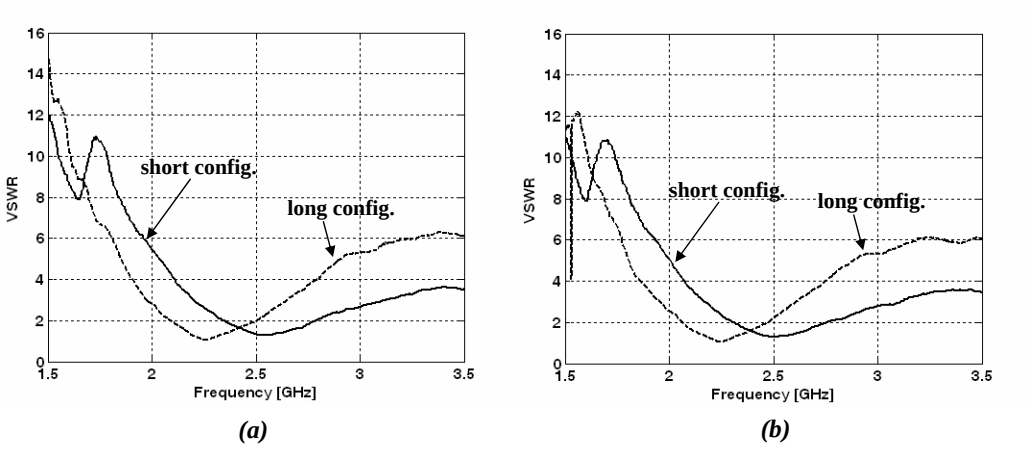

Figure 4.9: The measured VSWR for the "long" and "short" antenna configuration in a 2 element array with inter-element separation of $\lambda/4$ when (a) the other antenna is in the "short" configuration, and (b) the other antenna is in the "long" configuration.

4.3 Performance in clustered MIMO channel model

In this section, we evaluate the capacity performance of the proposed reconfigurable antenna in clustered MIMO channel models described in Section 3.2. The capacity is computed from the spatial correlation coefficients defined in Eq. (3.11).

The spatial correlation coefficients were numerically evaluated by employing realistic radiation patterns in the azimuthal plane (see Fig. 4.7) for all the switch configurations of a two element reconfigurable antenna array. The MIMO channel capacity was computed by using the spatial correlation coefficients in Eq. (3.11). A tight upper bound on the ergodic capacity for spatial multiplexing systems (with equal power allocation across the transmit antennas) [91], was adopted in this analysis. The upper bound for double sided correlated

MIMO channel capacity is expressed as:

$$C \leq log_2\Big[\sum_{k=0}^{N_{min}}\Big(\frac{SNR}{N_t}\Big)^k k! \sum_{1\leq i_1<i_2\ldots<i_k\leq N_t} |\mathbf{R}_{t_{i_1,i_2,\ldots,i_k}}^{i_1,i_2,\ldots,i_k}| \sum_{1\leq i_1<i_2\ldots<i_k\leq N_r} |\mathbf{R}_{r_{i_1,i_2,\ldots,i_k}}^{i_1,i_2,\ldots,i_k}|\Big] \quad (4.2)$$

where $N_{min} = min(N_r, N_t)$ and $|\mathbf{R}_{t_{i_1,i_2,\ldots,i_k}}^{i_1,i_2,\ldots,i_k}|$, $|\mathbf{R}_{r_{i_1,i_2,\ldots,i_k}}^{i_1,i_2,\ldots,i_k}|$ are the minor determinants of $\mathbf{R}_t$ and $\mathbf{R}_r$ (i.e., a determinant of the $k \times k$ matrix lying in the $i_1, i_2, ..., i_k$ rows and in the $i_1, i_2, ..., i_k$ columns of $\mathbf{R}_t$ and $\mathbf{R}_r$).

We first considered the performance of the reconfigurable array in single-sided correlated MIMO channels. In single-sided correlated channels, either $\mathbf{R}_t = \mathbf{I}$ or $\mathbf{R}_r = \mathbf{I}$, with the other matrix determined by the clustered MIMO channel model. Thus, the channel capacity was computed for a MIMO system employing the reconfigurable antenna at only one end of the link. Fig.4.10 shows the channel capacity achieved with the four possible array configurations as a function of the mean AOA (ϕ_c) of the cluster, for an angular spread of $\sigma_\phi = 30^\circ$ and $SNR = 20\,dB$. Fig.4.10 also shows the capacity of a double-sided uncorrelated 2×2 MIMO channel ($\mathbf{R}_t = \mathbf{R}_r = \mathbf{I}$) as a reference. It can be observed that for each antenna configuration, the capacity varies over the mean AOA of the cluster. The highest value of achievable capacity can be guaranteed by switching between the four array configurations, since each configuration outperforms the others in certain mean AOA ranges.

In order to complete a channel capacity analysis of the reconfigurable antenna in a clustered channel model, the channel capacity defined in Eq. (4.2) was computed for a double sided correlated channel (i.e. both $\mathbf{R}_t$ and $\mathbf{R}_r$ determined by the clustered MIMO channel model). In this case, the proposed reconfigurable antenna was used at both ends of the

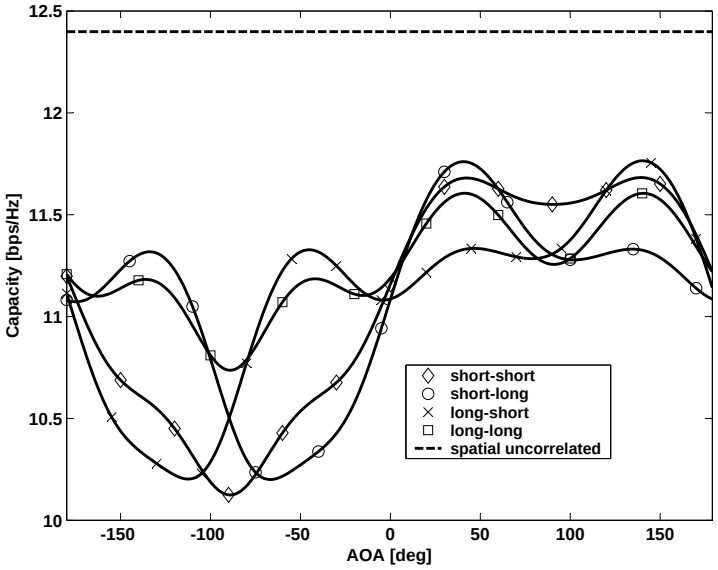

Figure 4.10: Single-sided correlated MIMO channel ergodic capacity for the four possible array configurations as a function of the cluster mean AOA, with SNR = 20 dB. The ergodic capacity for a double-sided uncorrelated channel is also shown as a reference.

MIMO link. The capacity of the channel was found according to Eq. (4.2) for each possible configuration of the transmitting and receiving antenna array, for a total of 16 different configurations. The capacity achievable with the reconfigurable antenna array was defined as the highest one among the 16 antenna configurations. Fig.4.11(a) depicts the double-sided correlated MIMO channel ergodic capacity of the reconfigurable antenna as a function of the cluster mean AOA and cluster angle spread (assuming these parameters to be the same at both the transmitter and the receiver side), with $SNR = 20\,dB$. In Fig.4.11(b) the ergodic capacity achievable with the same printed dipole in the "short" configuration (as specified previously, the most efficient in terms of radiation and matching) is reported as a reference non-reconfigurable antenna system. The results show the variation of the capacity

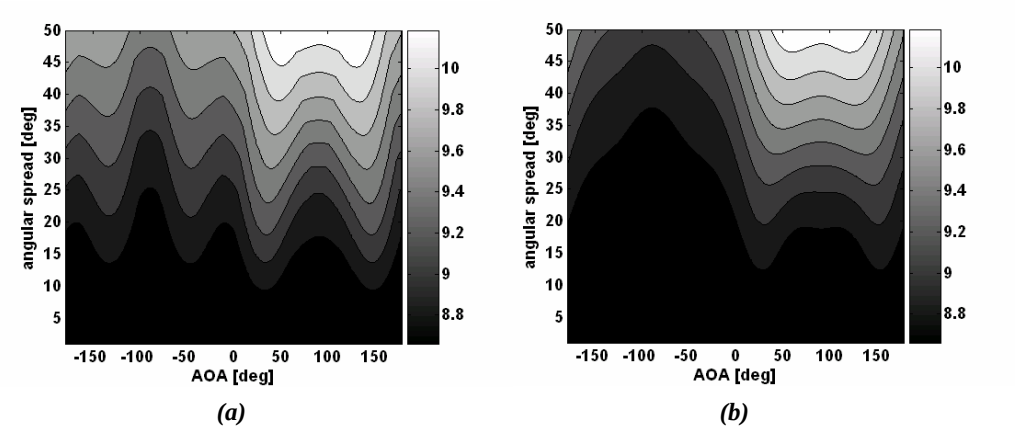

Figure 4.11: Contour plot of the double-sided correlated MIMO channel ergodic capacity for the (a) reconfigurable antenna array, and of the (b) non-reconfigurable $\lambda/2$ printed dipole as a function of the cluster mean AOA and per-cluster AS, with $SNR = 20\,dB$.

with the mean AOA of the cluster and the AS. The reconfigurable antenna outperforms the non reconfigurable printed dipole for every mean AOA and every AS. With respect to the single-sided correlated channel of Fig.4.10, the situation in Fig.4.11(a) shows the capacity achieved is lower, since both transmitter and receiver sides are correlated. However, the double-sided correlated channel better describes the real channel when closely spaced antenna array elements are used. Moreover, the relative capacity improvement achievable with the reconfigurable antenna in a double-sided correlated channel is higher than the capacity improvement achievable in a single-sided correlated channel.

The obtained results motivate then the use of this reconfigurable antenna in a MIMO link and demonstrate how a decision rule for switching configuration can be generated using

channel spatial correlation information (i.e. a function of mean AS and AOAs).

Since some limitations with the adopted clustered channel model have been recognized [92–94], in the next Sections, the RPDA performance is analyzed using computational electromagnetic simulation in an outdoor and indoor environment, and experimental field-testing in an indoor environment. In particular through electromagnetic simulations and experimental field-testing the effect of considering the full 3D antenna radiation pattern is investigated in realistic environments that consist of more than one cluster and in which the effect of cross-polarization is considered.

4.4 Ray tracing simulation results

In this Section, the RPDA is studied in terms of channel capacity, via numerical computation using an electromagnetic ray tracer, FASANT [95]. FASANT is a deterministic ray tracing program based on geometric optics and the uniform theory of diffraction. A 3D model of Austin downtown was simulated as the geometry input of FASANT. There was a transmission point located in the center of the model, at a height of $1.5m$, and a receiver, at a height of $1.5m$, moving along the streets, as shown in Fig.4.12(a), occupying 2400 different locations. Note that the orientation of the array has been selected such that the maximum degree of pattern diversity between the different antenna's configurations is in the azimuthal plane.

The radiation patterns obtained from HFSS antenna design software, for the different configurations of the antenna spaced by $\lambda/4$ were used in the ray tracing simulation both

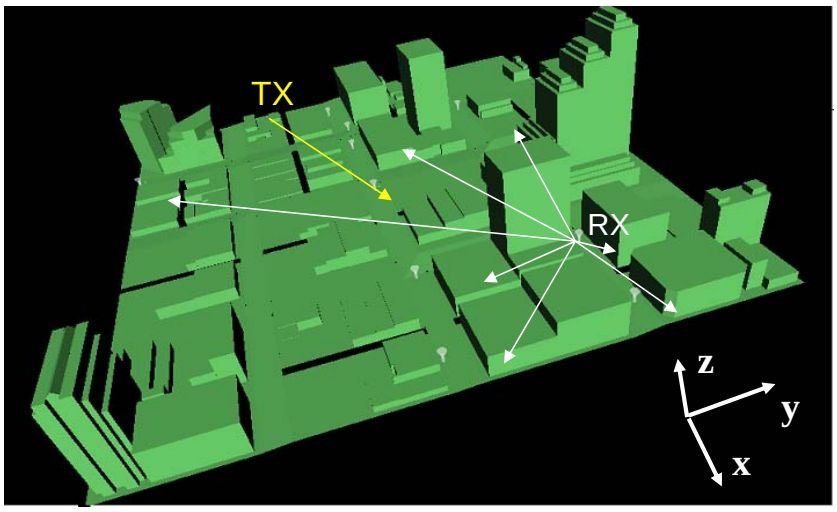

(a)

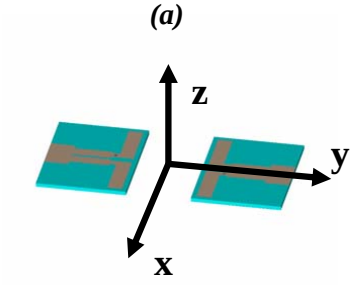

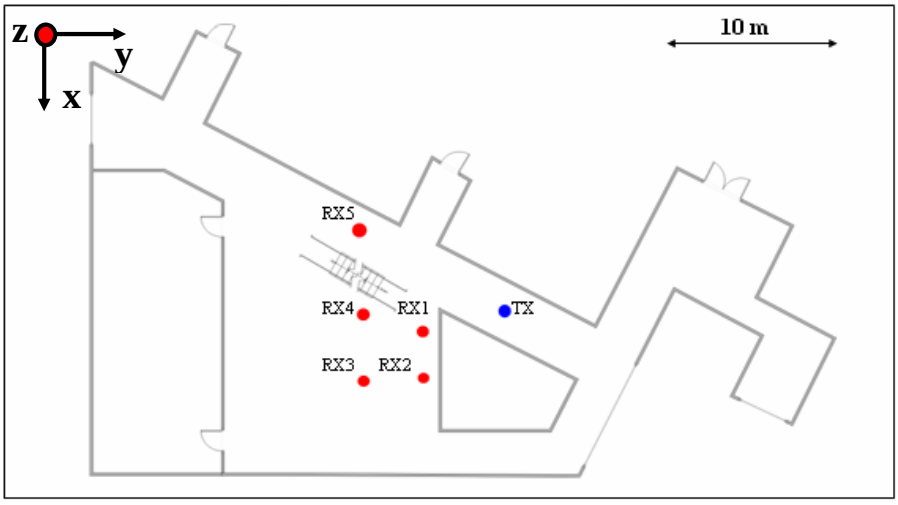

(b)

Figure 4.12: Outdoor and indoor environments models: (a) 3D model of downtown Austin (TX location is shown with some of the RX locations), (b) orientation of reconfigurable antenna array in the indoor environment illustrating the multiple receiver locations and the transmitter location.

at the receiver as well as at the transmitter in a 2×2 MIMO system. Ray tracing considers the effects caused by the superposition of the antenna's radiation patterns at the receiver and transmitter.

The channel matrix $\mathbf{H}$ was computed as described in [58]. To define the capacity of the MIMO communication link, a Frobenius normalization of the channel matrix was computed in order to remove the differences in path loss among a number of channel matrices [96]. Specifically, to preserve the relative antenna gain effects of each configuration, all the channel matrices for each receiver location were normalized with respect to the "short" configuration channel matrix. The normalization factor N_F is defined as:

$$N_F = \sqrt{\frac{\|\mathbf{H}_{\text{“}short\text{”}}\|_F^2}{N_t N_r}} \tag{4.3}$$

The capacity of the link was then determined, assuming a SNR of $20\,dB$, as [66]:

$$C = \log_2 \left[\det \left(\mathbf{I}_{N_r} + \frac{SNR}{N_t} \mathbf{H}\mathbf{H}^\dagger \right) \right] \tag{4.4}$$

where $\mathbf{I}_{N_r}$ is an $N_r \times N_r$ identity matrix.

The capacity of the channel was found in this way for each possible configuration of the transmitting and receiving antenna array, for a total of 16 different configurations per position, and the optimal solution of the reconfigurable antenna was the one which guaranteed the highest channel capacity. The channel capacity achieved using the reconfigurable antenna was compared with the capacity of a MIMO link where the same printed dipole

in the "short" configuration (as specified previously to be the most efficient in terms of radiation and matching) was used at the transmitter and receiver array. Based on the data collected from simulations, a cumulative distribution function (CDF) for the capacity was numerically obtained and shown in Fig.4.13(a), where one curve represents the CDF relative to a system where the reconfigurable antenna solution was used, and the other was relative to one where the "short" configuration (fixed antenna) was used. The percentage improvement in capacity that the system provided on a location-by-location basis, with respect to the fixed antenna solution, is shown in Fig.4.14. As shown by the dashed line the average percentage improvement in capacity results is 7% for a SNR of $20\,dB$, reaching peaks of 40% for certain receiver positions. It can also be observed, as shown in Section 4.3, that the operation of the system was dependent on the particular environment between the transmitter and the receiver.

4.5 Measurements results

The RPDA was then tested taking measurements on a 2×2 MIMO Orthogonal Frequency Division Multiplexing (OFDM) testbed communication system in an indoor environment. Each node of the experimental platform consisted of frequency agile transceivers operating in the ISM and UNII radio bands and a baseband process computer. The baseband chassis provided by National Instruments had two major functional roles. First, the unit contained the analog to digital (A/D) and (D/A) converters required for the two transceivers. The converters operated at $100MS/s$ with 14-bit quantization. Second, the baseband unit was a

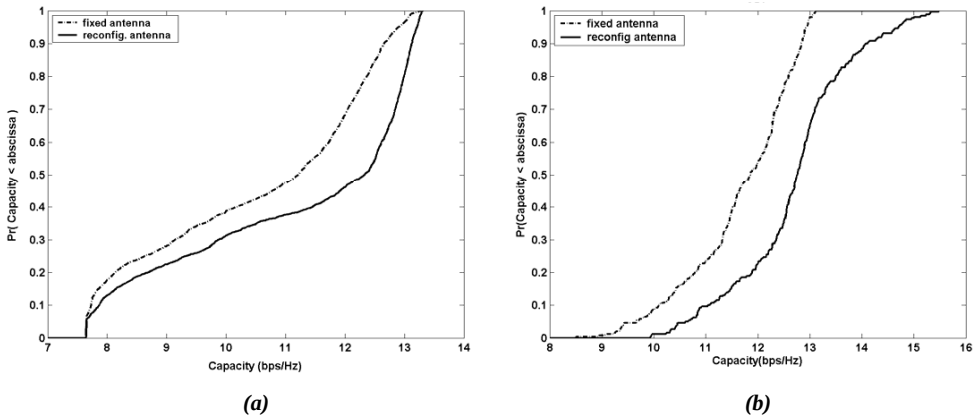

Figure 4.13: CDF of capacity for the reconfigurable and fixed antenna array in a (a) ray tracing simulated outdoor environment, and in a (b) measured indoor environment.

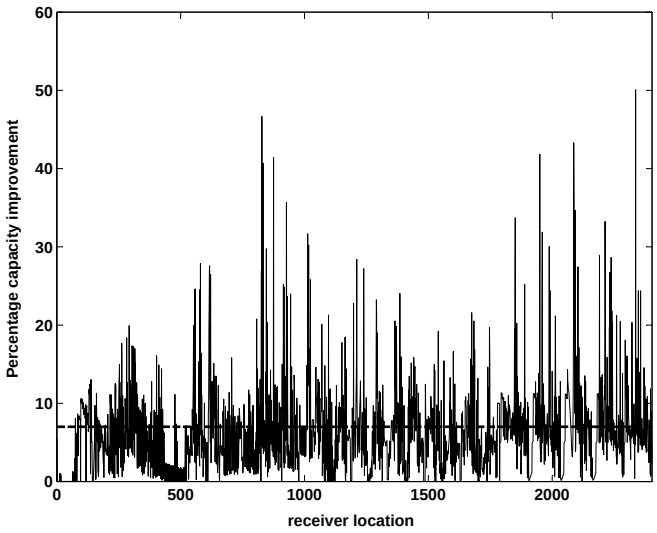

Figure 4.14: Percentage capacity improvement achieved with the reconfigurable antenna versus receiver location, and mean percentage capacity improvement (dashed line) in outdoor environment.

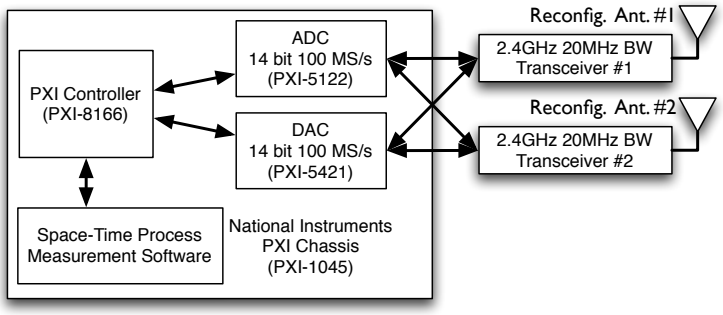

Figure 4.15: MIMO OFDM testbed block diagram

software defined radio (SDR) which allowed the physical layer to be flexible in implementing different experiments. An overview of the testbed can be seen in Fig.4.15. Further details on the channel sounder employed to collect field measurements are provided in Appendix A

Two nodes have been used for measurement. As shown in Fig.4.12(b), the measurements were taken in the hallway of the 3^{rd} floor of the Bossone Research building on Drexel University campus. The transmitter was stationary, while the receiver was moved between several different locations. The channel matrix was measured for 5 different locations of the receiver and for all 16 possible configurations of the antenna system. The measurements were performed at $2.484GHz$. We used BPSK to generate the analog baseband signal. The analog signal obtained was modulated using OFDM with the data being sent on each of the 52 sub-carriers. The spacing between each sub carrier was $312.5kHz$. A training pattern using binary phase shift keying (BPSK) was transmitted independently over the two transmitters. This training pattern was then received and used to estimate the channel

matrix [97]. The orientation of the array, depicted in Fig.4.12(b), has been selected such the maximum degree of pattern diversity between the different antenna's configuration is in the azimuthal plane.

To determine the capacity of the MIMO wideband communication link, a normalization of the channel matrix for each sub-carrier was computed using the Frobenius norm as described in Section 4.3, in order to remove the differences in path loss among a number of channel matrices [96]. Specifically, all the channel matrices for each receiver location and for each sub-carrier was normalized with respect to the "short" configuration channel matrix at the respective location and sub-carrier.

The capacity of the link was then determined using the equation:

$$C = \frac{1}{m}\sum_{i}^{m} \log_2 \Big[\det \Big(\mathbf{I}_{N_r} + \frac{SNR}{N_t} \frac{\mathbf{H}_i \mathbf{H}_i^{\dagger}}{N_{F_i}^2} \Big) \Big] \tag{4.5}$$

where m was the total number of sub-carriers. Since the channel was characterized over a broad frequency band, the capacity of the wideband channel was defined as an average of the capacities over all the m sub-carriers of the MIMO-OFDM link [98] and the optimal solution for the reconfigurable antenna was the one which guaranteed the highest average capacity.

In Fig.4.16 the percentage improvement in channel capacity, achieved with the novel reconfigurable antenna array with respect to a system where a fixed "short" configuration was used for every antenna array element at both transmitter and receiver, was plotted versus different SNR values for all 5 receiver locations. At each location the capacity improve-

ment was defined as the difference in capacity between the best configuration among the sixteen possible configurations (i.e. reconfiguring both transmit and receive arrays) of the reconfigurable antenna system and a 2×2 MIMO system with fixed, "short" configuration antennas. In order to define a "relative" improvement, the channel capacity improvement was normalized for each location with respect to the capacity measured with the "short" configuration antennas.

Table 4.5: Average measured percentage capacity improvement achievable with the RPDA with respect to the "short-short" configuration when used in a 2×2 MIMO OFDM system.

SNR [dB]	0	5	10	20	30
Percentage capacity improvement	28%	18%	10%	8%	5%

Fig.4.16 shows that the reconfigurable antenna solution increased MIMO link capacity with respect to a conventional, fixed antenna system. Only for receiver position 1 there was no improvement since, in that location, the best configuration of the reconfigurable antenna corresponded to the reference "short" configuration. On average, the novel antenna solution achieved a 10% improvement in capacity (with a peak of 28%) for a SNR of $10\,dB$ and 8% (with a peak of 16%) for a SNR of $20\,dB$ with respect to a system with a fixed antenna configuration. Fig.4.16 also shows how the improvement in capacity achieved with this novel antenna solution varied with receiver location and so with the particular multipath environment, as previously verified with simulations in Sections 4.3 and 4.4. Table 4.5 reports the values of average percentage capacity improvement for different values of SNR in a MIMO OFDM system.

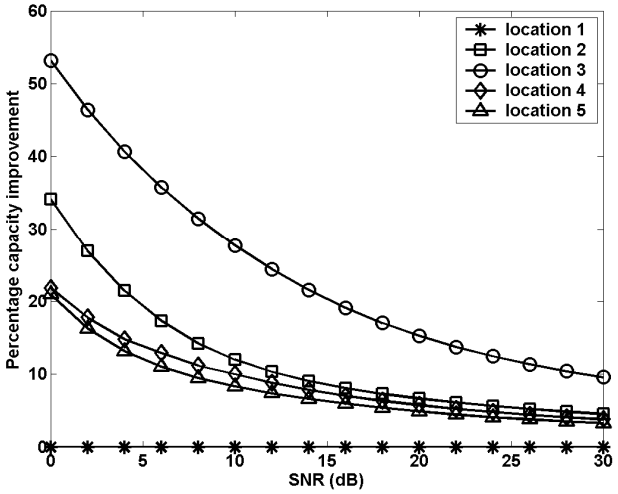

Figure 4.16: Percentage capacity improvement versus SNR for 5 different receiver locations in indoor environment (improvement defined as the normalized difference in capacity between the best configuration between the sixteen possible solutions of the reconfigurable antenna system and a 2×2 MIMO system with fixed length antennas).

A narrowband analysis of the channel, like the MIMO clustered channel model analysis (Section 4.3), could be performed by considering the channel on each OFDM sub-carrier to be an independent narrowband channel realization. This technique allows for a total of 260 narrowband channel realizations (5 locations times 52 sub-carriers for each location). For this narrowband analysis, results were shown in terms of the capacity CDF. In Fig.4.13(b) it was shown how the results from measurements were comparable to the results obtained from the simulation (Fig.4.13(a)) confirming the improvement that the reconfigurable MIMO antenna solution achieved in terms of capacity.

Fig.4.17 shows the percentage improvement in capacity achievable with the reconfigurable antenna in a narrowband channel for an indoor environment. The percentage im-

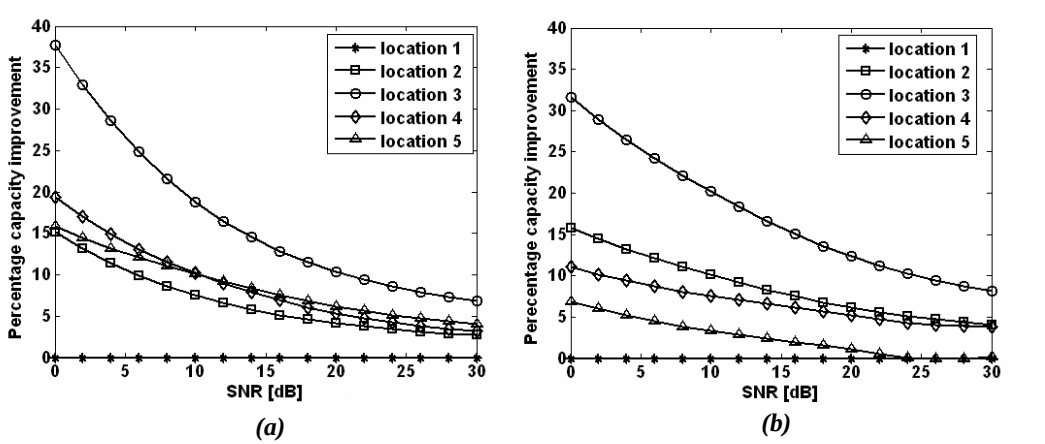

Figure 4.17: Percentage capacity improvement versus SNR for 5 different receiver locations in indoor environment for a narrow-band channel at $2.48\,GHz$: (a) results from measurements, (b) results from simulations.

provement is defined in the same way as in Fig.4.16, but it is calculated for a single subcarrier centered at $2.48\,GHz$. In Fig.4.17 the percentage improvement obtained through measurements for the five different locations of the receiver (Fig.4.17(a)) is compared with the one achieved through ray-tracing simulations conducted using FASANT, as in Section 4.4, for the same five locations and for the same frequency of $2.48\,GHz$ (Fig.4.17(b)). The results show a substantial agreement between the measured and the simulated results, confirming therefore the benefit of using the proposed reconfigurable antenna in indoor environments.

4.6 Summary

The achieved results demonstrates that the RPDA is an attractive solution for MIMO handheld devices (where space is an important constraint) to maintain good communication link capacity. The RPDA is the first demonstration of a reconfigurable antenna system for MIMO communications [43]. Only two switches are used per antenna element and a limited level of pattern diversity is achieved through this design. In the next chapters different reconfigurable antenna structures will be investigated in order to provide higher level of reconfigurability for higher capacity improvement while diminishing the space occupied by the antenna on the communication device.

Chapter 5: Reconfigurable circular patch antennas

In this chapter 2 novel reconfigurable multi element antennas that are capable of achieving increased levels of diversity with respect to the RPDA are presented. These antennas are based on a standard circular patch antenna design and they allow for an appreciable increase in the performance of MIMO systems while reducing the space occupied by the antenna on the communication device. With the circular patch design, a single antenna element can be used as a two element array by using multiple feed points. Two different types of reconfigurable circular patch antennas (RCPAs) are presented in this chapter: a RCPA with two different antenna configurations exploiting only pattern diversity (RCPA-PD) and a RCPA with three different antenna configurations exploiting both pattern and polarization diversity (RCPA-PPD). The benefits offered by each state (i.e., excited radiation pattern and polarization) of the RCPAs are investigated both in Line of Sight (LOS) and Non Line of Sight (NLOS) scenarios. The analysis shows the effectiveness of each array configuration in increasing the diversity level of the system and the amount of signal power received in LOS and NLOS communication links. The radiation efficiency and the level of pattern and polarization diversity of each configuration are investigated to explain the performance offered by this class of antennas in MIMO systems. Finally we show the difference in performance achievable with these antennas when employed in narrowband or broadband communication systems.

5.1 Circular patch: pattern and polarization diversity

The properties of circular microstrip antennas have been studied in [18, 99]. In [99] it was shown that, by exciting different electromagnetic modes of circular patch antennas, it is possible to obtain different radiation properties. In addition, by varying the size of the antennas as well as the feed location, different polarizations and radiation patterns can be generated in the far-field. In this chapter we use the orthogonality of the radiation patterns of circular patch antennas as a means to reduce correlation between the diversity branches of the MIMO array while increasing the SNR at the receiver.

As reported in [99], the electric field components excited in the far field for the n-th TM electromagnetic mode are defined, as a function of the circular patch antenna radius, ρ, as:

$$E_{\theta}^{(n)}(\phi,\theta) = e^{\frac{jn\pi}{2}}\frac{e^{-jk_0d}}{d}\frac{V_0}{2}k_0\rho[J_{n+1}(k_0\rho\sin\theta) - J_{n-1}(k_0\rho\sin\theta)]\cos[n(\phi-\phi_0)] \quad (5.1)$$

$$E_{\phi}^{(n)}(\phi,\theta) = -e^{\frac{jn\pi}{2}}\frac{e^{-jk_0d}}{d}\frac{V_0}{2}k_0\rho[J_{n+1}(k_0\rho\sin\theta) + J_{n-1}(k_0\rho\sin\theta)]\cos\theta\sin[n(\phi-\phi_0)] \quad (5.2)$$

where $J_n(k_0\rho\sin\theta)$ is the Bessel function of the first kind and order n, ϕ_0 is the reference angle corresponding to the feed point location on the antenna, V_0 is the edge voltage at $\phi = 0$, k_0 is the wavenumber, and d is the distance from the antenna. Varying the radius of the antenna, different electromagnetic modes can be excited according to [99]:

$$\rho = \frac{\chi_n^{'}\lambda}{2\pi\sqrt{\varepsilon_r}} \quad (5.3)$$

where ε_r is the dielectric permittivity of the substrate, λ is the wavelength and $\chi_n^{'}$ is the first

zero of the derivative of the Bessel function J_n. Different excited electromagnetic modes corresponds to different shapes of radiation and it is therefore possible to achieve pattern diversity by varying the radius of the circular patch. As shown in [99], it is also possible to rotate the radiation pattern in the azimuth plane by varying the feed point location along a circumference. Two different ports can be placed on the same circular patch to excite two orthogonal radiation patterns with the same electromagnetic mode. To achieve orthogonality between two radiation patterns, for a pair of the n-th modes, the feeds have possible azimuthal displacements of

$$\phi_2 - \phi_1 = \frac{(2q-1)\pi}{2n}, \;\; q = 1, 2, ..., n \tag{5.4}$$

where ϕ_1 and ϕ_2 are the azimuth displacements of feed point 1 and 2, respectively. Examples of the radiation patterns that can be excited at two orthogonal ports of the circular patch antenna for different modes are shown in Fig.5.1. The feed positions provide zero mutual resistance as long as the n-th mode exists alone. However, the presence of the other modes make some feed positions given by Eq. (5.4) better than others.

The radiation of a circular patch antenna is linear polarized independent from the excited electromagnetic modes. It is however possible to excite circular or elliptical polarization by properly modifying the antenna structure or its feeding network. For single probe feed types, circular polarization can be achieved through perturbation segments placed to the edge of the disk patch [100] or by using slots cut in the circular patch to properly phase shift the two

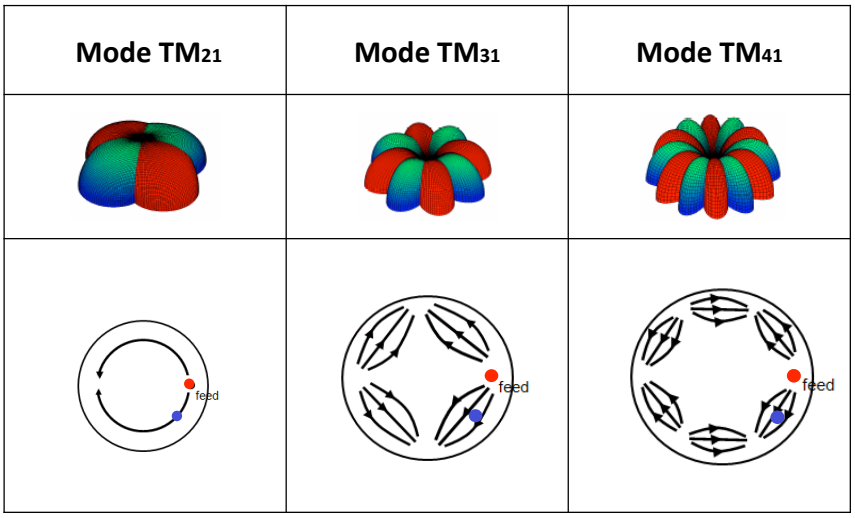

Figure 5.1: Radiation pattern and current distribution of two port circular patch antennas exciting different electromagnetic modes.

coexisting electromagnetic modes [101]. For double probe feed types, circular polarization is achieved employing 90° hybrid networks to generate a controlled phase shifting between the two ports of the antenna [102].

Such techniques for pattern and polarization control in circular patch antennas have been exploited to design two different types of RCPAs, discussed in Section 5.2.

5.2 Reconfigurable circular patch antennas

In this Section we introduce two different types of RCPAs: one that exploits only pattern diversity and one that exploits both pattern and polarization diversity. Both antennas have been designed to operate in the 2.4-2.5 GHz frequency band typical of an 802.11-like MIMO local area network.

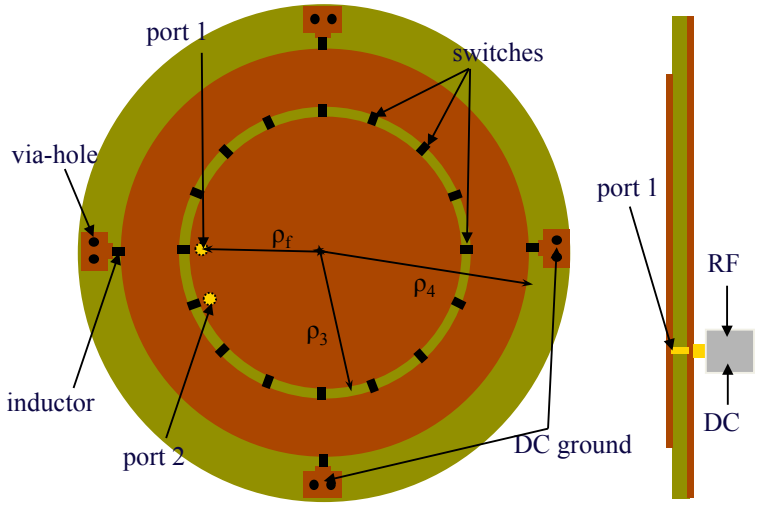

Figure 5.2: Schematic of the reconfigurable circular patch for pattern diversity (RCPA-PD).

5.2.1 Reconfigurable circular patch antenna for pattern diversity (RCPA-PD)

The Reconfigurable Circular Patch Antenna for Pattern Diversity (RCPA-PD) consists of a circular patch with two accessible coaxial ports that is capable of reconfiguring its radiation pattern at each port. Two different radiation patterns can be excited at each port by appropriately varying the current distribution over the patch. A detailed schematic of the RCPA is shown in Fig.5.2 and its photo is depicted in Fig.5.3. In order to change the current distribution on the antenna, the radius of the circular patch is varied. By varying the patch size, different electromagnetic modes of circular patch antennas can be excited and each excited mode generates a unique radiation pattern in the far-field [99].

The antenna is built on FR4 substrate and the radius of the circular patch is varied using PIN diodes switches strategically located over the antenna structure. Two different

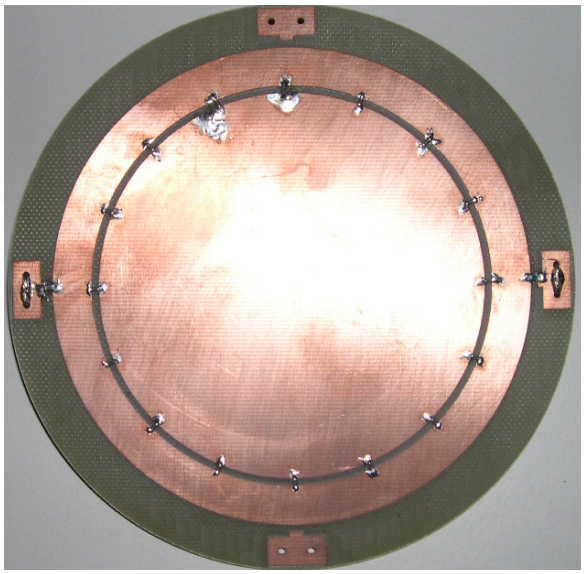

Figure 5.3: Reconfigurable circular patch for pattern diversity (RCPA-PD).

configurations of the antenna can then be defined at each port: *i*) when all the switches are turned off the electromagnetic mode TM_{31} is excited ("mode 3" configuration) and *ii*) when all the switches are turned on the electromagnetic mode TM_{41} is excited ("mode 4" configuration) at both ports.

As investigated through electromagnetic simulations in the finite difference time domain (FDTD) a minimum of sixteen switches are necessary in order to properly excite the electromagnetic mode TM_{41} at both the antenna ports. As depicted in Fig.5.4 the electric field in the antenna substrate, and therefore the current on the circular patch, is not distributed in the characteristic manner of mode TM_{41} when less than sixteen switches are placed on the antenna structure. Note also that the switches need to be placed where the electric field is maximum for mode TM_{41}. PIN diode switches (Infineon BAR 50-02V) with an isolation

of 18 dB and an insertion loss of 0.3 dB at a frequency of 2.5 GHz are used.

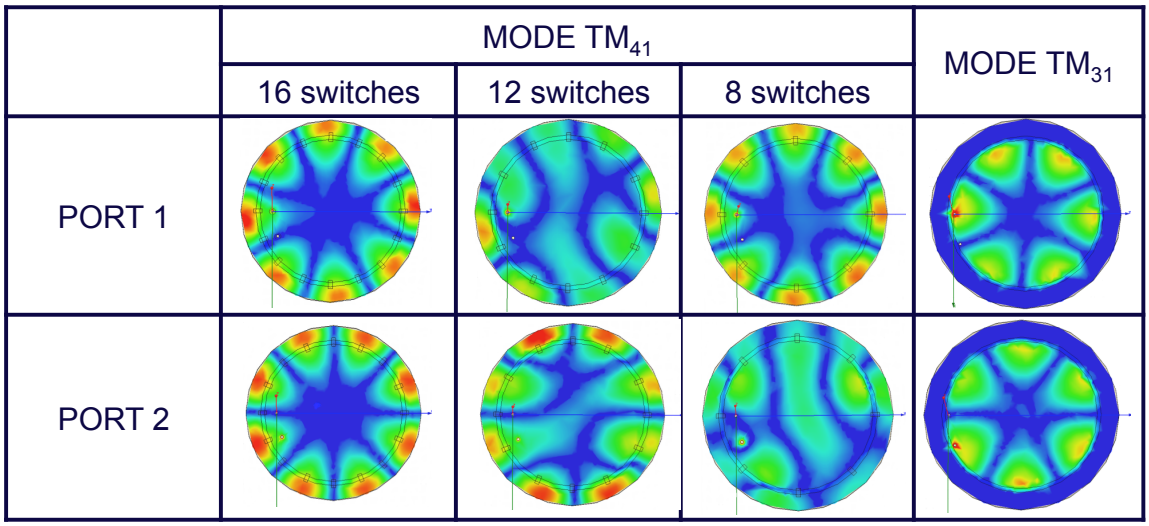

Figure 5.4: Electric field distribution in the antenna substrate for "mode 4" and "mode 3" configurations as a function of the number of switches. Distributions determined by simulation using HFSS

Four pads symmetrically located around the circular patch, are used to provide a ground for the biasing current of the PIN diodes. 1000 nH inductors are used to isolate the radio frequency signal from the DC ground. The DC bias (current of 10 mA and voltage of 0.7 V) is directly provided from one of the two feed points through a wideband coaxial bias-tee. The two ports on the antenna structure are separated by 25^o such that they are well isolated and the radiation patterns excited simultaneously at the two ports are spatially orthogonal to each other. The distance of the two ports from the center of the patch is strategically selected in order to have both ports matched at a frequency of 2.484 GHz for both antenna configurations. In Table 5.1 a summary of the structural parameters for the antenna is provided.

Table 5.1: RCPA-PD structural parameters

Dielectric	FR4 ($\epsilon_r = 4.4$)
Dielectric thickness	$1.524\,mm$
Feeds separation	25°
ρ_3	$3.9\,cm$
ρ_4	$4.6\,cm$
ρ_f	$3.82\,cm$

The scattering parameters of the antenna structure have been measured with a network analyzer and simulated using the finite-difference time-domain method HFSS antenna design software. Fig.5.5 shows the measured and simulated scattering parameters of the RCPA-PD determined at the two input ports over frequency, and for both antenna configurations ("mode 3" and "mode 4"). For both configurations, there is an isolation of about 20 dB and the return loss is below the target -10 dB at any port in the band of interest. The large isolation between the two ports allows for the generation of orthogonal radiation patterns, using a single antenna structure as a two element array. The -10 dB bandwidth of the RCPA is 1%, denoting the narrow-band characteristic of the RCPA-PD.

The measured radiation patterns of the RCPA-PD are shown in Fig.5.6 for both the antenna configurations in the azimuthal plane. It can be observed that the radiation patterns excited by "mode 3" and "mode 4" configurations are different, thus resulting in pattern diversity. "Mode 3" has six main beams compared to the eight of "mode 4" configuration. We note also that the radiation patterns excited at the two ports are orthogonal to one another: where there is a maximum in radiation at port 1, there is a null in radiation at port 2. The maximum directivity is 7 dB for "mode 3" and 9 dB for "mode 4".

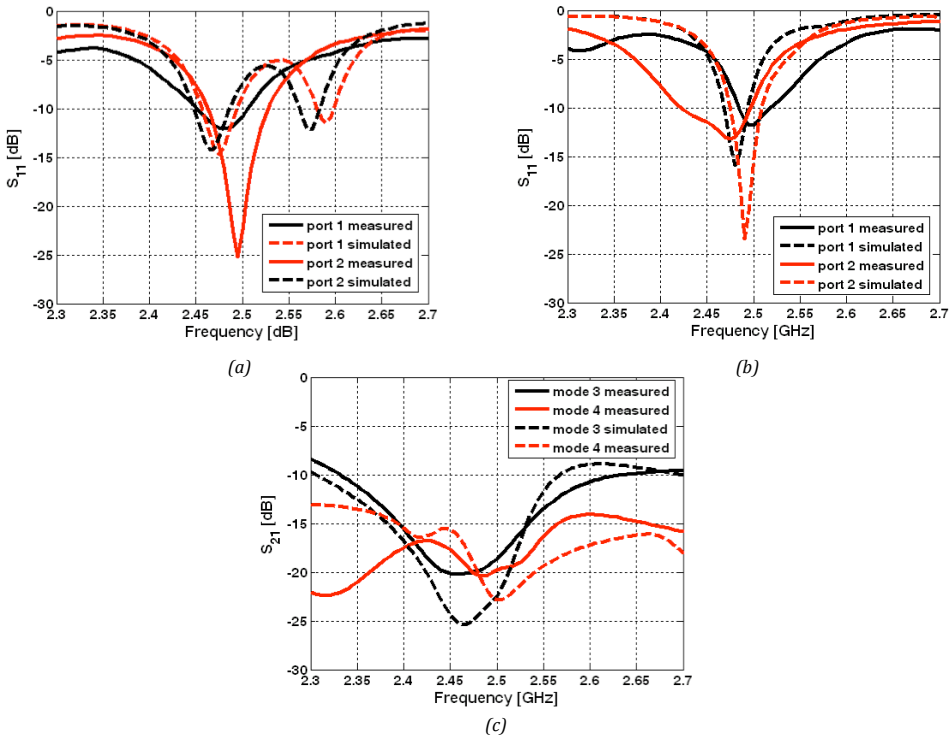

Figure 5.5: Measured and simulated scattering parameters for of the RCPA-PD (a)return loss"mode 3", (a)return loss"mode 4", (c)ports isolation.

The level of diversity between the patterns generated at the two ports of the array, as well as between the patterns generated at the same port for different configurations of the array, is estimated through the spatial correlation coefficient value of Eq. (4.1). Table 5.2 and Table 5.3 report the spatial correlation coefficient value between azimuthal patterns generated at two antenna ports and between azimuthal patterns of different configurations generated at the same port respectively. From Table 6.1 it can be noted that the patterns generated at the two ports of the RCPA-PD are spatially orthogonal for both the configurations. Moreover Table 6.2 shows the very high level of diversity ($r_{1,k,1,m} = 0.2$) existing

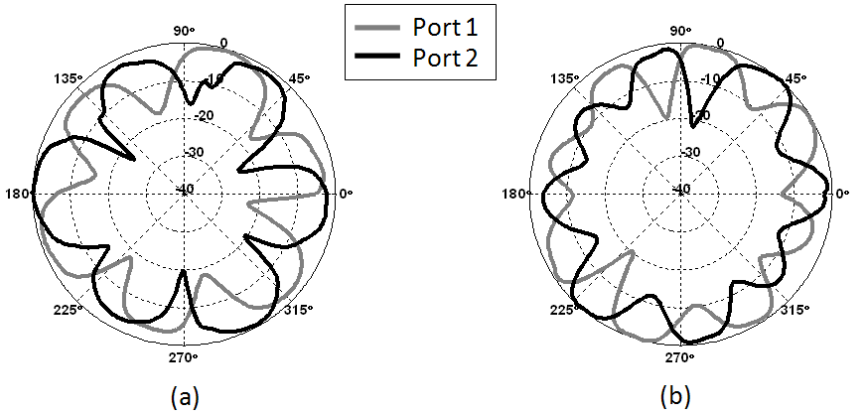

Figure 5.6: Measured radiation pattern (in dB) in the azimuthal plane at the two ports of the RCPA-PD in all its configurations for an operation frequency of $2.48\,GHz$:(a) port 1,"mode 3", port 2 "mode 3"; (b) port 1,"mode 4", port 2 "mode 4".

Table 5.2: Spatial correlation between patterns generated at two different ports of the RCPA-PD.

$mode3$	$mode4$
0.06	0.18

between the two configurations of the RCPA-PD.

The measured antenna radiation efficiency is reported in Table 5.4. We note that the antenna has a poor radiation efficiency because of the lossy substrate used for its fabrication (FR4 with $\tan\delta = 0.02$). As expected "mode 3" is the most efficient configuration since lower order modes are more efficient than higher order modes [99,103] and because no power is lost in the switches when "mode 3" is active.

Table 5.3: Spatial correlation between patterns generated at the same port of the RCPA-PD

	$E_{1,mode3}$	$E_{1,mode4}$
$E_{1,mode3}$	1	0.2
$E_{1,mode4}$	0.2	1

Table 5.4: Measured radiation efficiency of the RCPA-PD

	$Port1$	$Port2$
$mode3$	21%	17%
$mode4$	6%	5%

5.2.2 Reconfigurable circular patch antenna for pattern and polarization diversity (RCPA-PPD)

The Reconfigurable Circular Patch Antenna for Pattern and Polarization Diversity (RCPA-PPD), depicted in Fig.6.1 and 5.8, consists of a circular patch whose geometry can be changed by turning on and off the PIN diode switches located on the antenna structure in order to excite radiation patterns with different shapes and polarizations. Differences in the shape of the radiation pattern are achieved by exciting different electromagnetic modes in the antenna structure, while polarization diversity is obtained by phase shifting the two degenerate electromagnetic modes co-existing in the patch. Fourteen PIN diodes (switches D1), placed radially on the antenna, are positive biased and used to dynamically change the radius of the circular patch. Four PIN diodes (switches D2) are reverse biased and connect or disconnect two perturbation segments to the inner circular patch. Therefore, it is possible to define three configurations for this antenna: *i*) when both switches D1 and D2 are turned off, the electromagnetic mode TM_{21} is excited with elliptical polarization ("mode 2 elliptical" configuration), *ii*) when switches D1 are turned off and switches D2 are turned on, the electromagnetic mode TM_{21} is excited with linear polarization ("mode 2" configuration), and *iii*) when switches D1 are turned on and switches D2 are turned off, the electromagnetic mode TM_{31} is excited with linear polarization ("mode 3" configuration).

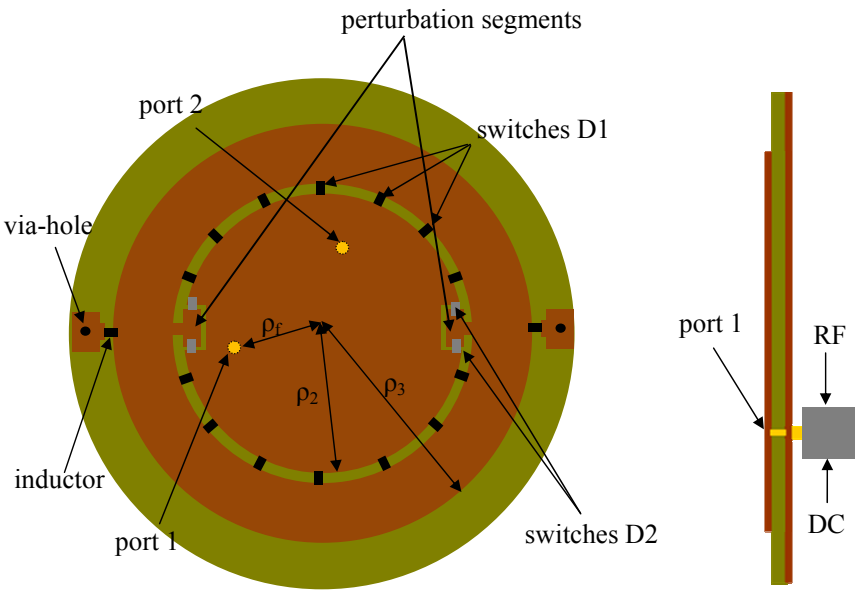

Figure 5.7: Schematic of the reconfigurable circular patch antenna for pattern and polarization diversity.

The antenna is fed through two coaxial ports separated by 135° such that the radiation patterns excited simultaneously at the two ports are orthogonal to each other, while maintaining high isolation between the ports.

Two pads, symmetrically located around the circular patch, are used to provide a ground for the biasing current of the PIN diodes. 1000 nH inductors are used to isolate the radio frequency signal from the DC ground. PIN diode switches (Infineon BAR50-02V) with an isolation of 18 dB and an insertion loss of 0.3 dB at a frequency of 2.5 GHz have been selected for this prototype.

The DC bias is directly provided from one of the two feed points through a wideband coaxial bias-tee. A summary of all the main structural parameters of the antenna is pro-

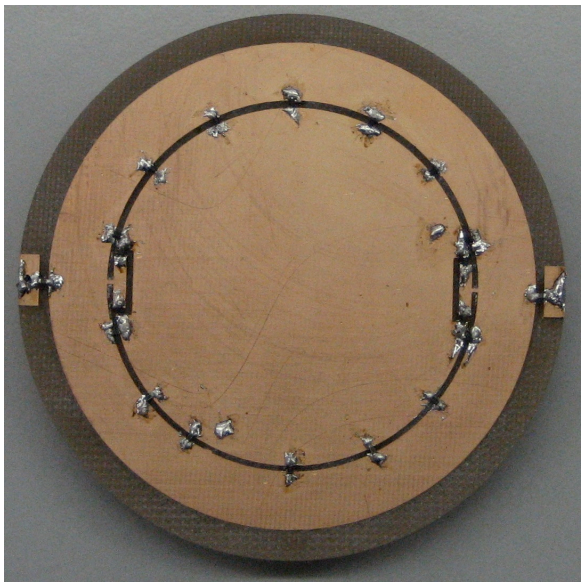

Figure 5.8: Reconfigurable circular patch for pattern and polarization diversity (RCPA-PPD).

Table 5.5: RCPA-PPD structural parameters

Dielectric	FR4 ($\epsilon_r = 4.4$)
Dielectric thickness	$1.524\,mm$
Feeds separation	130°
ρ_2	$2.78\,cm$
ρ_3	$3.65\,cm$
ρ_f	$2.53\,cm$

vided in Table 5.5.

Fig.5.9 shows the measured radiation patterns for all the antenna configurations in the azimuth plane. When "mode 2 elliptical" is selected, the radiation patterns at the two ports are orthogonal in polarization (right hand elliptical polarization is excited at port 1 and left hand elliptical polarization is excited at port 2), while when "mode 2" and "mode 3" are excited the patterns are orthogonal in space. The change in polarization between

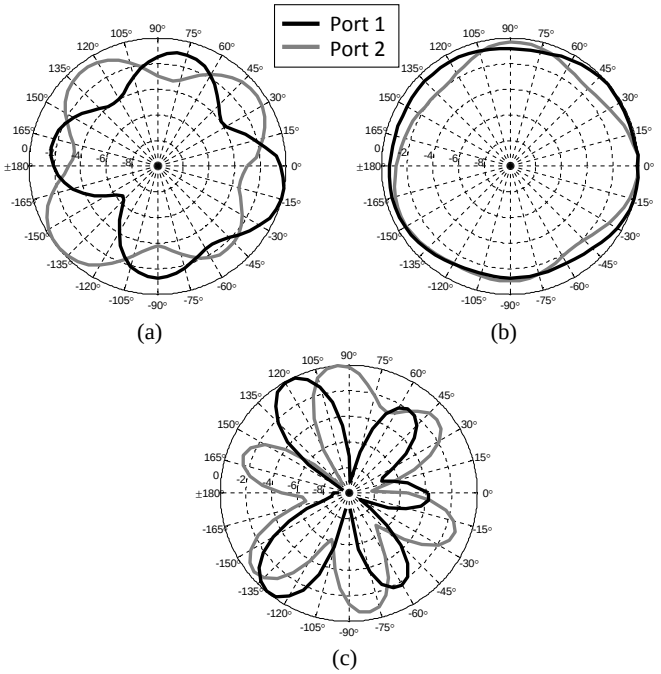

Figure 5.9: Measured radiation pattern (in dB) in the azimuthal plane at the two ports of the RCPA-PPD in all its configurations for an operation frequency of $2.48\,GHz$: (a)port 1,"mode 2", port 2 "mode 2"; (b)port 1,"mode 2 elliptical", port 2 "mode 2 elliptical"; (c)port 1,"mode 3", port 2 "mode 3"

Table 5.6: Spatial correlation between patterns generated at two different ports of the RCPA-PPD.

$mode2elliptical$	$mode2$	$mode3$
0.35	0.11	0.39

configurations "mode 2 elliptical" and "mode 2" can be observed in Fig.5.11, where the axial ratio is reported as a function of the azimuth angle for both configurations.

We estimated the level of diversity between the patterns generated at the two ports of the array, as well as between the patterns generated at the same port for different configurations of the RCPA-PPD, through the spatial correlation coefficient reported in Eq. (4.1).

Table 5.6 and Table 5.7 report the spatial correlation coefficient value between azimuthal

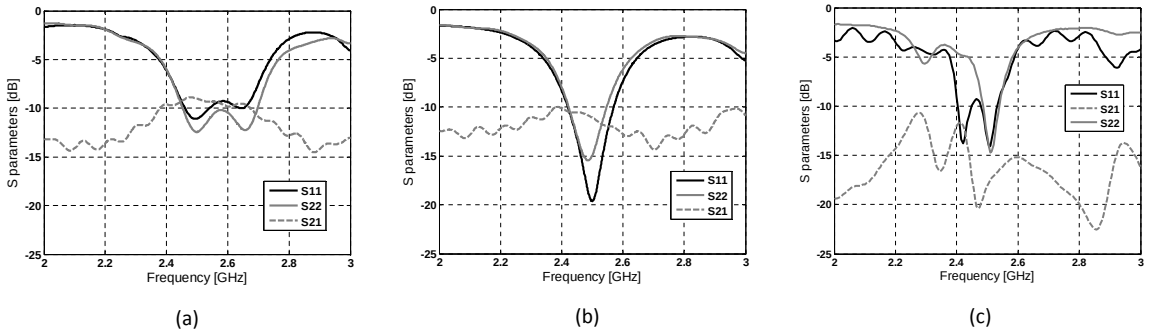

Figure 5.10: Measured scattering parameters for configuration (a)port 1,"mode 2", port 2 "mode 2"; (b)port 1,"mode 2 elliptical", port 2 "mode 2 elliptical"; (c)port 1,"mode 3", port 2 "mode 3".

Table 5.7: Spatial correlation between patterns generated at the same port of the RCPA-PPD.

	$E_{1,mode2elliptical}$	$E_{1,mode2}$	$E_{1,mode3}$
$E_{1,mode2elliptical}$	1	0.68	0.2
$E_{1,mode2}$	0.68	1	0.12
$E_{1,mode3}$	0.2	0.12	1

patterns generated at two antenna ports and between azimuthal patterns of different configurations generated at the same port respectively. It can be noted that the patterns generated at the two ports of the RCPA-PPD are orthogonal for all the configurations and that there is a good level of diversity ($r_{1,k,1,m} < 0.7$) between the three configurations.

Table 5.8 shows the measured radiation efficiency for all the antenna configurations. We observe that there are differences in radiation efficiency between the different configurations, mostly due to the different number of active PIN diodes between the antenna configurations and to the order of the excited electromagnetic mode [103]. "Mode 2 elliptical" is the most efficient configuration because all the switches are turned off and a lower order mode is excited, while "mode 3" is the least efficient configuration because the greatest number of PIN diodes are activated and the higher order of the excited mode. However overall the

Table 5.8: Measured radiation efficiency of the RCPA-PPD.

	$Port1$	$Port2$
$mode2elliptical$	31%	31%
$mode2$	22%	27%
$mode3$	7%	8%

radiation efficiency is low due to the high losses introduced by the substrate (FR4 with tanδ = 0.02).

The antenna has been designed to operate at a frequency of 2.484 GHz, in the 802.11n band. Fig.7.8 shows the measured scattering parameters of the proposed RCPA-PPD. All the configurations are matched for a target return loss of 10 dB and the isolation between the two ports is higher than 9 dB. The -10 dB bandwidth of the RCPA-PPD is 1%, denoting the narrow-band characteristic of the proposed design.

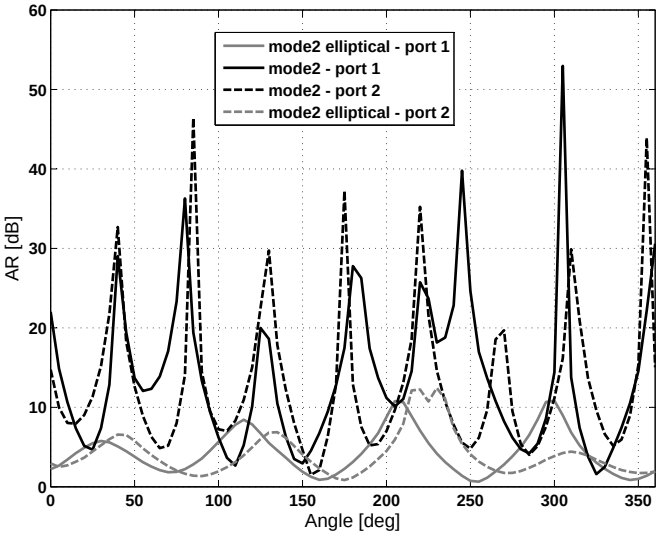

Figure 5.11: Measured axial ratio in the azimuth plane for configurations "mode 2" and "mode 2 elliptical" at the two ports of the RCPA.

5.3 Experimental setup and channel model

The RCPAs presented in the previous Section have been used as a building block of a MIMO system employing spatial multiplexing as a transmission technique. Assuming that the channel is unknown at the transmitter, the achievable channel capacity per single frequency tone is defined as [66]:

$$C = \log_2 \left[\det \left(\mathbf{I}_{N_r} + \frac{SNR}{N_t} \mathbf{H}\mathbf{H}^{\dagger} \right) \right] \tag{5.5}$$

To remove the effect of path loss, each measured channel matrix, $\mathbf{G} \in C^{N_r \times N_t}$, is normalized such that:

$$\mathbf{H} = \mathbf{G} \sqrt{\frac{N_t N_r}{\|\mathbf{G}\|_F^2}} \tag{5.6}$$

where $\|\mathbf{G}\|_F$ is the Frobenius norm of the measured channel matrix.

Employing different antenna configurations at the receiver and at the transmitter results in different amount of received power and therefore different signal-to-noise ratios. In order to keep the difference in signal-to-noise-ratio between the different antenna configurations we calculate the channel capacity for a given value of noise at the receiver, v, as in [104]. We define therefore the average SNR as:

$$SNR = \frac{P_t \sum_{i=1}^{N_r} \sum_{j=1}^{N_t} |g_{i,j}|^2}{N_r v} \tag{5.7}$$

where $g_{i,j}$ are the entries of the measured channel matrix $\mathbf{G}$ and P_t is the transmitted power at each antenna element. Note that by using this method for calculating the achievable channel capacity, it is possible to independently study the effects of system diversity and received signal power [104].

In broadband MIMO systems that employ Orthogonal Frequency Division Multiplexing (OFDM) modulation similar to the IEEE 802.11n standard, the channel matrix is determined for each subcarrier and the overall achievable channel capacity is averaged over all the subcarriers:

$$C_{OFDM} = \frac{1}{m}\sum_{i}^{m} \log_2 \left[\det \left(\mathbf{I}_{N_r} + \frac{SNR_i}{N_t} \mathbf{H}_i \mathbf{H}_i^{\dagger} \right) \right] \tag{5.8}$$

where $\mathbf{H}_i$ and SNR_i are the normalized channel and the measured SNR at the receiver for the i-th subcarrier respectively.

The channel capacity achievable using the RCPAs in a 2×2 MIMO communication system was determined through field measurements in an indoor environment. The measurement campaign took place on the 3^{rd} floor of the Bossone building at Drexel University. Both the transmitter and the receiver were located at a height of 1.5 meters. The transmitter was kept fixed in the middle of the hallway while the receiver was moved to different locations, as shown in Figure 5.12.

The same MIMO OFDM testbed used to measured the performance of the RPDA was used to extract the channel matrix for each antenna configuration at the transmitter and at the receiver. Further details on the MIMO OFDM testbed can be found in Appendix A.

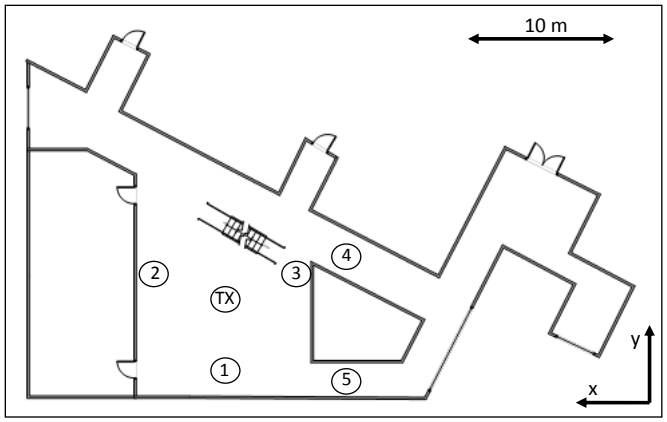

Figure 5.12: Indoor environment measurement setup.

The measurements were performed at $2.484\,GHz$ transmitting 22 dBm at each antenna port ($P_t = 22\ dBm$). We used binary phase shift keying (BPSK) to generate the analog baseband signal. The analog signal obtained was modulated using OFDM with the data being sent on each of the 52 sub-carriers. The spacing between each sub carrier was $312.5\,kHz$. A training pattern using BPSK was transmitted independently over the two transmitters. This training pattern was then received and used to estimate the channel matrix [97].

The antennas at the receiver were placed on a positioner and were moved to 40 different positions at displacements of $\lambda/10$ (where λ is the wavelength at the frequency of operation) along the y-axis for receivers 1,2, and 3 and along the x-axis for receiver 4 and 5 to capture small scale fading effects. At each position, 100 noisy channel estimates were captured and averaged, so as to get the channel response between each receiver-transmitter pair. When the RCPA-PD was used, a total of 4 link configurations were measured (2 array configurations at the transmitter and 2 at the receiver) while for the RCPA-PPD, 9 channel

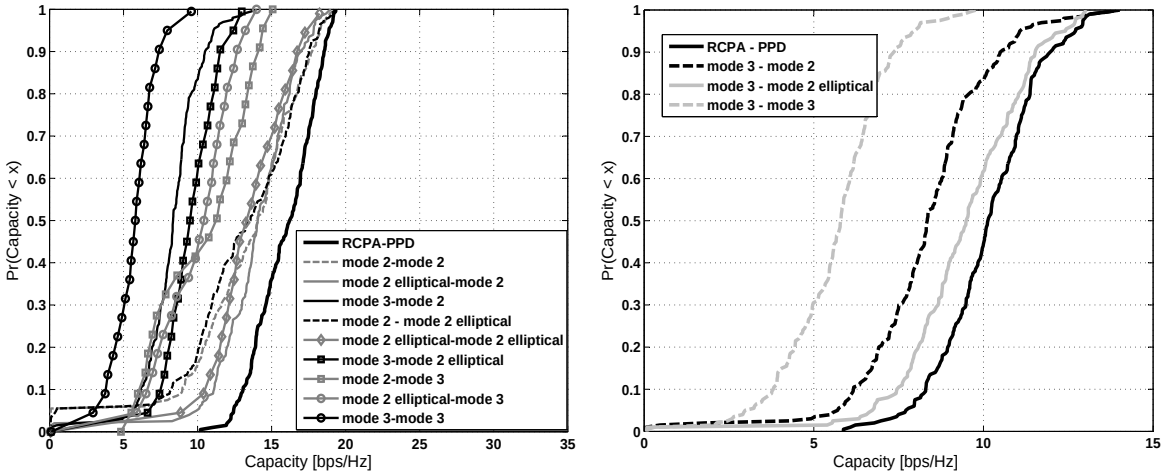

Figure 5.13: Measured capacity CDF of the RCPA-PPD used in a 2×2 MIMO OFDM system. Reported are the CDF curves of the RCPA-PPD and of all the possible antenna configurations in a link (TX-RX) for a noise level $v = 1nW$. (a) RCPA-PPD used at both transmitter and receiver, (b) RCPA-PPD used only at the receiver.

matrices were measured per location (3 array configurations at the transmitter and 3 at the receiver).

5.4 RCPAs performance

In this Section we investigate the results achievable with the RCPAs in a 2×2 MIMO communication link. In particular we look at the performance achievable with the RCPA-PD and RCPA-PPD when they were employed at one or both ends of the communication link. We investigate the benefits offered by each antenna configuration in LOS and NLOS wireless channels scenarios and we look at the differences existing in achievable performance when using this type of reconfigurable antennas in narrowband or broadband MIMO systems. If not specified, when the RCPAs are employed only at the receiver, configuration “mode 3”

was used at the transmitter.

5.4.1 RCPAs at one and both ends of the communication link

Fig.5.13(a) shows the capacity cumulative distribution function (CDF) measured when employing the RCPA-PPD at the receiver and at the transmitter of a MIMO OFDM system. The results achievable with the RCPA-PPD are reported together with the CDF of all the 9 possible antenna configurations in a link. It can be noted that the channel capacity improvement achievable with the RCPA-PPD with respect to the most radiation efficient configuration ("mode 2 elliptical - mode 2 elliptical") is 18% with a probability of 50%. The improvement becomes much higher if we consider results relative to the less efficient antenna configurations. The improvement with respect to the least efficient system configuration ("mode 3 - mode 3") is 166% with a probability of 50%. As expected the antenna configurations that exhibit high radiation efficiency overall perform better than those with poor radiation efficiency; however as shown in subsection 5.4.2 there are also conditions where the RCPA configuration with the lowest efficiency outperforms the others.

Fig.5.14(a) shows the capacity CDF for the RCPA-PD used at both ends of the communication link. We observe that with this antenna that excites only high order modes, the achievable capacity improvement with respect to the most efficient system configuration ("mode 3 - mode 3") is 7% with a probability of 50%. The improvement achievable with the RCPA-PD is lower than the one offered by the RCPA-PPD mainly because this antenna has only two configurations and one of them ("mode 4") is much less efficient than the other one. The higher the excited mode, the lower the radiation efficiency, and the lower

Table 5.9: Percentage capacity improvement achievable for a probability of 50% when using the RCPA-PD and the RCPA-PPD with respect to a system that employes circular patch antennas operating in "mode 3". Noise level $v = 100\ nW$.

	RCPA-PD at one end	RCPA-PD at both ends	RCPA-PPD at one end	RCPA-PPD at both ends
η non normalized	4%	7%	9%	18%
$\eta = 100\%$	11%	21%	20%	28%

the chance of selecting that antenna configuration [53]. Note however that the capacity improvement achievable relative to "mode 3 - mode 3" grows for low values of capacity and probability. The gain is 20% with a probability of 5% and the less radiation efficient configurations are used mainly when the stronger configuration "mode 3 - mode 3" receives a poor signal. Table 5.9 summarizes the percentage capacity improvement achievable with the RCPA-PD and the RCPA-PPD.

We investigated also the simpler scenario that consists of using the RCPAs only at one end of the 2×2 MIMO OFDM communication link. Fig.5.13(b) and Fig.5.14(b) show the capacity CDF for the RCPA-PPD and the RCPA-PD respectively. In this case, the percentage capacity improvement is 9% and 4% with a probability of 50% for the RCPA-PPD and the RCPA-PD respectively relative to the most radiation efficient system configuration. As expected the achievable gain decreases when using the reconfigurable antennas only at the receiver/transmitter since the number of link configurations decreases.

To show the performance achievable with these types of antennas independently from the relative differences in radiation efficiency between the array configurations, in Fig.5.15 we report the capacity CDF obtained with the RCPA-PPD (Fig.5.15(a)) and the RCPA-PD

Table 5.10: Average channel capacity with efficiency normalization for the RCPA-PPD and the RCPA-PD used at the receiver. Noise level $v = 100\ nW$

RCPA-PPD		
TX/RX antenna	Capacity [bps/Hz]	% Decrement
mode 2/RCPA-PPD	10.4	13%
mode 2 elliptical/RCPA-PPD	10.2	15%
mode 3/RCPA-PPD	9.88	20%
RCPA-PD		
TX/RX antenna	Capacity [bps/Hz]	% Decrement
mode 3/RCPA-PD	9.77	11%
mode 4/RCPA-PD	9.70	12%

(Fig.5.15(b)) assuming that all the antenna configurations have equal radiation efficiency. We set the radiation efficiency to be 100% for all the antenna configurations by scaling each coefficient of the measured channel matrix, $\mathbf{G}$, as:

$$\frac{|g_{i,j}|^2}{\eta_i \eta_j} \tag{5.9}$$

where η_i and η_j are the radiation efficiency of the antenna configuration used at the i-th receiver and j-th transmitter respectively. Using this approach, we quantify the gains that derive only from the level of pattern diversity existing between the antenna configurations. We observe that the improvement derived only from diversity is high: when using the reconfigurable antennas at both ends of a transmission link the capacity gain is 28% and 21% with a probability of 50% with respect to the most capacity achieving system configuration for the RCPA-PPD and the RCPA-PD respectively. The difference in capacity improvement between the two systems is mostly due to the number of link configurations (9 for the RCPA-PPD and 4 for the RCPA-PD), the higher the number of uncorrelated configurations, the

higher the diversity gain [42]. From Fig.5.15 we can also directly compare the difference existing in achievable capacity between a system that adopts the proposed RCPAs only at the receiver and a system that employs the reconfigurable arrays at both ends of the communication link. The capacity improvement that derives from using the RCPAs at one end of the communication link is 20% and 11% with a probability of 50% for the RCPA-PPD and the RCPA-PD respectively. These capacity improvements are measured with respect to a system that adopts the RCPAs only at the receiver and that employs "mode 3" configuration at the transmitter. The capacity improvement is higher for the RCPA-PPD than for the RCPA-PD mainly because of the different number of array configurations and because the other configurations of the RCPA-PPD ("mode 2" and "mode 2 elliptical") are more capacity achieving than "mode 3" when used at the transmitter in the selected testing environment. Table 5.10 shows the capacities achievable for different antenna modes used at the transmitter and illustrates that the capacity improvement achievable using the RCPAs at both ends of the communications is dependent on the antenna configuration used at the transmitter when employing the reconfigurable antenna only at the receiver. We note that the capacity improvement drops to 15% and 13% when using configurations "mode 2 elliptical" and "mode 2" at the transmitter respectively. We can then conclude that the capacity improvement achievable using the proposed RCPA designs at both ends of the communication link rather than at one end lies in between 10% and 20%. Table 5.9 summarizes the percentage capacity improvement achievable with the RCPA-PD and the RCPA-PPD when a radiation efficiency of 100% is assumed.

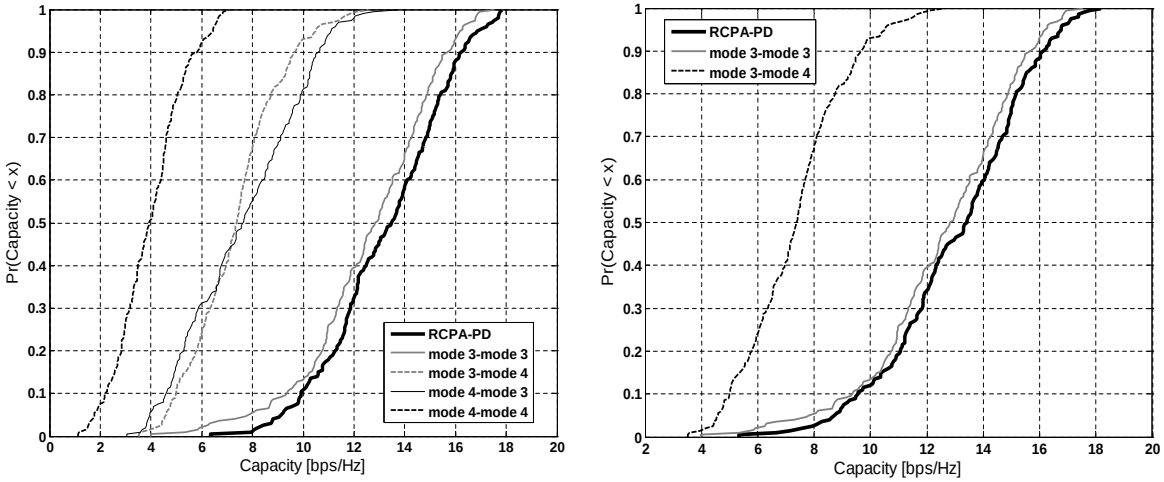

Figure 5.14: Measured capacity CDF of the RCPA-PD used in a 2×2 MIMO system. Reported are the CDF curves of the RCPA-PD and of all the possible antenna configurations in a link (TX-RX) for a noise level $v = 1nW$. (a) RCPA-PD used at both transmitter and receiver, (b) RCPA-PD used only at the receiver.

5.4.2 RCPA configuration performance

To investigate the benefits offered by each configuration of the RCPAs, in terms of system diversity and amount of signal power received, we plot the average achievable channel capacities as a function of the actual received SNR by each configuration of the RCPA-PPD and RCPA-PD. We conduct this analysis employing the RCPAs only at the receiver of a 2×2 MIMO OFDM system and using the "mode 3" configuration at the transmitter. Fig.5.16(a) shows the measured capacities achievable with the RCPA-PPD in a LOS scenario (receiver position 1,2, and 3 of Fig.5.12). We observe that the configuration "mode 2" on average achieves the best performance. In particular we note that for a given noise power level, v, the average received SNR varies greatly among the different configurations and that all the capacities curve lie on the same line. Therefore in a LOS scenario the difference in per-

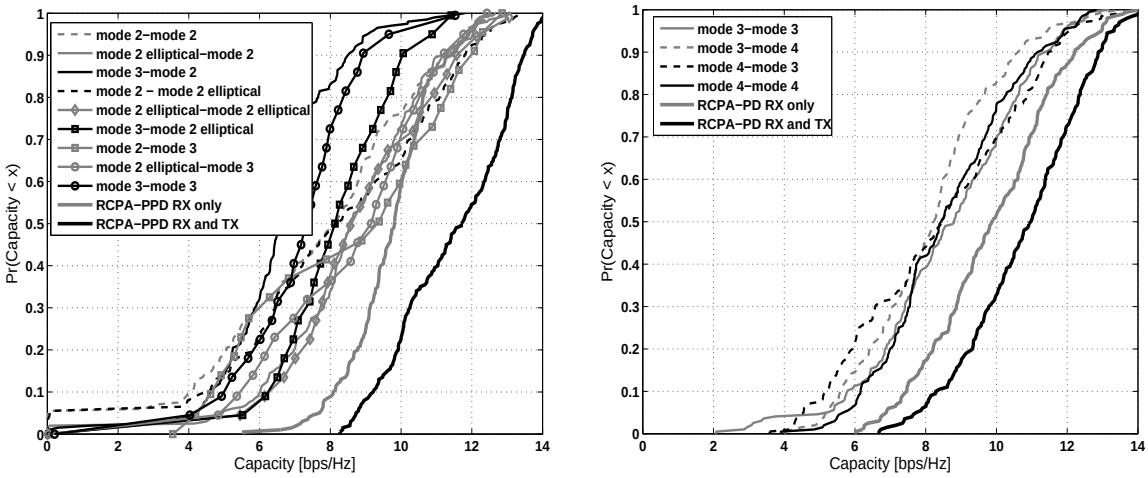

Figure 5.15: Measured capacity CDF of (a) the RCPA-PPD and (b) the RCPA-PD used in a 2×2 MIMO system, assuming radiation efficiency equal to 100% for all the antenna configurations. Reported are the CDF curves of the RCPAs and of all the possible antenna configurations in a link (TX-RX) for a noise level $v = 100nW$.

formance between the antenna configurations is due to differences in received signal power and not in diversity. Since configuration "mode 3" has the lowest radiation efficiency, it offers the worst performance in LOS scenarios. The difference in performance between the configurations "mode 2" and "mode 2 elliptical" is also dependent on the type of antenna used at the transmitter. Fig.5.17(a) shows the same capacity curves as Fig.5.16(a), when the transmitter employs the configuration "mode 2 elliptical". In this case, we note that the configuration "mode 2 elliptical" outperforms "mode 2" due to the better polarization alignment between the transmitter and the receiver.

Fig.5.16(b) reports the measured capacities achievable with the RCPA-PPD in a NLOS scenario (receiver position 4 and 5 of Fig.5.12). We see that in a NLOS scenario overall the configuration "mode 2 elliptical" behaves better than the other configurations because

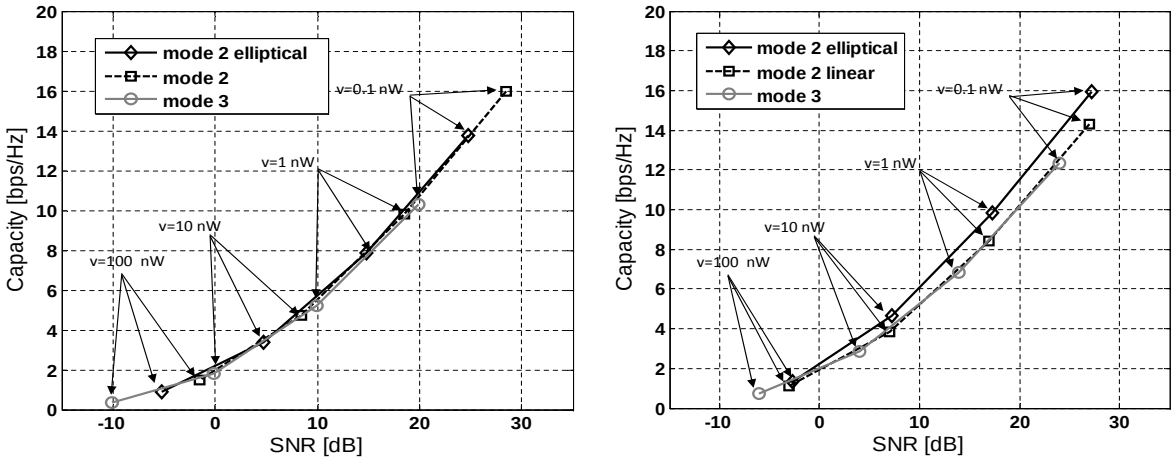

Figure 5.16: Measured capacities of a 2×2 MIMO system employing the RCPA-PPD only at the receiver as a function of the received SNR. Each group of data points corresponds to a specific level of noise power. (a) LOS scenario and (b) NLOS scenario.

it provides the highest diversity. For the same value of SNR at the receiver, mode 2 elliptical is the highest capacity achieving configuration. "Mode 3" is on average the worst configuration both in LOS and NLOS scenario due to its very poor radiation efficiency. Note however that in some locations, due to its high degree of pattern diversity, "mode 3" outperforms all the other configurations. This can be clearly observed in Fig.5.17(b) which shows the capacity curves for each RCPA-PPD configuration for a particular NLOS location.

The same capacity curves are reported in Fig.5.18(a) for the RCPA-PD operating in LOS and NLOS scenarios. Similar to the results of the RCPA-PPD, we note that the highest capacity achieving configuration is "mode 3" because of its higher radiation efficiency with respect to "mode 4". Note however that for the RCPA-PD, there are some locations where the least efficient "mode 4" outperforms the most radiation efficient "mode 3" (see

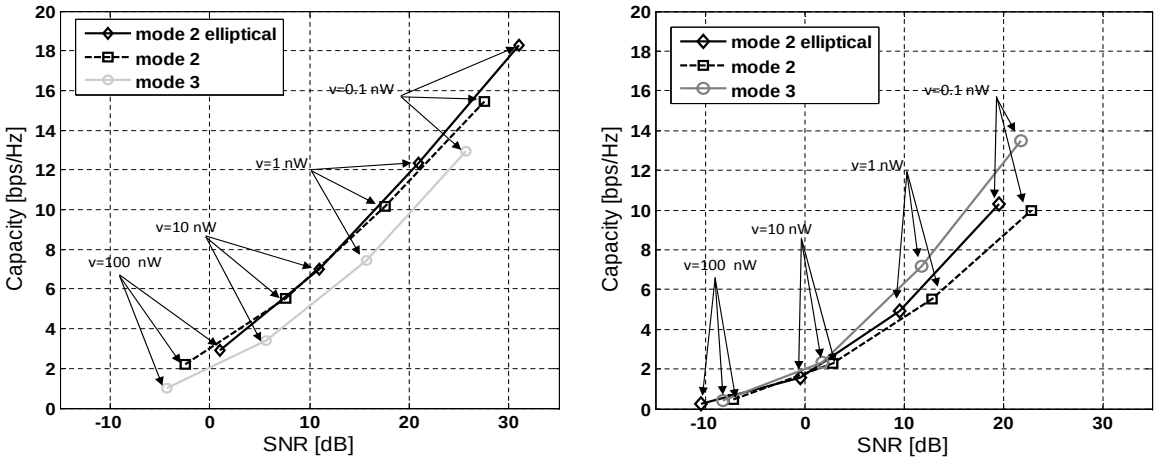

Figure 5.17: Measured capacities of a 2×2 MIMO system employing the RCPA-PPD only at the receiver as a function of the received SNR. Each group of data points corresponds to a specific level of noise power. (a) LOS scenario employing "mode 2 elliptical" at the transmitter (b) one NLOS location employing "mode 3" at the transmitter.

Fig.5.18(b)). In particular, this happens when the configuration "mode 3" does not receive a strong signal, in agreement with the conclusions drawn in Section 5.4.1.

These results demonstrate the strength of each configuration in the RCPAs. It is very effective to have a configuration that exploits polarization diversity because of its consistent behavior in both LOS and NLOS scenarios. Configurations that excite lower order modes to achieve pattern diversity overall perform better than configurations with higher order modes because they allow the receiver to collect more signal power due to their high radiation efficiency. However it is possible to increase the diversity of the RCPA system by increasing the efficiency of those configurations that excite higher order modes. Note that this efficiency increase can be achieved by designing the RCPAs on a substrate with low losses [103].

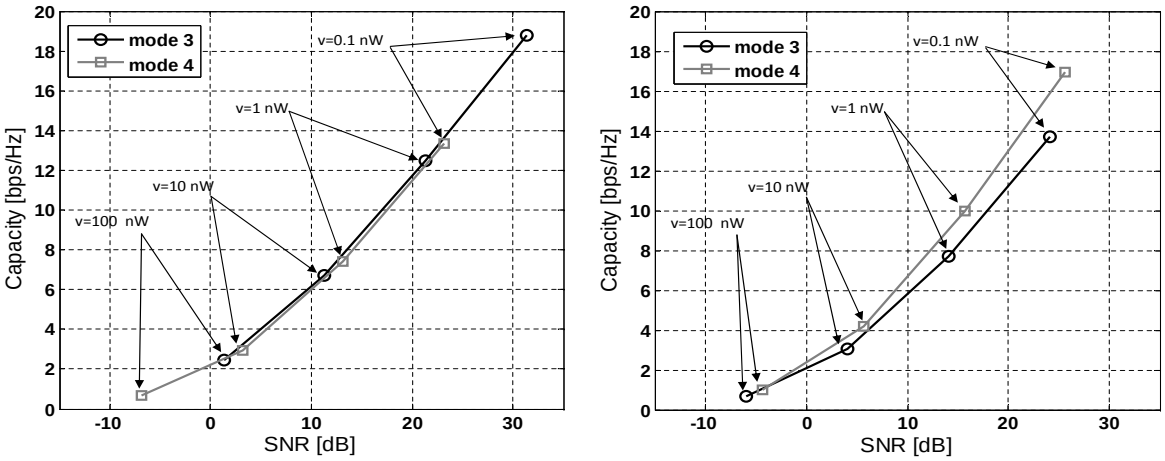

Figure 5.18: Measured capacities of a 2×2 MIMO system employing the RCPA-PD only at the receiver as a function of the received SNR. Each group of data points corresponds to a specific level of noise power. (a) average over 120 locations (b) single location.

5.4.3 Narrowband vs broadband capacity

The results presented so far illustrate RCPA performance in broadband MIMO OFDM systems. In this section we consider also the case of using the antenna in a narrowband MIMO system. To simplify our analysis we study only the case of the RCPA-PPD employed at the receiver.

Fig.5.19 reports the measured capacity curves for all the RCPA-PPD configurations as a function of the OFDM subcarriers for two different receiver locations. We observe that in some cases (Fig.5.19(a)) the highest capacity achieving configuration varies with the selected subcarrier, while in other cases (Fig.5.19(b)) there is one configuration that outperforms the others over all the subcarriers, independently from the receiver location. In general, however, it is clear that the achievable capacity improvement offered by a reconfigurable

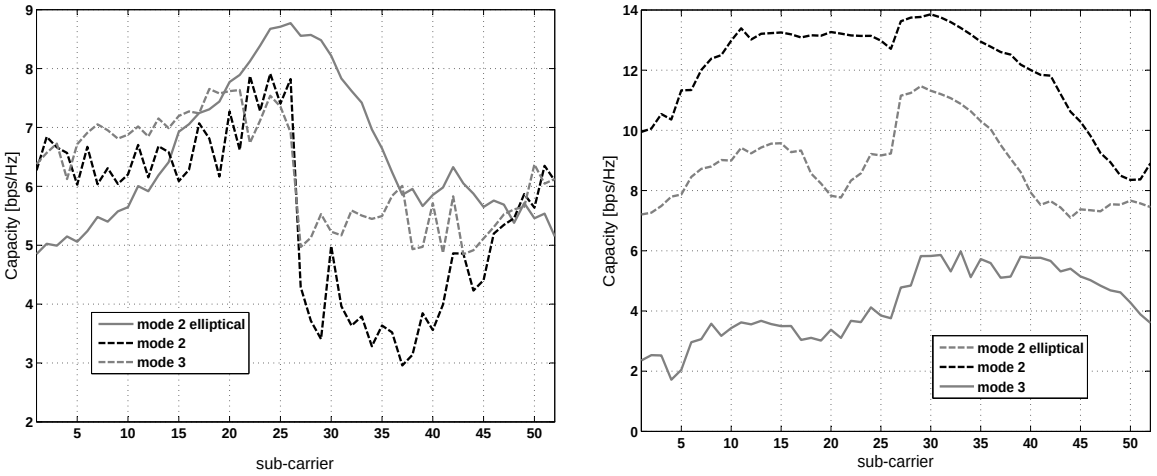

(a) (b)

Figure 5.19: Measured capacities of a 2×2 MIMO system employing the RCPA-PPD only at the receiver as a function of the subcarriers for two different locations (a) and (b). Noise power level $v = 1nW$.

multi element antenna used in a narrowband MIMO system is frequency dependent.

Fig.5.20 reports the capacity CDF of the RCPA-PPD used only at the receiver in a narrowband (only one subcarrier) MIMO system. We observe that the percentage capacity improvement offered by the RCPA-PPD is 20% higher with a probability of 50% with respect to the most efficient link configuration ("mode3 - mode 2 elliptical"). The same antenna operating in an OFDM system (Fig.5.13(b)) exhibits instead a percentage capacity improvement of only 9%. Note however that even if there is a difference in the overall performance the highest capacity achieving configuration is still "mode 2 elliptical" and the lowest is "mode 3".

To show that the capacity improvement is on average higher when employing the RCPAs in a narrowband channel with respect to a broadband channel we calculated the percentage

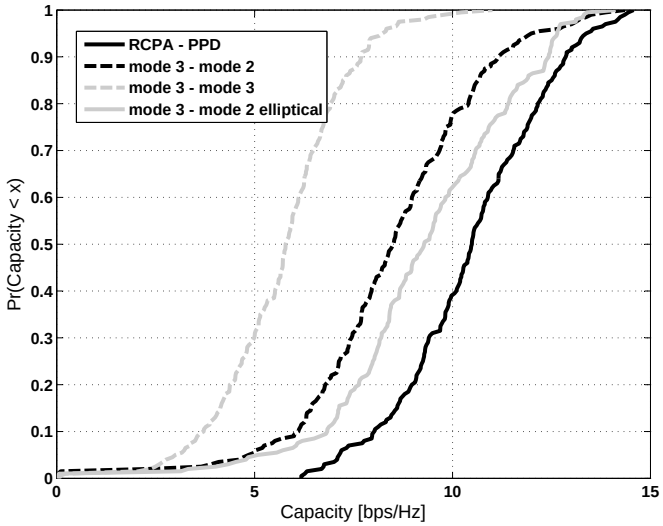

Figure 5.20: Measured capacity CDF of the RCPA-PPD used at the receiver of a 2×2 MIMO narrowband system. Reported are the CDF curves of the RCPA-PPD and of all the possible antenna configurations in a link (TX-RX) for a noise level $v = 1nW$.

capacity improvement achievable with the RCPA-PPD per subcarrier for a probability of 50% and averaged the improvement over all 52 subcarriers. Figure 5.21 shows this percentage capacity improvement calculated for all the subcarriers and compares it with the percentage capacity improvement achievable in a broadband channel. The proposed RCPA-PPD achieves an average percentage capacity improvement of 17.5% when employed only at the receiver in a narrowband channel relative to the 9% improvement achievable in a broadband channel.

5.5 Summary

The circular patch antenna is a good candidate for developing compact multi element reconfigurable antennas. The RCPA-PPD and the RCPA-PD showed that it is possible to

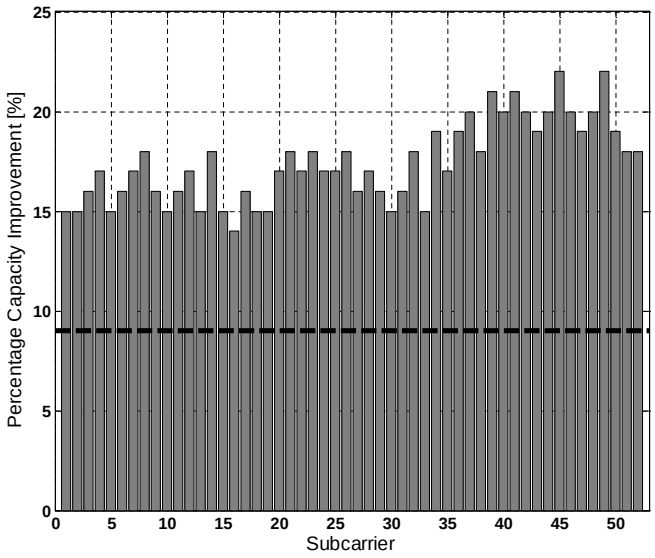

Figure 5.21: Measured average percentage capacity improvement per subcarrier for a noise level $v = 1nW$. The dashed line represents the average percentage capacity improvement for a broadband channel.

achieve both pattern and polarization reconfigurability with a compact structure. Results showed a significant channel capacity improvement when using RCPAs relative to non reconfigurable circular patches. In particular, it is very effective to have a configuration that exploits polarization diversity because of its consistent behavior in both LOS and NLOS scenarios. On the other hand the RCPA-PD allows for generation of more pure radiation patterns than the RCPA-PPD because the feed points location can be selected without corrupting the antenna polarization. In addition, configurations that excite lower order modes to exploit pattern diversity are preferable over configurations that work with higher order modes because of their higher radiation efficiency.

In order to effectively use the RCPAs in a MIMO communication a control algorithm is required to select the antenna configuration without the need of switching between all the

antenna configurations prior selecting the optimal one. This topic is addressed in the next Chapter by means of an analysis of RCPAs-PD performance in clustered channel model.

Chapter 6: Configuration selection scheme for pattern RCPAs

To optimally use reconfigurable antennas in MIMO systems it is necessary to know the channel response between the transmitter and the receiver for each antenna configuration. However, estimating the channel response for each antenna configuration at the transmitter and at the receiver has been demonstrated to be power consuming and to have a detrimental effect on the performance of the reconfigurable MIMO system [42]. The negative effect of channel estimation on the performance of the communication system increases proportionally with the number of antenna configurations, reaching the point where the losses, caused by imperfect channel estimation, may be higher than the capacity gain offered by reconfigurable antennas [42].

In order to overcome this channel estimation problem, in this chapter we propose a method that allows multi element reconfigurable antennas to select the antenna configuration at the receiver without any extra power consumption or modifications to the data frame of a conventional, non reconfigurable MIMO system. This configuration selection scheme does not aim to maximize the throughput for each particular channel realization, but it selects the antenna configuration that, on average, increases the spectral efficiency of the communication link. While the only existing technique for antenna configuration selection in reconfigurable MIMO antenna systems [42] uses instantaneous channel information to switch antenna configuration, the selection algorithm proposed in this chapter is based on

second order wireless channel statistics.

The adaptive algorithm we present in this paper is shown to be effective for pattern reconfigurable antennas, though its use can also be extended to other classes of antennas. We present this configuration selection scheme analyzing the performance achievable with pattern reconfigurable circular patch antennas, like the RCPA-PD presented in Chapter 5. An analysis of the performance of these antennas, in terms of ergodic channel capacity and Bit Error Rate (BER), is conducted using the clustered channel model described in Section 3.2. Through this approach we show that the array configuration selection is directly linked to *i*) the spatial characteristics of the wireless channel (angle spread of the power angular spectrum), *ii*) the levels of pattern diversity existing between the elements of the reconfigurable array, *iii*) the differences in radiation efficiency and input impedance between the various antenna configurations, and *iv*) the average system SNR.

6.1 MIMO system with reconfigurable antennas

We consider a MIMO system employing reconfigurable arrays that are capable of P different configurations. Assuming a flat fading channel, the signal collected at the receiver is related to the signal outgoing from the transmitter through the relation:

$$\mathbf{y}_{p,q} = \mathbf{H}_{p,q}\mathbf{x}_{p,q} + \mathbf{n}_{p,q} \tag{6.1}$$

where $\mathbf{y}_{p,q} \in C^{N_r \times 1}$ is the signal vector at the receiver array, $\mathbf{x}_{p,q} \in C^{N_t \times 1}$ is the signal vector at the transmit antenna array, $\mathbf{n}_{p,q} \in C^{N_r \times 1}$ is the complex additive white Gaussian

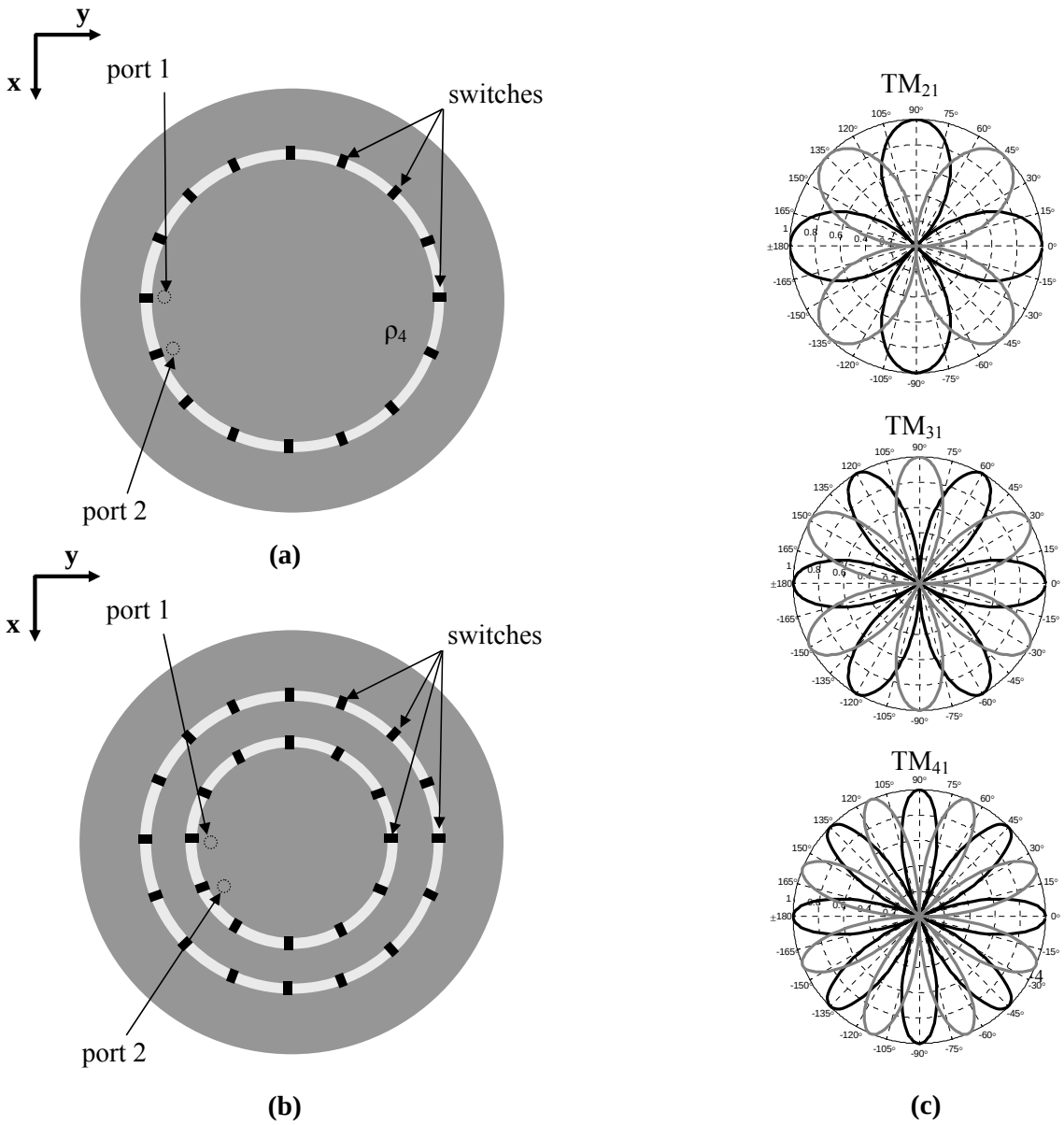

Figure 6.1: (a) Schematic of the Reconfigurable Circular Patch Antenna RCPA with two antenna configurations (e.g. TM_{31}, TM_{41}) and (b) RCPA with three antenna configurations (e.g. TM_{21}, TM_{31} and TM_{41}). (c) Radiation patterns excited in the azimuthal plane at the two ports of the RCPA for different electromagnetic modes.

noise (AWGN) vector with variance σ_n^2 and $\mathbf{H}_{p,q} \in C^{N_r \times N_t}$ is the channel transfer matrix.

The subscripts p-th and q-th refer to the array configuration employed at the transmitter

and receiver multi element antenna respectively.

According to the Kronecker model [84], the transfer channel matrix $\mathbf{H}_{p,q}$, is defined as:

$$\mathbf{H}_{p,q} = \mathbf{R}_{r_q}^{1/2} \mathbf{H}_w \mathbf{R}_{t_p}^{1/2} \tag{6.2}$$

where $\mathbf{R}_{t_p}$ and $\mathbf{R}_{r_q}$ denote respectively the receive and transmit spatial correlation matrices for the p-th configuration of the receiving array and for the q-th configuration of the transmitting array respectively. $\mathbf{H}_w \in C^{N_r \times t}$ is a matrix of complex Gaussian fading coefficients.

To perform estimation of the channel response, $\mathbf{H}_{p,q}$, we consider a pilot assisted estimation that uses minimum mean square error (MMSE) receivers (e.g. [105]). A training sequence composed of L symbols is transmitted with a period of T symbols, and used by the receiver to estimate the channel response. We assume, as is common [106] [107] [108], that the pilot signals assigned to the different transmit antennas are mutually orthogonal. This assumption implies that the total transmitted data per pilot sequence is equal to $T - LN_t$ symbols.

We also consider that the transmitted power is uniformly distributed across the N_t transmit antenna elements. According to [109] we can then express the amplitude of the data symbol as:

$$A = \sqrt{\frac{T}{((T - LN_t) + \zeta^2 L)} \frac{P_{av}}{N_t}} \tag{6.3}$$

where P_{av} is the average transmit power from all transmit antennas and ζ is a parameter that relates the amplitude of the data symbols to the amplitude of the training symbols A_p, so that $A_p = \zeta A$. The percentage of power allocated to the training symbols, μ is then given by [109]:

$$\mu = \frac{L\zeta^2}{(T - LN_t) + L\zeta^2} 100[\%] \tag{6.4}$$

For such communication systems, assuming perfect knowledge of the spatial correlation information at the transmitter and at the receiver, we can then define a lower bound of the achievable ergodic channel capacity [110] as:

$$C \geq \frac{T - LN_t}{T} \times E_{\hat{\mathbf{H}}_{p,q}}[\log_2 \det(\mathbf{I} + \frac{P_{av}}{N_t} \hat{\mathbf{H}}_{p,q} \hat{\mathbf{H}}_{p,q}^{\dagger} (\boldsymbol{\Upsilon} + \sigma_n^2 \mathbf{I})^{-1})] \tag{6.5}$$

where $\hat{\mathbf{H}}_{p,q}$ is the estimated transfer channel matrix and $\boldsymbol{\Upsilon}$ is the covariance matrix of the random vector $\mathbf{H_e x_p}$, with $\mathbf{H_e}$ being the MMSE estimation error on $\mathbf{H}_w$ (i.e. $\mathbf{H_e} = \hat{\mathbf{H}}_w - \mathbf{H}_w$); $\mathbf{I}$ is a $N_r \times N_r$ identity matrix and $(\dagger)$ denotes a complex conjugate transpose operation. Note that the term $\frac{T-LN_t}{T}$ is introduced because L temporal signatures per each transmit antenna are allocated to the pilot. The covariance matrix, $\boldsymbol{\Upsilon}$, is defined as

$$\boldsymbol{\Upsilon} = \sigma_{H_e}^2 P_{av} \mathbf{R}_{r_q} \tag{6.6}$$

where $\sigma_{H_e}^2$ is the variance of the MMSE estimation error on $\mathbf{H}_w$. For this communication

system $\sigma^2_{H_e}$ is defined as [105]:

$$\sigma^2_{H_e} = \left(\frac{1}{1 + \frac{\rho_p L_p}{N_t}} \right) \tag{6.7}$$

where $\rho_p = \frac{\zeta A}{\sigma^2_n}$ and L_p is the length of the subtraining sequence of L, allocated to estimate the channel transfer matrix for a particular antenna configuration at the transmitter and at the receiver [42] ($L_p \in (0, L]$). Note that as ζ approaches ∞ the ergodic channel capacity is that of a system that assumes perfect channel state information at the receiver (p-CSI).

6.2 Reconfigurable circular patch antennas

In this section a general overview of the main characteristics of pattern reconfigurable antennas is provided. These antennas will be used as part of a reconfigurable MIMO system to present a novel antenna configuration selection scheme.

Pattern RCPAs like the one presented in Section 5.2.1 are antennas that can dynamically change the shape of their radiation patterns by varying the size of the circular patch. Each antenna has two feed points and acts as a two element array. As depicted in Fig.6.1 the two feed points on the antenna structure are separated such that the radiation patterns excited at the two ports are orthogonal to each other. By simultaneously turning on and off the switches located radially on the antenna, it is possible to vary the current distribution on the antenna structure and excite different TM electromagnetic modes, each corresponding to a particular shape of radiation pattern.

As reported in Section 5.1, the electric field components excited in the far field by each

port of the antenna for the n-th TM electromagnetic mode are defined, as a function of the circular patch antenna radius, ρ, as:

$$E_{\theta,1}^{(n)}(\phi,\theta) = e^{\frac{jn\pi}{2}} \frac{e^{-jk_0 d}}{d} \frac{V_0}{2} k_0\rho[J_{n+1}(k_0\rho\sin\theta) - J_{n-1}(k_0\rho\sin\theta)]\cos[n(\phi-\phi_0)]$$

$$E_{\phi,1}^{(n)}(\phi,\theta) = -e^{\frac{jn\pi}{2}} \frac{e^{-jk_0 d}}{d} \frac{V_0}{2} k_0\rho[J_{n+1}(k_0\rho\sin\theta) + J_{n-1}(k_0\rho\sin\theta)]\cos\theta\sin[n(\phi-\phi_0)]$$

$$E_{\theta,2}^{(n)}(\phi,\theta) = e^{\frac{jn\pi}{2}} \frac{e^{-jk_0 d}}{d} \frac{V_0}{2} k_0\rho[J_{n+1}(k_0\rho\sin\theta) - J_{n-1}(k_0\rho\sin\theta)]\sin[n(\phi-\phi_0)]$$

$$E_{\phi_2}^{(n)}(\phi,\theta) = -e^{\frac{jn\pi}{2}} \frac{e^{-jk_0 d}}{d} \frac{V_0}{2} k_0\rho[J_{n+1}(k_0\rho\sin\theta) + J_{n-1}(k_0\rho\sin\theta)]\cos\theta\cos[n(\phi-\phi_0)]$$

where $E_{\theta,<1,2>}$ and $E_{\phi,<1,2>}$ are the θ and ϕ components of the electric fields excited at port 1 and port 2 of the RCPA.

To propose a novel antenna configuration selection scheme we will consider RCPAs capable of exciting three different electromagnetic modes (i.e. configurations) at both ports: TM_{21}, TM_{31} and TM_{41}. The radiation patterns that are excited in the azimuthal plane with such RCPAs are shown in Fig.6.1(c). We note that the patterns excited at the two ports of the RCPA, for the same antenna configuration, are orthogonal to each other and that variations between radiation patterns of different RCPA modes occur in the number of lobes and in their beamwidth. To quantify the level of diversity existing between radiation

Table 6.1: Spatial correlation between patterns generated at two different ports of the RCPA for the same configuration - $\hat{r}_{1,k,2,k}$

$\hat{r}_{1,TM_{21},2,TM_{21}}$	$\hat{r}_{1,TM_{31},2,TM_{31}}$	$\hat{r}_{1,TM_{41},2,TM_{41}}$
0.63	0.63	0.63

Table 6.2: Spatial correlation between patterns generated at the same port of the RCPA - $\hat{r}_{1,k,1,m}$

	$\mathbf{E}_{1,TM_{21}}$	$\mathbf{E}_{1,TM_{31}}$	$\mathbf{E}_{1,TM_{41}}$
$\mathbf{E}_{1,TM_{21}}$	1	0.80	0.85
$\mathbf{E}_{1,TM_{31}}$	0.80	1	0.81
$\mathbf{E}_{1,TM_{41}}$	0.85	0.81	1

patterns excited at the ports of the RCPA, we use the spatial correlation coefficient defined in Eq. (4.1).

Table 6.1 shows the level of diversity existing between radiation patterns excited at the two ports of the array for each antenna configuration ($\hat{r}_{1,k,2,k}$), while Table 6.2 reports the level of diversity existing between the different antenna configurations ($\hat{r}_{1,k,1,m}$). We observe that the correlation values between radiation patterns excited at the two ports of the array are small enough for all the configurations (≤ 0.7) to provide significant diversity gain [89]. Table 6.2 shows that the correlation between different configurations is about 0.8 for all the states. Although this value is large, as discussed in Section 6.5, the differences between the array configurations are high enough to provide an improvement in terms of spectral efficiency and BER with respect to non reconfigurable circular patch antennas.

Differences between the various antenna configurations (and electromagnetic modes) exist not only in the shape of the excited radiation patterns, but also in the level of radiation

efficiency, η, defined as:

$$\eta = \frac{Q_T}{Q_R} \tag{6.8}$$

where Q_T is the antenna total quality factor and Q_R is the radiation quality factor; Q_T takes into account dielectric, conduction and radiation losses while Q_R is a figure of merit for only the radiation losses. They are defined, for a circular patch antenna, as [103]:

$$Q_T = \left(\frac{1}{h\sqrt{\pi\mu f\sigma}} + \tan\delta + \frac{h\mu f (k_0\rho)^2 I_1}{240[\chi_n'^2 - n^2]} \right)^{-1} \tag{6.9}$$

$$Q_R = \left(\frac{240[\chi_n'^2 - n^2]}{h\mu_s f (k_0\rho)^2 I_1} \right) \tag{6.10}$$

where f is the frequency of operation, μ_s is the substrate dielectric permeability, h is the substrate thickness and σ is the conductivity of the material used to build the circular patch. $\tan\delta$ is a figure of merit that takes into account the substrate losses and I_1 is defined as:

$$\begin{aligned} I_1 = \int_0^{\pi} \Big[\big(J_{n+1}(k_0\rho\sin\theta) - J_{n-1}(k_0\rho\sin\theta) \big)^2 + \\ + (\cos\theta)^2 \big(J_{n+1}(k_0\rho\sin\theta) + J_{n-1}(k_0\rho\sin\theta) \big)^2 \Big] \sin\theta d\theta \end{aligned} \tag{6.11}$$

In Fig.6.2 the radiation efficiency is reported as a function of the dielectric permittivity for different configurations of a RCPA matched at 5.2 GHz and built on a substrate of

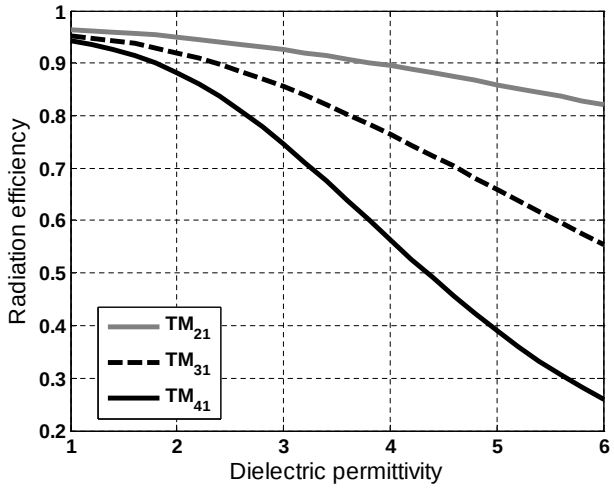

Figure 6.2: RCPA radiation efficiency for different antenna configurations as a function of the substrate dielectric permittivity. $h = 1.59$ mm, $\sigma = 5.8 \times 10^7$ S/m, $f = 5.2$ GHz and $tan\delta = 0.0009$.

thickness $h = 0.159$ mm and tan$\delta = 0.0009$. It can be observed that the level of radiation efficiency is different for each antenna configuration, as is true for most of the electrically reconfigurable antennas proposed in the literature. For the RCPAs we can note that the lower electromagnetic modes are more efficient than the higher modes. Also we observe that when the dielectric permittivity value increases, the radiation efficiency decreases.

In the following analysis we will consider two different types of RCPAs that differ in antenna substrate and level of radiation efficiency. A summary of the main characteristics of these two antennas is reported in Table 6.3.

6.3 RCPAs performance in clustered channel model

In this Section we show how the ergodic channel capacity is related to the wireless channel power angular spectrum, antenna radiation efficiency, level of pattern diversity, input

Table 6.3: RCPAs characteristics

	RCPA-1	RCPA-2
substrate	Rogers RT-duroid 5880	Rogers R03003
ε_r	2.2	3
$\eta_{TM_{21}}$	0.94	0.88
$\eta_{TM_{31}}$	0.91	0.81
$\eta_{TM_{41}}$	0.87	0.66
$\rho_{TM_{21}}$	0.33λ	0.28λ
$\rho_{TM_{31}}$	0.45λ	0.39λ
$\rho_{TM_{41}}$	0.57λ	0.49λ
S_{11}	0	0

impedance of each antenna configuration and average system SNR.

6.3.1 Clustered channel model and RCPA spatial correlation

According to [8] and the definition of spatial correlation introduced in Eq. (3.11), the theoretical spatial correlation coefficients of a two port RCPA is defined as:

$$\begin{aligned} r_{l,m,l,m}(\phi_c,\sigma_\phi) =& \frac{(1-|S_{11_{l,m}}|)\eta_{l,m}}{(1-e^{-\sqrt{2}\pi/\sigma_\phi})}\frac{(n\sigma_\phi)^2}{1+2(n\sigma_\phi)^2}\times\Big[1-e^{-\sqrt{2}\pi/\sigma_\phi}+\frac{\cos^2(n\phi_c)}{(n\sigma_\phi)^2}\times \\ & \times\left(1-e^{-\sqrt{2}\pi/\sigma_\phi}\cos(n\pi)\right)\Big] \end{aligned} \tag{6.12}$$

$$\begin{aligned} r_{j,k,j,k}(\phi_c,\sigma_\phi) =& \frac{(1-|S_{11_{j,k}}|)\eta_{j,k}}{(1-e^{-\sqrt{2}\pi/\sigma_\phi})}\frac{(n\sigma_\phi)^2}{1+2(n\sigma_\phi)^2}\times\Big[1-e^{-\sqrt{2}\pi/\sigma_\phi}+\frac{\sin^2(n\phi_c)}{(n\sigma_\phi)^2}\times \\ & \times\left(1-e^{-\sqrt{2}\pi/\sigma_\phi}\cos(n\pi)\right)\Big] \end{aligned} \tag{6.13}$$

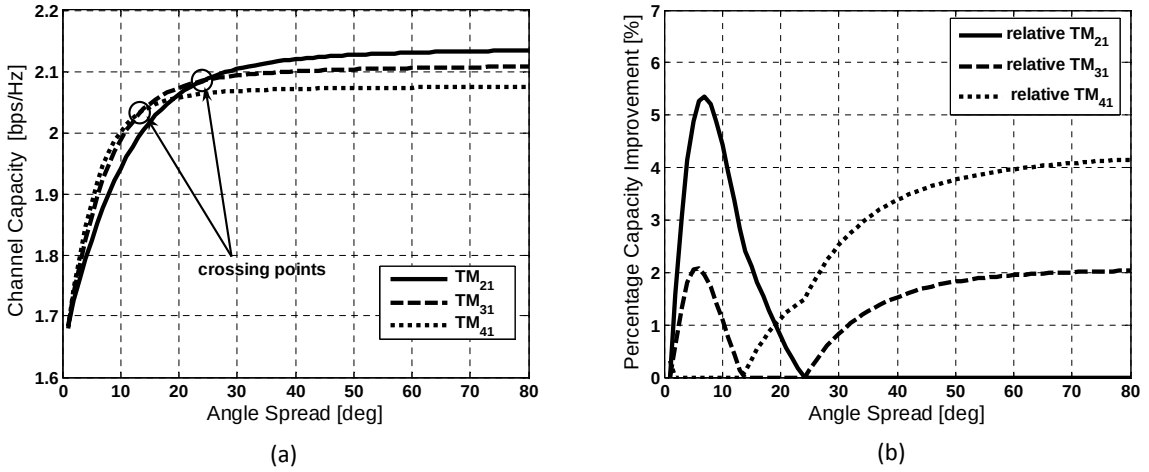

Figure 6.3: (a) Channel capacity curves for three different antenna configurations (TM_{21}, TM_{31} and TM_{41}) as a function of the angle spread (AS) for a 2×2 MIMO system employing the RCPA-1 at the receiver. (b) Percentage capacity improvement, as a function of the angle spread (AS), achievable when using the RCPA-1 in the same 2×2 MIMO system relative to a non reconfigurable antenna system employing circular patch antennas operating in mode TM_{21}, TM_{31} and TM_{41}. SNR = 5 dB.

$$r_{j,k,l,m}(\phi_c, \sigma_\phi) = \frac{\sqrt{(1 - |S_{11_{l,m}}|)\eta_{l,m}(1 - |S_{11_{j,k}}|)\eta_{j,k}}}{2} \times \frac{(\sin n\phi_c)}{1 + 2(n\sigma_\phi)^2} \tag{6.14}$$

where we have assumed $\int_{4\pi} P(\Omega)|\mathbf{E}_{ref}(\Omega)|^2 d\Omega = 1$. We observe that the input impedance, efficiency and AS of the power angular spectrum describing the wireless channel, act as scaling factors of the spatial correlation coefficient.

Knowing the spatial correlation coefficient for each antenna configuration allows us to compute the transfer channel matrix $\mathbf{H}_{p,q}$ as in Eq. (6.2). We will consider only single sided correlated MIMO channels. In particular, we use RCPAs only at the receiver while at the transmitter we assume $\mathbf{R}_t = \mathbf{I}$. We make this assumption because we present an antenna

configuration selection technique for the receiver, independently from the transmitter. The fact that $\mathbf{R}_t = \mathbf{I}$ does not affect the following analysis, which would not change for $\mathbf{R}_t \neq \mathbf{I}$.

The ergodic channel capacity achievable for each RCPA configuration can then be calculated according to Eq. (6.5) for the case of perfect channel state information at the receiver ($\zeta \longrightarrow \infty$), as discussed in Section 6.1. The following analysis is performed in the single cluster channel model [67], and the spatial correlation information is determined as in (3.11), using configuration TM_{21} as a reference antenna.

6.3.2 Effect of RCPA spatial correlation on configuration selection

In Fig.6.3(a) the average channel capacity achievable for some configurations of a reconfigurable circular patch antenna is reported as a function of the AS of the PAS, for a SNR = 5 dB. The ergodic channel capacity values are averaged over all azimuthal angles ($\phi_c \in [0, 2\pi)$) of the incoming PAS. Note that these results of channel capacity have been determined for a RCPA built on a Rogers RT-duroid 5880 substrate and for a condition of perfect matching for all the antenna configurations (RCPA-1). Refer to Table 6.3 for a summary of the antenna related parameters.

We observe that the achievable average channel capacity varies as a function of the PAS angle spread. In particular each antenna configuration outperforms the others for a certain range of angle spread. In Fig.6.4 we show the same ergodic channel capacity of Fig.6.3(a) for a RCPA built on Rogers R03003 substrate (RCPA-2). The parameters for RCPA-2 are also described in Table 6.3. As shown in this table, RCPA-2 is characterized by different values

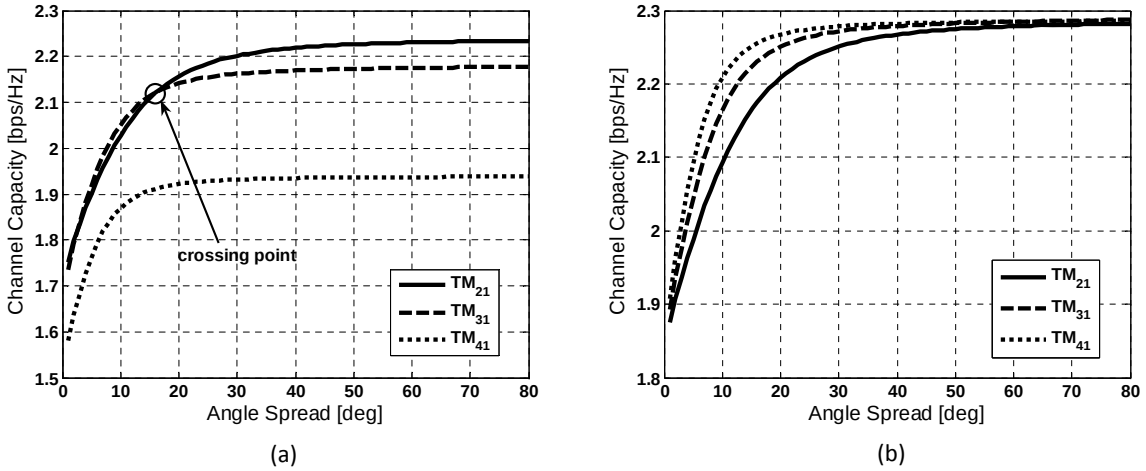

Figure 6.4: Channel capacity curves for three different antenna configurations (TM_{21}, TM_{31} and TM_{41}) as a function of the angle spread (AS) for a 2×2 MIMO system employing (a) the RCPA-2 at the receiver, (b) an ideal RCPA with unitary radiation efficiency for all the antenna configurations. SNR = 5 dB.

of radiation efficiency with respect to RCPA-1. A comparison of Fig.6.3(a) with Fig.6.4 shows that the crossing points of the channel capacity traces vary as a function of the radiation efficiency of the configuration. This effect can be better explained by looking at the average channel capacity curves relative to an ideal RCPA having unit efficiency for all its configurations (Fig.6.4 (b)). We note that, in this case, configuration TM_{41} outperforms the other configurations for low AS while for large AS all the configurations perform the same. This happens because, at low AS, higher order modes are characterized by larger pattern diversity with respect to lower modes, while at high AS, the level of pattern diversity is similar for all the antenna modes, as demonstrated in [8]. On the other hand, the radiation efficiency, that is larger for lower order modes than for higher modes, determines configuration TM_{21} to have the best performance at high AS, as depicted in Fig.6.3(a) and Fig.6.4.

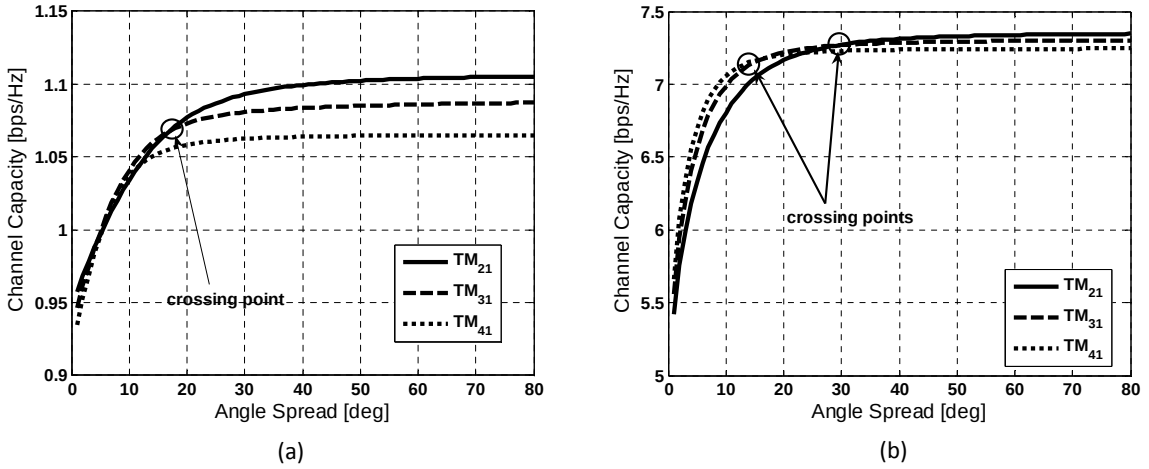

Figure 6.5: Channel capacity curves for three different antenna configurations (TM_{21}, TM_{31} and TM_{41}) as a function of the angle spread (AS) for a 2×2 MIMO system employing the RCPA-1 at the receiver. (a) SNR = 0 dB, (b) SNR = 20 dB.

A similar conclusion could be drawn if we considered a variation in input impedance among the different antenna configurations. In fact, according to Eq. (6.12), (6.13) and (6.14), the antenna matching condition (represented by S_{11}) scales the spatial correlation coefficients in the same way as the efficiency.

These results demonstrate the possibility of selecting the antenna configuration at the receiver based on PAS angle spread knowledge, once the average system SNR is known. In Fig.6.3(b) we show the percentage capacity improvement achievable when using RCPAs relative to a non reconfigurable antenna system (i.e. fixed radius circular patch antennas operating in mode TM_{21}, TM_{31} and TM_{41}). It can be noted that, for the system of Fig.6.3(b), using angle spread information to switch between configurations leads to an average improvement of up to 5% with respect to a system that does not employ reconfigurable antennas.

6.3.3 Effect of average system SNR on configuration selection

As shown in Eq. (6.5) the ergodic channel capacity of a MIMO system does not depend only on the spatial correlation, but also on the system average SNR. In Fig.6.5 the average channel capacity achievable for the different configurations of RCPA-1 is shown as a function of the AS of the PAS, for a SNR = 20 dB (Fig.6.5(a)) and SNR = 0 dB (Fig.6.5(b)). We note that the achievable channel capacity is, as expected, higher for the system with SNR = 20 dB than that of the same system with average SNR = 5 dB (Fig.6.8(a)) and SNR = 0 dB. We also observe that the angle spread crossing points of the capacity curves, for different antenna configurations, shift with varying average system SNR. Using the same reconfigurable antenna, at SNR = 20 dB, the AS crossing points values are higher with respect to a system with SNR = 0 dB.

In Fig.6.6 the AS crossing points for configurations $TM_{41} - TM_{31}$ and $TM_{31} - TM_{21}$ are reported as a function of the system average SNR, for a MIMO system that employs RCPA-1 at the receiver. We observe that as the value of average system SNR increases, the AS crossing point values increase as well. This effect can be explained if we consider that the channel capacity of MIMO systems can be increased in two ways: i) increasing the system diversity and ii) increasing the amount of signal power received. The system diversity is reflected in the antenna correlation coefficient, while the signal power received is influenced by the antenna efficiency and input impedance. Intuitively, at high SNR, since the received amount of power can not be greatly modified by varying the antenna efficiency and input impedance, the level of antenna diversity is the dominant contribution to the

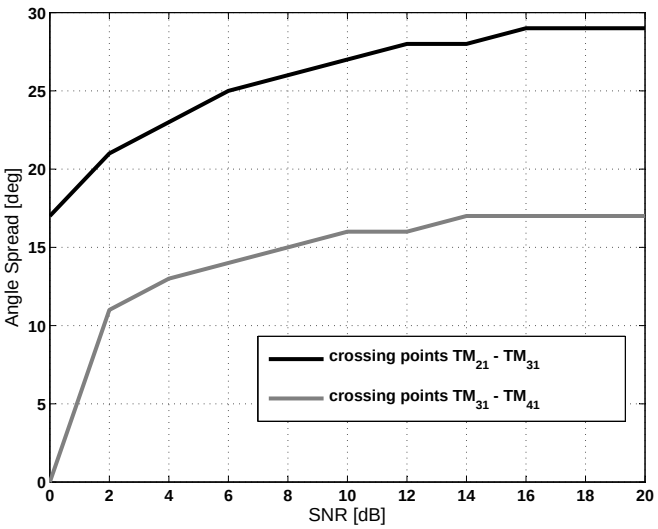

Figure 6.6: Angle spread crossing points versus SNR for configurations $TM_{21} - TM_{31}$ and $TM_{31} - TM_{41}$.

achievable channel capacity. At low SNR, instead, small variation in antenna efficiency and input impedance can greatly effect the amount of received signal power, and therefore antenna efficiency and input impedance are dominant contributions on the channel capacity trend. As shown in Fig.6.5(a) we note that at low SNR the most efficient antenna (TM_{21}) has larger advantage with respect to the other configurations. On the other hand at high SNR (Fig.6.5(b)) the configuration with the lowest spatial correlation (TM_{41}) outperforms the others for more values of angle spread with respect to the same system at lower SNR.

These results demonstrate therefore the possibility of selecting the antenna configuration at the receiver based on knowledge of PAS angle spread and average system SNR.

6.4 Selection algorithm

A parameter of discrimination between the different wireless channel scenarios is the reciprocal condition number of the transmit/receive correlation matrices, defined as [111] [112]:

$$D_\lambda = \frac{\lambda_{max}}{\lambda_{min}} \tag{6.15}$$

where λ_{max} and λ_{min} are the maximum and minimum eigenvalues of the transmit and receive correlation matrices.

In Fig.6.7 reciprocal condition number is plotted as a function of the angle spread of the PAS for a RCPA (RCPA-1) operating in mode TM_{21}. For each value of AS, there is a corresponding value of reciprocal condition number; in particular for low values of AS the reciprocal condition number is high and vice-versa. We can therefore map, given the average system SNR, the values of AS that define a switching point between two configurations (as shown in Fig.6.3(a)) to reciprocal condition number. In Table 6.4, a mapping of reciprocal condition number to corresponding values of AS regions is presented. Note that, given the results of Fig.6.3(a), only three regions of D_λ need to be specified; each region corresponds to a particular antenna configuration at the receiver. This mapping procedure is necessary since the PAS angle spread is difficult to estimate, while the transmit/receive spatial correlation matrices can be estimated using standard techniques [113] [114]. Note that the mapping procedure varies with the average system SNR, as explained in Section 6.3.3. Therefore an antenna table, like the one of Table 6.4, need to be generated for each

average SNR value.

According to this channel parametrization, it is therefore possible to use second order wireless channel statistics together with the average SNR, in order to determine receiver array configuration. Note that this approach allows the system to select the antenna configuration using the spatial correlation matrix of only one reference antenna configuration without the need of estimating the channel response over each antenna configuration. This greatly simplifies channel estimation in reconfigurable MIMO systems (discussed further in Section 6.5). In the example of Table 6.4 the antenna configuration TM_{21} has been selected as arbitrary reference antenna.

An algorithm that allows for the selection of the antenna configuration at the receiver, without estimating the channel transfer matrix for each antenna configuration, can then be summarized as follows:

OFF LINE OPERATIONS

1. Antenna tables, like the one of Table 6.4, that maps the optimal antenna configuration at the receiver to the range of reciprocal number are built, one for each average SNR value, using the clustered channel model approach described in Section 6.3.

ON LINE OPERATIONS

2. The average system SNR is determined and used to select the corresponding antenna table generated in step 1.

3. The receiver spatial correlation is determined for a reference receiver antenna configuration which is used to determine the channel reciprocal condition number, D_λ.

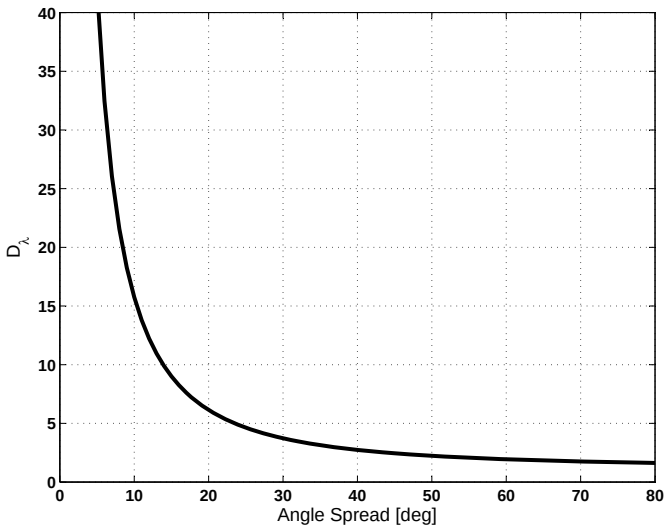

Figure 6.7: Reciprocal condition number, D_λ, as a function of the angle spread for the antenna configuration TM_{21} used at the receiver in a 2×2 MIMO system.

4. The information of the reciprocal condition number, D_λ, is used together with the antenna table generated in step 1 to select the antenna configuration at the receiver.

We observe that the proposed selection algorithm requires the channel second order statistics to be constant over the configuration selection procedure [115]. Estimation of the spatial correlation matrix could then be conducted using standard techniques [113] [114]. Once the channel correlation is estimated and the antenna configuration is selected, the L symbols of the pilot sequence can be used to estimate the channel for signal detection as discussed in Section 6.1.

Table 6.4: Relationship of angle spread to reciprocal condition number for SNR = $5dB$

AS	D_λ	CONFIGURATION
$[0^o, 13^o)$	$(11, \infty)$	TM_{41}
$[13^o, 23^o)$	$(5, 11]$	TM_{31}
$[23^o, 360^o)$	$(0, 5]$	TM_{21}

6.5 Effect of pilot assisted estimation on the channel capacity and BER

The performance achievable with the proposed configuration selection scheme is evaluated for a MIMO system like the one described in Section 6.1, including the effect of imperfect channel estimation (np-CSI) (ζ finite), in terms of ergodic channel capacity and BER. We also compare the performance of such a selection scheme to that achievable with a system that detects the optimal antenna configuration by exhaustively estimating the channel transfer matrix for every possible antenna configuration [42]. According to the system in [42], the results presented in this section are based on the frame structure of the IS-136 standard. IS-136 is based on Time Division Multiple Access (TDMA) technology where each frame length is 40 ms. Each IS-136 frame consists of $T = 162$ symbols, of which $L = 32$ symbols are used for training purposes.

In case of a configuration selection scheme like the one described in [42], in order to evaluate the optimal antenna configuration, the L symbols allocated for channel estimation are subdivided into P subtraining sequences of length $L_p = \frac{L}{P}$, where P is the number of array configurations at the receiver. Each subtraining sequence is used to estimate the transfer channel matrix for a particular antenna configuration. According to this approach the achievable ergodic capacity can then be computed as described in Eq. (6.5).

Table 6.5: MIMO system configuration

	2×2 MIMO	2×6 MIMO
RCPA type	RCPA-1	RCPA-1
array configurations states (P)	3	10
$\mu_{proposed\ algorithm}$	6%	11%
$\zeta_{proposed\ algorithm}$	0.44	0.58
$\mu_{standard\ algorithm}$	10%	20%
$\zeta_{standard\ algorithm}$	0.61	0.88

Note that contrary to this selection approach, the selection algorithm proposed in this work always has $L_p = L$ independently of the number of receiver antenna configurations. In this way, a better estimation of the channel matrix can be obtained, resulting in better signal detection, and therefore, higher achievable channel capacity and lower BER. The technique in [42] always selects the optimal antenna configuration based on the channel scenario that maximizes the receive signal-to-noise ratio, while the proposed selection scheme selects the antenna configuration that on average increases the spectral efficiency of the communication link.

6.5.1 Ergodic channel capacity

In Fig.6.8(a) the channel capacity achievable with a RCPA (RCPA-1) employed at the receiver of a 2×2 MIMO link is reported as a function of the AS, for a system that employs the proposed selection scheme including the effects of imperfect channel estimation (proposed algorithm np-CSI) or assuming perfect channel estimation (proposed algorithm p-CSI) ($\zeta \rightarrow \infty$). The Figure also shows results for a system that selects the antenna configuration after exhaustively estimating the channel for each configuration including the

effects of imperfect channel estimation (standard np-CSI) or assuming perfect channel estimation (standard p-CSI). These results are obtained for $P_{av} = 1$, a SNR = 5 dB, and an allocated power to the training sequence, μ, optimal for each selection scheme. A summary of the system configuration is shown in Table 6.5. Note that the adopted RCPA is capable of switching between modes TM_{21}, TM_{31} and TM_{41} and thus in this case $P = 3$. It can be observed that the imperfect channel estimation causes a decrease in overall system performance. Note in particular, that the loss in capacity is higher for the selection scheme that needs to estimate the channel P times (one estimation per antenna configuration) every training sequence than for the proposed approach that instead estimates the channel only for a single antenna configuration. The percentage capacity improvement achievable when using such a selection scheme with RCPAs is reported in Fig.6.8(b) relative to non reconfigurable antenna systems operating in different modes, and an RCPA system that selects the antenna configuration after exhaustively estimating the channel for all possible configurations. In terms of its ergodic capacity, on average the improvement achievable with the proposed selection algorithm is 9% with respect to the technique in [42]. Note also that using the RCPAs at the receiver together with the technique in [42] performs worse than employing non reconfigurable circular patch antennas. This happens because, using the technique in [42], the imperfection in channel estimation is so high so as to appreciably decrease the system achievable channel capacity. Note in fact that, according to the technique in [42], as the number of receiver antenna configurations increases, the imperfection in channel estimation increases and consequently the achievable channel capacity decreases.

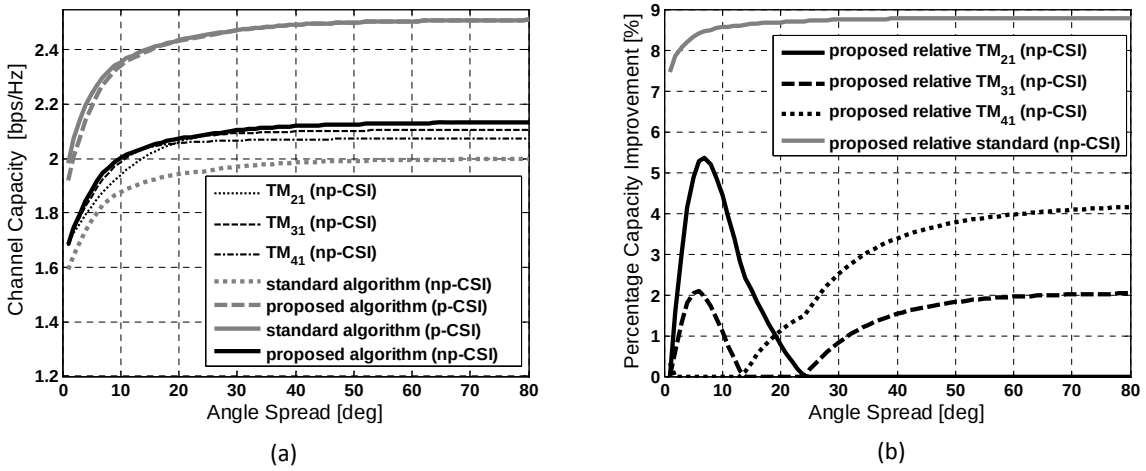

Figure 6.8: (a) Achievable channel capacity as a function of the angle spread (AS) for a 2×2 MIMO system, with RCPA-1 at the receiver, that employs:(i) the proposed selection scheme including the effects of imperfect channel estimation (proposed algorithm np-CSI), (ii) the proposed selection scheme assuming perfect channel estimation (proposed algorithm p-CSI), (iii) an algorithm that selects the antenna configuration after estimating the channel for all possible configuration including the effects of imperfect channel estimation (standard np-CSI) and, (iv) a standard algorithm assuming perfect channel estimation (standard p-CSI). The curves relative to the channel capacity achievable with non reconfigurable circular patch antennas operating in different modes assuming non-perfect channel estimation are also reported. (b) Percentage capacity improvement, as a function of the angle spread (AS), for the same 2×2 MIMO system that employs RCPA-1 at the receiver with the proposed selection algorithm relative to non reconfigurable antenna systems operating in different modes (proposed relative TM_{21}, TM_{31} and TM_{41}) and RCPA system that selects the antenna configuration after exhaustively estimating the channel for all possible configurations (proposed relative standard (np-CSI)). SNR = 5 dB.

In Fig.6.9 the channel capacity achievable with the proposed selection scheme is determined for a 2×6 MIMO system employing RCPAs only at the receiver for a SNR = 5dB. The MIMO system configuration is shown in Table 6.5. In this case three RCPAs, built on Rogers RT-duroid 5880 substrate (RCPA-1), are used at the receiver with spatial separation of multiple wavelengths, such as to be uncorrelated one with the other. A

total of ten possible array configurations can then be selected at the receiver ($P = 10$[1]), using a RCPA that is capable of switching between modes TM_{21}, TM_{31} and TM_{41}. At the transmitter we assume $\mathbf{R}_t = \mathbf{I}$. Since the number of antenna configurations is higher than the 2×2 MIMO case (where $P = 3$) the capacity improvement achievable using the proposed selection scheme is higher. The improvement is in fact almost 20%. As explained in [42], the greater the number of array configurations, the worse the channel transfer matrix detection, and therefore the worse the channel capacity. This problem is addressed by the proposed selection scheme that needs to estimate the channel for a single antenna configuration independently of the number of array configurations.

6.5.2 Bit error rate

An analysis of the proposed configuration selection algorithm performance, in terms of BER, has been conducted for a 2×2 MIMO system employing RCPA-1 antennas at the receiver. The modulation scheme considered is BPSK without any additional coding. BER values have been calculated assuming perfect decoupling at the receiver of the two Single Input Single Output (SISO) links comprising the 2×2 MIMO system.

In Fig6.10(a) BER curves are reported as a function of the SNR for an angle spread of 10^o. The reported curves are specific to: i) a system that employs the proposed selection scheme including the effects of imperfect channel estimation (proposed algorithm np-CSI),

[1]P is determined as the combinations of the number of configurations, K, per RCPA that can be repeated up to J times in the array. $P = \frac{(K+J-1)!}{J!(K-1)!}$. In case of six elements antenna array at the receiver, three RCPA are used and therefore $J = 3$. In this case, using an RCPA with three different configurations ($K = 3$), we obtained $P = 10$.

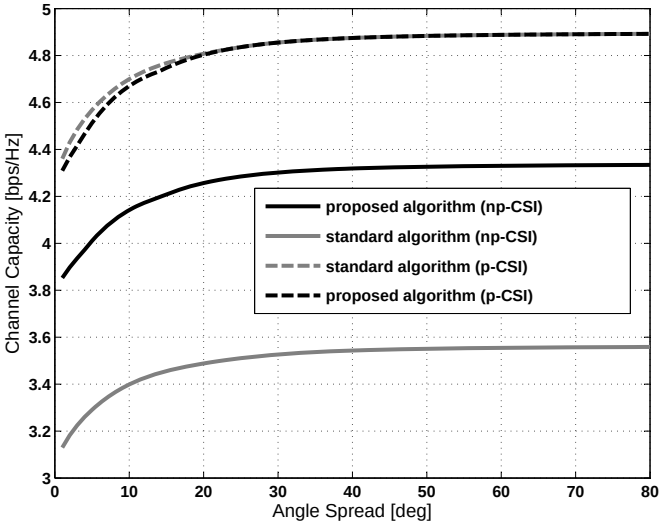

Figure 6.9: Achievable channel capacity as a function of the angle spread (AS) for a 2×6 MIMO, with RCPAs (RCPA-1) at the receiver, that employs:(i) the proposed selection scheme including the effects of imperfect channel estimation (proposed algorithm np-CSI), (ii) the proposed selection scheme assuming perfect channel estimation (proposed algorithm p-CSI),(iii) an algorithm that selects the antenna configuration after estimating the channel for all possible configuration including the effects of imperfect channel estimation (standard np-CSI) and, (iv) a standard algorithm assuming perfect channel estimation (standard p-CSI). SNR = 5 dB.

ii) a system that selects the antenna configuration after exhaustively estimating the channel for each configuration including the effects of imperfect channel estimation (standard algorithm np-CSI) and, *iii*) a system assuming perfect channel estimation (standard algorithm p-CSI). The Figure also shows results for a system equipped with non reconfigurable circular patch antennas operating in modes TM_{21}, TM_{31} and TM_{41}.

We note that the proposed algorithm achieves an appreciable gain with respect to a standard selection algorithm that selects the antenna configuration after exhaustively estimating the channel for each configuration. In particular we note that a gain of 1.8 dB is achieved for a BER of 0.1. This gain is not due to an improvement in the diversity

order of the system, but to the fact that with the proposed algorithm the channel is better estimated than with the standard algorithm. Specifically, in the proposed algorithm, the training sequence is entirely allocated to estimate the channel for a single antenna configuration, instead of being allocated to estimate the channel for all possible array configurations. This effect can be better observed by comparing the BER curve of a system with perfect channel estimation (standard algorithm p-CSI) with the BER curves of systems with imperfect channel estimation (proposed algorithm np-CSI and standard algorithm np-CSI). In Fig.6.10(a) we observe that in systems with imperfect channel estimation the BER curves are shifted to the right at higher SNR. To explain this result we note that imperfect channel estimation impacts the SNR level at the receiver [42]. In particular, for a system that selects the antenna configuration after exhaustively estimating the channel for each configuration, the quality of channel estimation diminishes as the number of array configurations, P, is increased. Thus the SNR level at the receiver is degraded [42]. Unlike a standard algorithm, the proposed configuration selection scheme, estimates the channel for a single antenna configuration and therefore the quality of channel estimation remains the same, independent of the number of array configurations. This improved channel estimation leads to a better SNR level at the receiver. Note also that the BER curve slope for the proposed algorithm is less steep than the one corresponding to the standard algorithm; therefore the diversity order of the system that uses the proposed algorithm is degraded with respect to a system that uses the standard algorithm. This diversity order degradation is due to the fact that the proposed selection algorithm does not select the optimal antenna configuration for each

particular channel realization, but it selects the antenna configuration that, on average, increases the spectral efficiency of the communication link. Finally we observe that in the case of low angle spread (e.g. AS=10^o), the proposed algorithm always selects configuration TM_{41}, which is the one that on average outperforms the other configurations in terms of channel capacity.

In Fig.6.10(b) the same BER curves are shown for an angle spread of 60^o. A similar gain is achieved using the proposed algorithm with respect to a system that selects the antenna configuration after exhaustively estimating the channel for each configuration. However we observe that, different from the case of Fig.6.10(a), at high AS the proposed algorithm always selects configuration TM_{21}. Recall that TM_{21} on average outperforms the other configurations, according to the results of Section 6.3. Also, at high AS, the BER curve slope remains the same for all the different configurations; therefore the level of diversity provided by the different configurations is the same. The diversity level also effects the trend of the BER curves for the proposed algorithm (proposed algorithm np-CSI) and the standard algorithm (standard algorithm np-CSI). Unlike the results from Fig.6.10(a), at high AS, the BER curve slope is the same for both systems; therefore, at high AS, the two systems are characterized by the same diversity order.

6.6 Summary

The selection technique presented in this Chapter delivers performance similar to those achievable with an optimal selection scheme, without any extra power consumption or

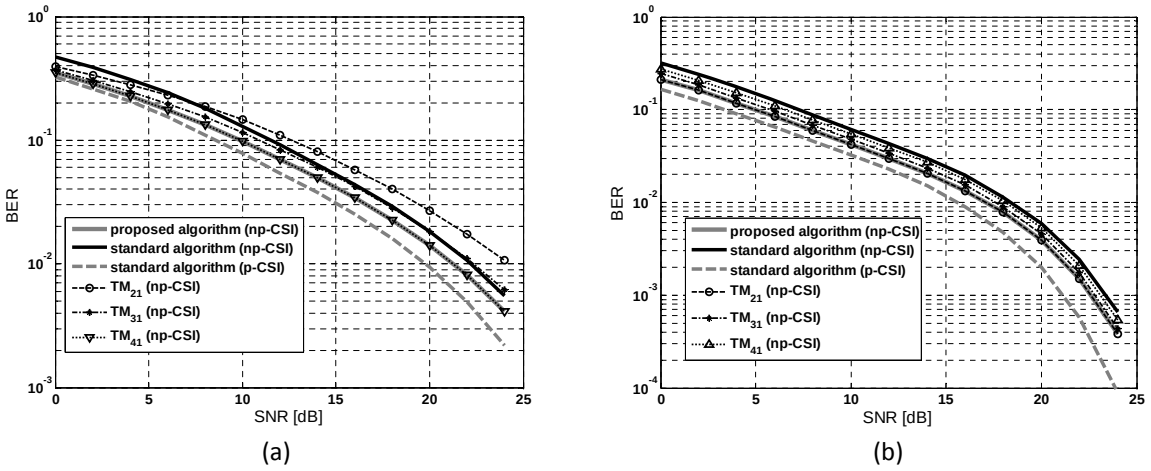

Figure 6.10: BER versus SNR for a 2×2 MIMO system, with RCPA-1 at the receiver, that employs:(i) the proposed selection scheme including the effects of imperfect channel estimation (proposed algorithm np-CSI), (ii) an algorithm that selects the antenna configuration after estimating the channel for all possible configuration including the effects of imperfect channel estimation (standard np-CSI) and, (iii) a standard algorithm assuming perfect channel estimation (standard p-CSI). The BER curves relative to non reconfigurable circular patch antennas operating in different modes assuming non-perfect channel estimation are also reported. (a) AS=10^o and (b) AS=60^o.

modifications to the data frame of a conventional, non reconfigurable MIMO system.

A relative capacity gain is achievable with respect to a reconfigurable antenna MIMO system that selects the antenna configuration after estimating the channel for all the possible antenna configurations. In particular we have demonstrated that the higher the level of reconfigurability in the receiving antenna element, the higher the benefit offered by our proposed algorithm. The diversity order of a system that adopts the proposed algorithm falls in between the upper bound of a system that adopts a standard configuration selection algorithm and the lower bound of a system that employs non reconfigurable antennas. On the other hand we observe that the proposed algorithm allows for better channel estimation (and thus, higher receiver SNR) than a standard configuration selection scheme.

The functionality of this selection scheme is dependent on the differences existing between the antenna configurations of the reconfigurable antenna array. This fact motivates the need to develop reconfigurable antennas for MIMO systems jointly with the characteristics of the proposed selection algorithm.

Chapter 7: Two port reconfigurable CRLH leaky wave antenna

As demonstrated in previous chapters, the benefits achievable with reconfigurable arrays in MIMO systems grow with the number of antenna configurations. However, designing multi element antennas with several efficient configurations, all characterized by high gain, good impedance matching and high pattern diversity, is a difficult task.

In this chapter a novel leaky wave antenna (LWA) [116] built using metamaterial microstrip structures is presented. We show that composite right left handed (CRLH) metamaterials [117,118] can be effectively used to achieve high radiation pattern reconfigurability without scarifying gain, impedance matching, or compactness. This antenna design is, in essence, a CRLH microstrip structure incorporating varactor diodes for fixed-frequency voltage-controlled operation. Angle scanning at a fixed frequency is achieved by modulating the capacitances of the structure by adjusting the bias voltage applied to the varactors. Ideally an infinite number of radiation patterns can be excited for increased system diversity. Two separate ports are located on the same antenna structure so that a single physical antenna can be used as a two element array for reduced antenna space occupation on the communication device. We define the performance achievable with this highly reconfigurable array when employed in a 2×2 802.11n like MIMO communication system. Field measurements collected in Line of Sight (LOS) and Non Line of Sight (NLOS) scenarios are used to determine the system achievable channel capacity and to quantify the level of power

saving achievable for a fixed transmission rate with such antenna compared to a reference non reconfigurable antenna system. Analysis conducted in realistic cluster channel models are then used to provide a complete understanding of the achievable performance of this antenna structure in different environments.

7.1 Generalities of leaky wave antennas

A leaky wave is a traveling wave that progressively leaks out power while it propagates along a waveguiding structure. Such structures are usually used as antennas to achieve high directivity. Leaky wave antennas are fundamentally different from resonating antennas, in the sense that they are based on a traveling wave as opposed to a resonating wave mechanism. The antenna size is not related to the antenna resonant frequency but to its directivity.

The radiation properties of a leaky wave antenna are related to the propagation constant along the direction of the waveguide, $\gamma = \alpha - j\beta$ (where α is the attenuation constant and β is the phase constant), and to the propagation constant perpendicular to this direction, $k_\perp$. The two propagation constants are related as:

$$k_\perp = \sqrt{k_0^2 - \beta^2} \tag{7.1}$$

where k_0 is the free space wave number.

If the wave is slower than the velocity of light (slow wave region) and so $k_0 < \beta$, the perpendicular propagation constant, $k_\perp$, is imaginary and therefore no radiation occurs,

and the wave is guided. If in contrast the wave is faster than the velocity of light (fast wave region) and so $k_0 > \beta$, the perpendicular propagation constant is real and radiation occurs. In particular, radiation occurs under the angle

$$\theta = sin^{-1}\left(\frac{\beta}{k_0}\right) \tag{7.2}$$

where θ is the maximum beam angle from the broadside direction. Thus, the radiation angle can be controlled by frequency in a leaky wave antenna. The attenuation constant, α, determines instead the radiated power density per unit length. For large values of α most of the power is leaked in the first part of the waveguiding structure, while for small values of α, leakage occurs slowly and highly directivity is achieved.

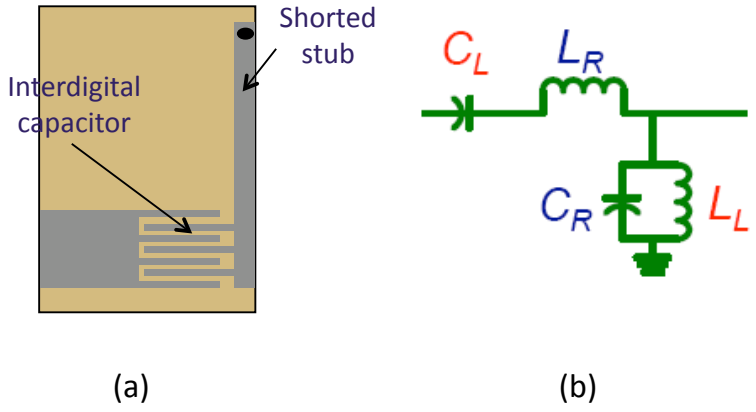

Figure 7.1: CRLH transmission line unit cell: (a)schematic, (b)equivalent circuit model.

In conventional microstrip structures wave leakage is achieved exciting higher order modes [119] and this requires a complicated feeding structure. Moreover standard waveg-

uiding structures do not allow to achieve full beam scanning from back-fire to end-fire, but their radiation capabilities are limited to few scanning angles [120].

7.2 CRLH leaky wave antennas

A dominant mode frequency-scanned LW antenna can be implemented using composite right left handed (CRLH) transmission lines. A CRLH transmission line is implemented by inserting an artificial series capacitance and a shunt inductance into a conventional transmission line, which has an intrinsic series inductance and shunt capacitance. The general representation of the CRLH transmission line and its equivalent circuit model are shown in Fig.7.1. It consists of an interdigital capacitor and a shorted shunt stub representing a series capacitance and a shunt inductance, respectively.

Loading a common transmission line with a series capacitance and shunt inductance allows modification of the typical propagation characteristic of right handed (RH) materials which are characterized by a positive propagation constant, $\beta > 0$. In CRLH transmission lines the material propagation behavior shifts with frequency from RH (characterized by $\beta > 0$) to left handed (LH)(characterized by $\beta < 0$). This effect has been demonstrated in [117, 118, 121, 122] and it can be observed in the dispersion diagram of Fig.7.2. According to the CRLH transmission line dispersion diagram there are four distinct regions: the LH-guided region, the LH-leaky region, the RH-leaky region and the RH-guided region.

Fig.7.3 illustrates the operating principle of the CRLH LW antenna. According to Eq. (7.2), backfire radiation is achieved at the frequency f_{BF} where $\beta = -k_0$ (point A

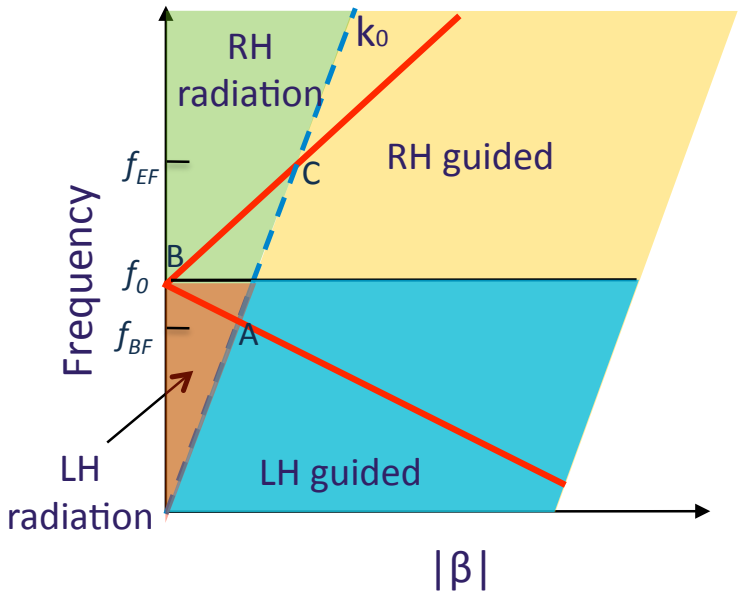

Figure 7.2: Dispersion diagram of a CRLH transmission line unit cell.

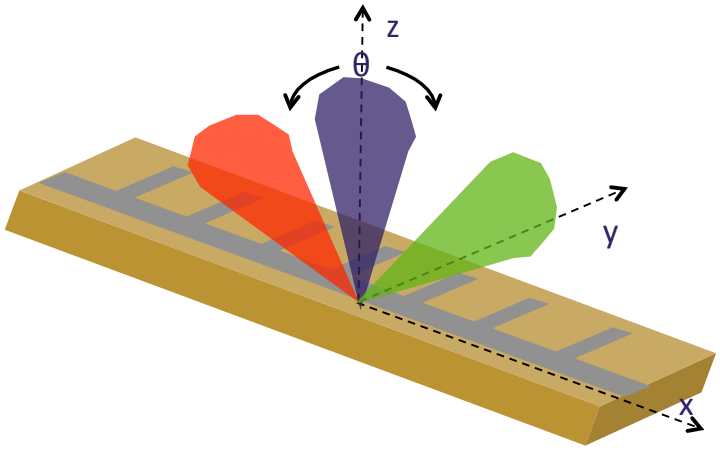

Figure 7.3: Working principle of a CRLH leaky wave antenna.

in Fig.7.2), broadside radiation is achieved at the frequency f_0 where $\beta = 0$ (point B in Fig.7.2) and endfire radiation is achieved at the frequency f_{EF} where $\beta = k_0$ (point C in

Fig.7.2). This backfire to endfire scanning capability, first demonstrated experimentally in [122] and explained by the CRLH concept in [123] , is a very unique feature for a LW antenna, which cannot be obtained in conventional LW structures.

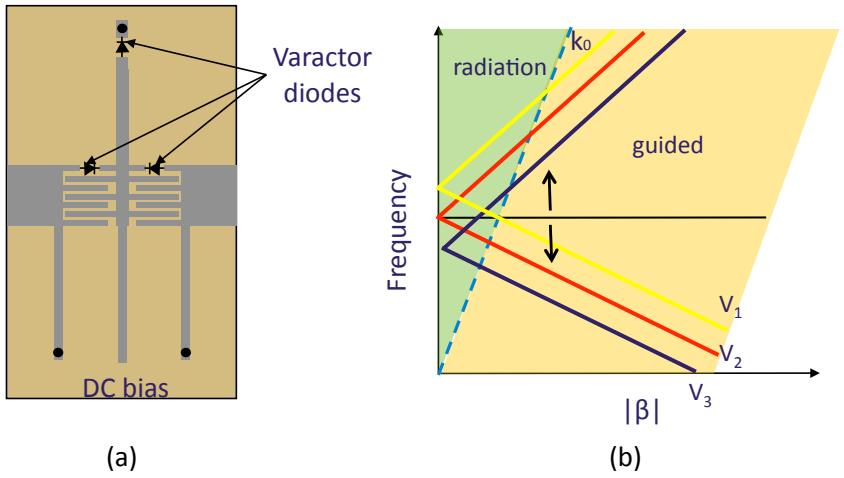

Figure 7.4: (a) tunable CRLH unit cell and (b) its dispersion diagram.

The frequency scanned nature of these LW antenna is however a disadvantage that has limited their applications in modern communication systems, generally requiring fixed frequency operation for effective channelizing. In CRLH LW antennas, since the main radiation beam angle is a function of the propagation constant along the structure, it is possible to steer the beam by LC parameters tuning at a fixed frequency of operation. In this case varactor diodes can be integrated along the structure, in each cell, to provide continuously variable capacitances via the control of their reverse bias voltage V. A first prototype of an electronically scanned CRLH LW antenna has been proposed in [124] and its working principle is described in the dispersion diagram of Fig.7.4. Varying the applied

bias voltage V it is possible to shift the propagation characteristics of the transmission line and achieve different propagation constants, β, for a fixed frequency of operation.

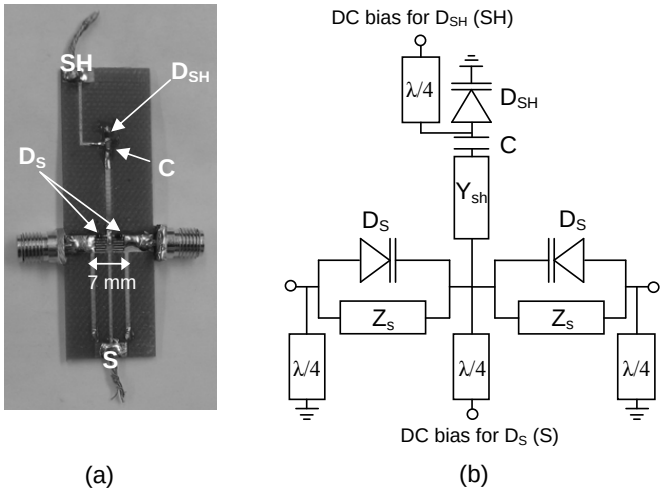

Figure 7.5: CRLH tunable unit cell: (a)picture, (b)circuit model.

7.3 Reconfigurable leaky wave antenna

The design of the LWA unit cell is shown in Fig.7.5. In order to achieve CRLH behavior, we implemented the unit cell by inserting an artificial series capacitance and a shunt inductance into a conventional microstrip line by means of an interdigital capacitor and a shorted stub respectively. To dynamically tune the handedness of the unit cell two varactor diodes (D_S) are placed in parallel with the microstrip series interdigital capacitor and one varactor diode (D_{SH}) is placed in series with the shunt inductor similar to the design in [124]. Two independent bias networks are used to separately tune the varactors D_S ("S" bias) and

Table 7.1: Unit cell structural paramters.

Dielectric	FR4 ($\epsilon_r = 4.4$)
Dielectric thickness	$1.524\,mm$
Stub length	$19\,mm$
Interdigital capacitor width	$3.1\,mm$
Period p	$7\,mm$
C	$0.5\,pF$
Varactor capacitance	$1.3 - 7.3\,pF$

D_{SH} ("SH" bias). A capacitor (C = 0.5 pF) is used to decouple the two DC bias networks and quarter wave transformers are employed to prevent the RF signal from flowing to DC ground. By using two independent DC bias networks, it is possible to adjust the unit cell reactance in order to keep the Bloch impedance close to 50 Ω while shifting the unit cell electrical characteristic from left hand to right hand.

The unit cell is built on a FR4 substrate with dielectric constant, ϵ, of 4.4 and a length, p, of 7 mm. We used Skyworks SMV1413 varactor diodes with a measured capacitance that varies continuously from 1.3 pF (for a bias voltage of 40 Volt) to 7.3 pF (for a bias voltage of 0 Volt). A summary of the main characteristics of the unit cell structure is reported in Table 7.1.

Fig.7.6 shows the measured dispersion diagram of the proposed unit cell for five different configurations of "S" and "SH" DC bias voltages. Table 7.2 shows the measured Bloch impedance for the same voltage combinations at a frequency of 2.45 GHz. We note that the proposed unit cell design allows for continuous shifting of the propagation constant, β, for a fixed frequency of operation while keeping the Bloch impedance close to 50 Ω. This unit cell design is then suitable for building reconfigurable CRLH LWAs with good matching

Table 7.2: Bloch impedance.

CONFIGURATION	IMPEDANCE
S=40V SH=30V	$40 + j25\Omega$
S=35V SH=30V	$28 + j15\Omega$
S=30V SH=10V	$20 + j10\Omega$
S=25V SH=0V	$30 + j25\Omega$
S=17V SH=0V	$48 + j30\Omega$

over the entire set of generated scanning beams.

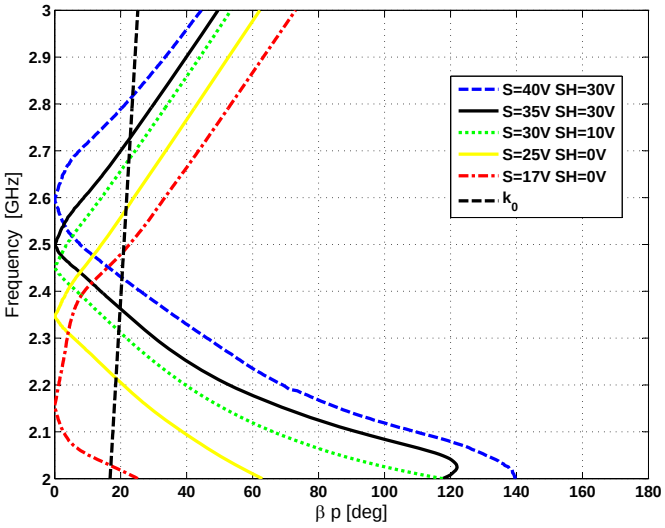

Figure 7.6: Dispersion diagram of the proposed unit cell for five different bias voltage combinations.

For a selected frequency of operation, in the fast wave region of the unit cell, $\beta < k_0$, radiation is occurs as described in Eq. (7.2).

Fig.7.7 shows a prototype of a two port reconfigurable leaky wave antenna built with the unit cell structure of Fig.7.5. The antenna is composed of 25 unit cells and has been

designed to operate in a 802.11n MIMO WLAN at a frequency of 2.45 GHz. The design is 17.5 cm long and it allows for excitation of two independent beams (one per port) that can be steered from back-fire to end-fire. Since a common antenna structure is used for the two ports, the excited beams are steered together symmetrically with respect to the broadside direction. Ideally, since the varactor capacitance allows for continuous tuning, an infinite number of configurations can be selected for the proposed two element array.

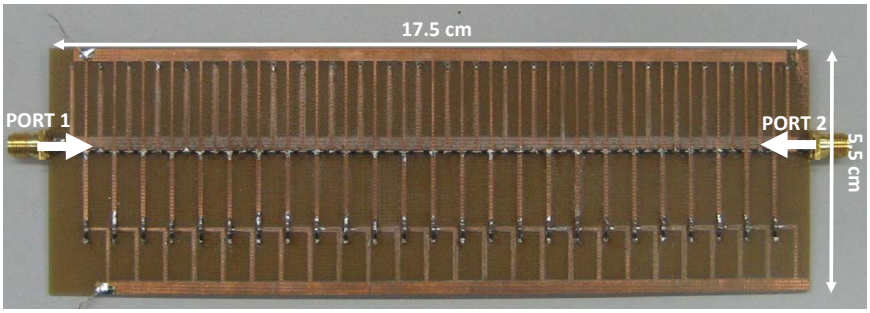

Figure 7.7: Two port reconfigurable leaky wave antenna.

Fig.7.8 shows the measured scattering parameters for five different array configurations (each corresponding to a specific combination of "S" and "SH" voltages). We observe that both ports are matched at the frequency of 2.45 GHz with respect to a 10 dB target return loss. The isolation between the two ports is higher than 10 dB for all the configurations and allow for two decoupled array elements coexisting within the same antenna structure. Minor differences between the two ports are attributable to fabrication imperfections.

Fig.7.9 shows the measured radiation patterns excited at the two ports for the same

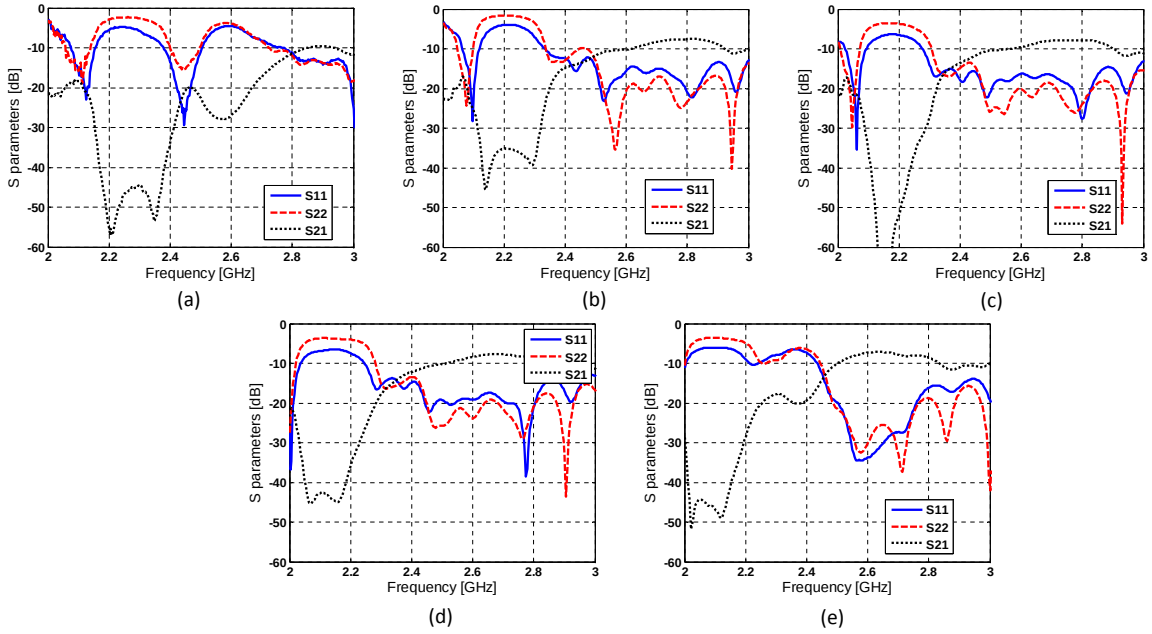

Figure 7.8: Measured scattering parameters for five different configuration of the proposed reconfigurable LWA: (a)S=40V SH=30V, (b)S=35V SH=30V, (c)S=30V SH=10V, (d)S=25V SH=0V, (e)S=17V SH=0V

five different array configurations of Fig.7.8. The beam can be effectively steered over 115^o in the elevation plane with minor differences between the two ports. The beam scanning direction of the proposed antenna structure can be predicted using the dispersion diagram information as [124]:

$$\theta_1 = sin^{-1}\left(\frac{\beta(S,SH)}{k_0}\right) = -\theta_2 \tag{7.3}$$

where θ_1 and θ_2 are the scanning angles at port 1 and port 2. As summarized in Tables 7.3 and 7.4, we note that the antenna measured scanning direction agrees well with the one predicted using the measured propagation constant of a single unit cell. We also note

that the proposed two port reconfigurable LWA has highest gain in the broadside direction and that the half power beamwidth (HPBW) varies while steering the beam. In particular we observe that the highest gain (6.2 dBi) is achieved for directions close to broadside, while it diminishes when moving at endfire and backfire. However all possible antenna configurations have a gain higher than 0.5 dBi.

Table 7.3: Main radiation characteristics of five antenna configurations of the proposed reconfigurable LWA. Frequency =2.45 GHz. Port 1

CONFIGURATION	HPBW	Gain [dBi]	Direction(expected)
S=40V SH=30V	53^o	1.6	-55^o(-55^o)
S=35V SH=30V	31^o	3.6	-18^o(-20^o)
S=30V SH=10V	20^o	4.4	-10^o(-5^o)
S=25V SH=0V	29^o	2.1	16^o(20^o)
S=17V SH=0V	40^o	0.8	60^o(52^o)

To validate that the proposed antenna design is a suitable solution for MIMO communications we determined the level of pattern diversity between the patterns generated at the two ports of the array through the spatial correlation coefficient value of Eq. (4.1) Table 7.5 reports the spatial correlation coefficient value between the patterns generated at two antenna ports for five different array configurations.

It can be noted that for all five selected array configurations, the envelope correlation is below the target value of 0.7 and thus the reconfigurable LWA is capable of providing significant diversity gain. We also note that the array configurations that suffer from low gain (S=40V SH=30V and S=17V SH=0V) exhibit higher pattern diversity than high gain configurations (S=30V SH=10V, S=35V SH=30V and S=25V SH=0V); a good balance

Table 7.4: Main radiation characteristics of five antenna configurations of the proposed reconfigurable LWA. Frequency =2.45 GHz. Port 2

CONFIGURATION	HPBW	Gain [dBi]	Direction(expected)
S=40V SH=30V	42^o	2.6	$50^o(55^o)$
S=35V SH=30V	38^o	5.8	$22^o(20^o)$
S=30V SH=10V	28^o	6.2	$10^o(5^o)$
S=25V SH=0V	48^o	2.7	$-15^o(-20^o)$
S=17V SH=0V	34^o	0.7	$-61^o(-52^o)$

Table 7.5: Envelope correlation for the radiation patterns excited at the two ports of the reconfigurable LWA for five different configurations

CONFIGURATION	ENVELOPE CORRELATION
S=40V SH=30V	0.15
S=35V SH=30V	0.30
S=30V SH=10V	0.62
S=25V SH=0V	0.38
S=17V SH=0V	0.28

between the level of pattern diversity and the antenna gain is then guaranteed for all the configurations.

7.4 System model and experimental setup

We study the performance of the RLWA in a wideband MIMO systems employing spatial multiplexing as a transmission technique. Assuming that the channel is unknown at the transmitter, the achievable channel capacity per channel sub-band centered at the frequency tone, f_k, is defined as [66]:

$$C_k = \log_2 \left[\det \left(\mathbf{I}_{N_r} + \frac{SNR_k}{N_t} \mathbf{H}_k \mathbf{H}_k^{\dagger} \right) \right] \tag{7.4}$$

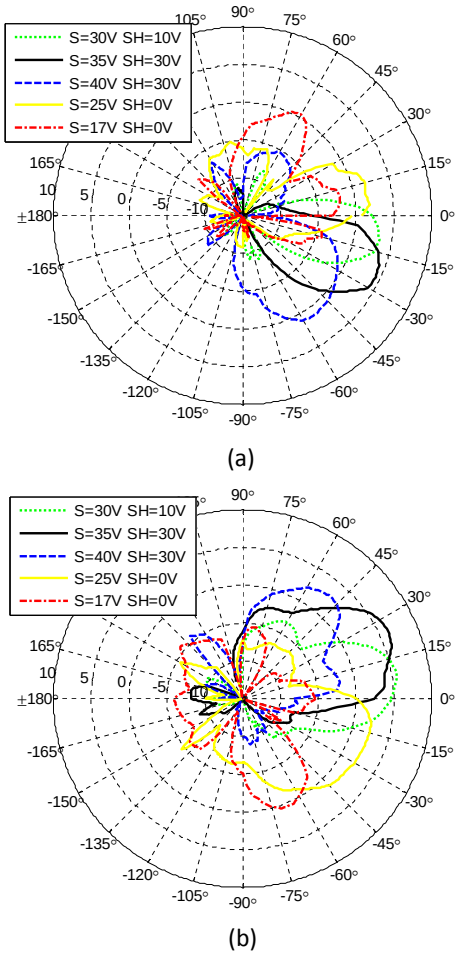

Figure 7.9: Measured radiation pattern excited at the two ports of the reconfigurable LWA for five different configurations: (a)port 1, (b)port 2. Frequency = 2.45 GHz.

where SNR_k is the average signal-to-noise-ratio over all receiver array elements for the k-th sub-band. To remove the effect of path loss, each measured channel matrix, $\mathbf{G}_k \in C^{N_r \times N_t}$, is normalized such that:

$$\mathbf{H}_k = \mathbf{G}_k \sqrt{\frac{N_t N_r}{\|\mathbf{G}_k\|_F^2}} \tag{7.5}$$

where $\|\mathbf{G}_k\|_F$ is the Frobenius norm of the measured channel matrix.

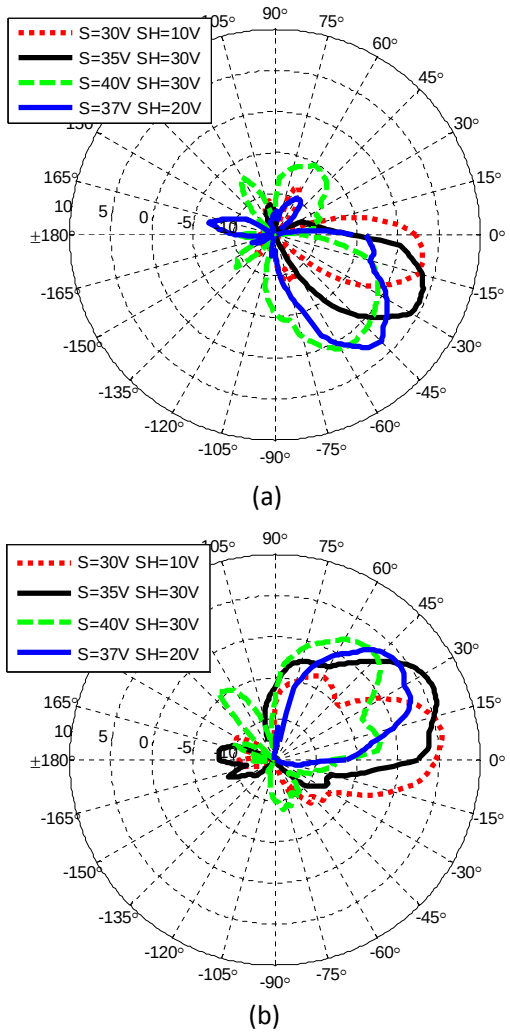

Figure 7.10: Measured radiation pattern excited at the two ports of the reconfigurable LWA for four different configurations employed to collect field measurements: (a)port 1, (b)port 2. Frequency = 2.45 GHz.

Employing a reconfigurable antenna capable of exciting different shapes of radiation pattern results in different amounts of received power per configuration and therefore dif-

ferent signal-to-noise ratios. In order to keep the difference in signal-to-noise-ratio between the different antenna configurations we calculate the channel capacity for a given value of noise at the receiver, v, as in [104]. We define therefore the average SNR_k per sub-band as:

$$SNR_k = \frac{P_t \sum_{i=1}^{N_r} \sum_{j=1}^{N_t} |g_{i,j}^k|^2}{N_r v} \tag{7.6}$$

where $g_{i,j}^k$ are the entries of the measured channel matrix $\mathbf{G}_k$ and P_t is the transmitted power at each antenna element.

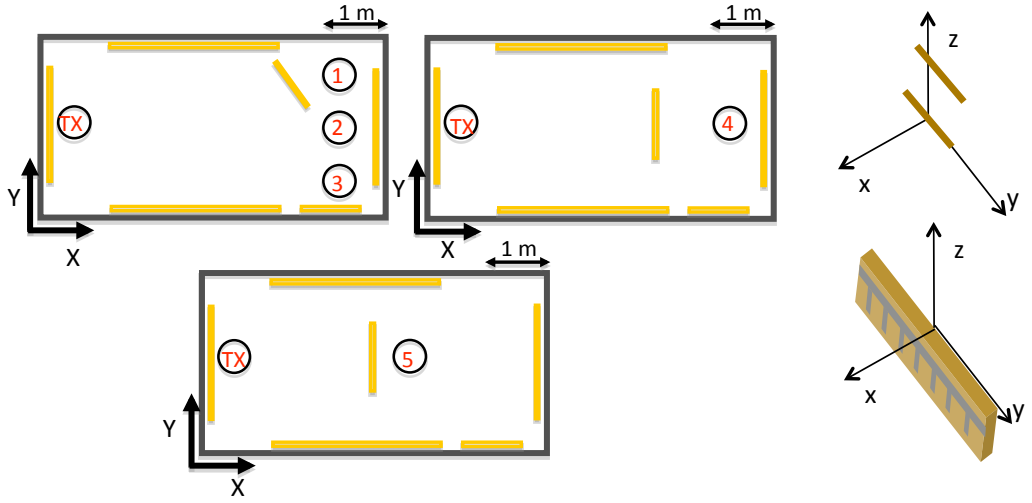

Figure 7.11: Experimental setup and antenna displacement in a semi-anechoic chamber with metallic foils displaced in the indoor environment to act as scatterers.

The channel capacity, C_W, for the wideband MIMO system is defined as:

$$C_W = \frac{1}{m} \sum_{k}^{m} C_k \tag{7.7}$$

where m is the number of sub-bands composing the wideband spectrum. The maximum throughput for the wideband MIMO system is then:

$$R_{max} = \Delta f \sum_{k}^{m} C_k \tag{7.8}$$

where Δf is the bandwidth of each sub-band.

Using the RLWA in a MIMO system, different radiation patterns can be generated and thus the channel matrix, $\mathbf{G}$, between the transmitter and the receiver can be dynamically changed. The proper choice of the RLWA configuration is the one which increases the system diversity and/or the received signal power to maximize the channel capacity for a particular multipath environment.

We measured the performance achievable with the RLWA when used at the receiver of a 2×2 MIMO system in a controlled indoor environment. We conducted channel measurements in a 4×7 meter semi-anechoic chamber with metallic foils displaced on the walls and in the middle of the chamber to generate a multipath environment. The layout of the indoor environment is shown in Fig.7.11. Both the transmitter and the receiver were located at a height of 1.5 meters. The transmitter was kept fixed in the middle of the hallway while the receiver was moved to five different locations, covering both LOS (locations 2 and 3) and NLOS (locations 1, 4 and 5) locations. The antennas at the receiver were moved to 10 different positions at displacements of $\lambda/10$ (where λ is the wavelength at the frequency of operation) along the y-axis.

We used a four port vector network analyzer (Agilent ENA-C) to extract the channel

matrix between the transmitter and the receiver. Two ports of the vector network analyzer were connected to the two transmitting array elements and two ports were connected to the receiving array. The channel matrix, $\mathbf{G}_k$, was extracted from the scattering parameters transmitting 10 dBm of power at each port for a frequency sub-band of 125 KHz. At each position, 100 noisy channel estimates were captured and averaged, so as to get the channel response between each receiver-transmitter pair. A frequency scan over 20 MHz with center frequency of 2.45 GHz was conducted to collect data for 160 sub-bands.

At the transmitter we used two dipoles with gain of 2.2 dBi spaced one wavelength apart in the z direction to provide high decorrelation between the two array elements [5]. The dipoles have been oriented along the y-axis to provide polarization alignment between the transmitter and the receiving RLWA. To provide a fair analysis of the gains of the RLWA, we measured the channel matrix by also substituting the RLWA at the receiver with another set of the same dipoles spaced one wavelength apart. An array of dipoles was selected as a reference antenna system because of its widespread use in wireless communications and its omnidirectional radiation pattern that allows for the generation of a rich multipath environment and to receive signals incoming from different directions.

For the sake of simplicity, in this chapter we selected a representative subset of all the possible array configurations to determine the achievable performance of this reconfigurable antenna system with respect to standard non reconfigurable arrays. Fig.7.10 shows the measured radiation patterns of the four selected antenna configurations for the two ports of the RLWA. We selected the array configurations with higher gain and capable of offering

complete coverage in the elevation plane from -55^o to +50^o.

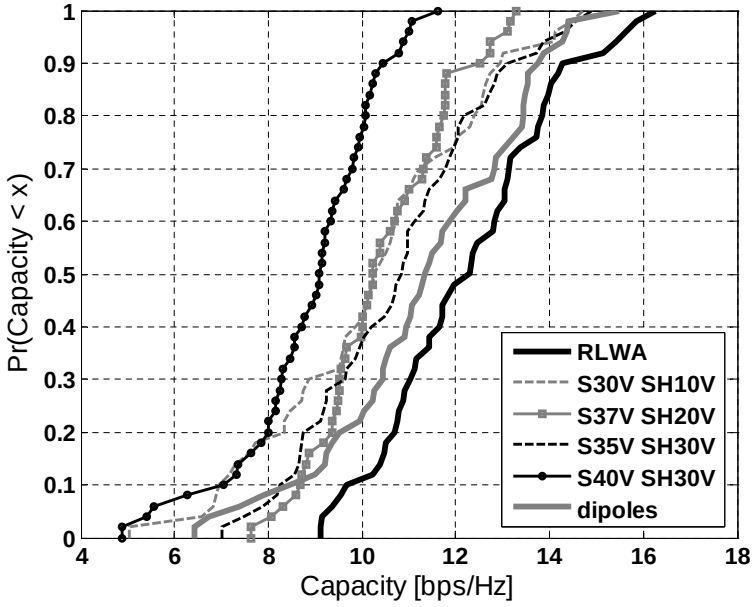

Figure 7.12: Comulative distribution function of the achievable channel capacity for a noise level v=1nW.

7.5 Experimental results

The collected channel measurements were used to evaluate the performance of the RLWA, in terms of achievable channel capacity and power saving for a fixed target of transmission rate. We used Eq. (7.7) to determine the capacity achievable for each of the four selected antenna configurations for a broadband system using a band of 20 MHz. We also determined the power, P_t, required to guarantee a maximum transmission rate of R_{max} = 300 Mbit/s for both the RLWA and the array of dipoles, using the water-filling power allocation scheme [1].

We could then determine the amount of power that can be saved using the RLWA with respect to the reference array as:

$$\Delta P_t = P_t^{RLWA} - P_t^{reference} \tag{7.9}$$

where P_t^{RLWA} and $P_t^{reference}$ are the amounts of power transmitted (in dBm) when the RLWA and the reference array of dipoles are respectively used.

7.5.1 Channel capacity

Fig.7.12 reports the capacity cumulative distribution function (CDF) determined for the RLWA and the array of dipoles for a noise value of $v = 1$ nW. For a probability of 50% the RLWA channel capacity improvement is 9% with respect to the array of dipoles and 15% with respect to the most capacity achieving RLWA configuration (S=35V SH=30V). In particular, we observe that the array of dipoles outperforms all the RLWA configurations thanks to its capability of receiving a good signal independently from its direction of arrival. On the other hand, a single RLWA configuration, due to its high directivity, can not effectively collect a strong signal for every multipath scenario. By properly switching between the RLWA configurations, it is instead possible to collect two strong and uncorrelated signals at the ports of the RLWA, leading to enhanced performance. Table 7.6 summarizes the percentage capacity improvement achievable with the RLWA when used at the receiver of a 2×2 MIMO system.

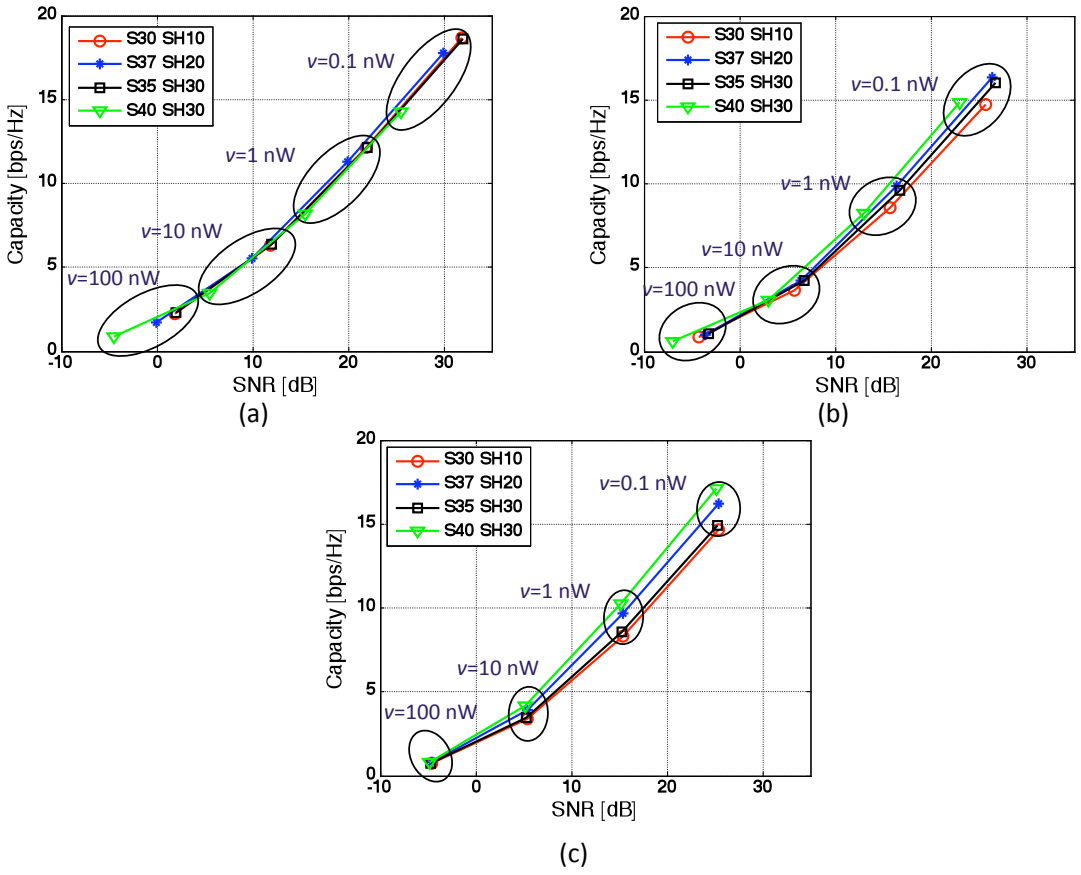

Figure 7.13: Measured capacities of a 2×2 MIMO system employing the RLWA at the receiver as a function of the received SNR. Each group of data points corresponds to a specific level of noise power. (a) LOS scenario, (b) NLOS scenario, and (c) single NLOS location.

Fig.7.13(a) and Fig.7.13(b) show the average achievable channel capacities as a function of the actual received SNR by each configuration of the RLWA. Fig.7.13(a) shows the capacity curves for the LOS channels (locations 2, and 3) and Fig.7.13(b) for the NLOS channels (locations 1,4, and 5). We observe that, on average, in LOS scenarios the configurations (S=30V SH=10V, S=35V SH=30V) with higher gain and proper alignment with the transmitter outperform the others. In particular we note that for a given noise power level, v, the average received SNR varies greatly among the different configurations and

Table 7.6: Percentage capacity improvement achievable for a probability of 50% when using the RLWA at the receiver of a 2×2 wideband MIMO system. Noise level $v = 1\ nW$.

	Capacity improvement
with respect to dipoles	9%
with respect to S=40V SH=30V	43%
with respect to S=37V SH=20V	21%
with respect to S=35V SH=30V	15%
with respect to S=30V SH=10V	21%

that all the capacities curve lie on the same line. Therefore in a LOS scenario the difference in performance between the antenna configurations is due to differences in received signal power and not in diversity. On the other hand, when using the RLWA in NLOS scenarios, we observe that, since the capacity curves do not lie on the same line, the difference in performance between the array configurations are due to differences in both received signal power and diversity. In particular we measured that configurations S=35V SH=30V and S=37V SH=20V outperforms the other configurations. This effect can be better observed looking at the capacity curves for a single location. Fig.7.13(c) shows the channel capacities as a function of the actual received SNR for a location of receiver 4. In this case we note that the configuration S=40V SH=30V, which is characterized by the lowest gain and the highest pattern diversity [48], outperforms all the other. The capacity gain achieved using configuration S=40V SH=30V is only due to the higher diversity respect to the other RLWA configurations, since the SNRs at the receiver are almost the same for all the antenna configurations.

7.5.2 Power saving

Fig.7.14 shows a histogram of the difference in transmitted power, ΔP_t, between the RLWA and the array of dipoles for a fixed target of transmission rate $R_{max} = 300$ Mbit/s. The RF power saving achievable using the RLWA with respect to the array of dipoles is on average of 3.2 dB. This means that the RLWA achieves the same performance of the array of dipoles using only half of the RF power. In particular we observed that the power saving is higher for the LOS locations (4.3 dB) than for the NLOS locations (2.5 dB). This happens because when the multipath is scarce (LOS locations) the high RLWA directivity helps receiving a strong signal, a lot higher than the one received by the dipoles. In presence of high multipath the level of received signal by the RLWA and the dipoles is instead comparable. In NLOS scattered channel scenarios the ability of dipoles to capture multipath, given the broader angular spread of their radiation pattern, compensates for the lower antenna gain and allows to collect a signal power comparable to the one received by a directional antenna like the RLWA.

We observe that such RF power saving comes at the cost of DC power consumption necessary to drive the varactor diodes on the RLWA. The DC power consumption varies with the excited radiation configuration. Table 7.7 shows the measured DC power consumption for each of the four RLWA configurations. To achieve a transmission rate of $R_{max} = 300$ Mbit/s in this testing environment, the average DC power consumption is 105 mW. Accounting also for these losses, the power saving achievable using the RLWA, in a system with a noise level of v=10 nW, is 1.5 dB with respect to the array of dipoles. We remark

Table 7.7: DC power consumption per RLWA configuration

CONFIGURATION	POWER CONSUMPTION (mW)
$S = 30V SH = 10V$	0.1
$S = 35V SH = 30V$	3.5
$S = 37V SH = 20V$	172
$S = 40V SH = 10V$	558

that this result is obtained with a RLWA not specifically optimized for low DC power consumption. To drastically reduce the DC power consumption and maximize the total power saving the RLWA design can be revised such that the same varactor diodes could be used with lower actuation voltage (i.e. biasing the varactor diodes for higher values of capacitance) or alternatively a different varactor diode could be selected.

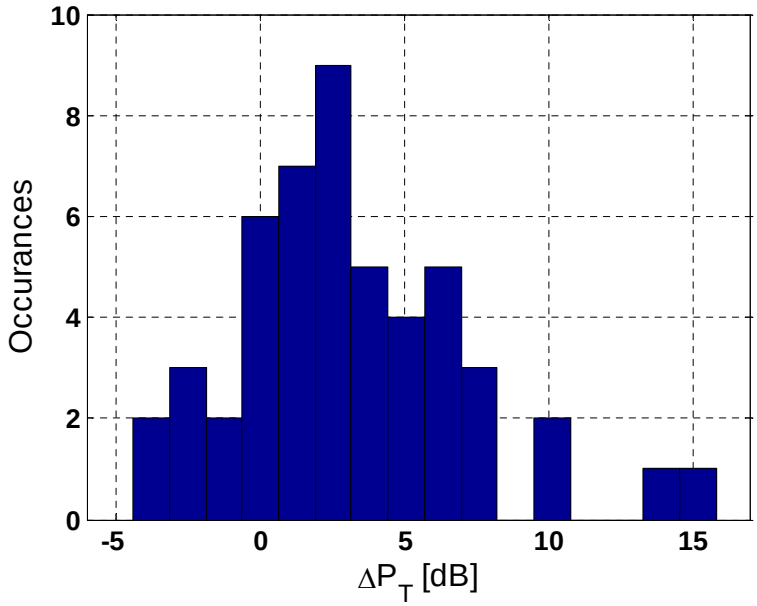

Figure 7.14: Distribution of ΔP_T for a fixed transmission rate of 300 Mbit/s.

7.6 RLWA in different channel scenarios

To provide a complete understanding of the performance offered by the different array configurations of the RLWA, we performed a performance analysis of the RLWA in different simulated clustered channel models. We consider four typical channel models, with different degrees of spatial selectivity, based on the IEEE 802.11n standard channel models described in [67]. These models are defined as follows:

- **Model 1** (NLOS, high AS): zero-mean correlated Rayleigh fading model, with K=-∞ dB, AS$\in$ $[28^o, 55^o]$, N_c=6 (consistent to "Model F, NLOS" in [67]).
- **Model 2** (NLOS, low AS): zero-mean correlated Rayleigh fading model, with K=-∞ dB, AS$\in$ $[22.4^o, 24.6^o]$, N_c=2 (consistent to "Model C, NLOS" in [67]).
- **Model 3** (LOS, low K-factor): correlated Ricean model, with K-factor K=2 dB, AS$\in$ $[22.4^o, 24.6^o]$, N_c=2 (consistent to "Model C, LOS" in [67]).
- **Model 4** (LOS, high K-factor): correlated Ricean model, with K-factor K=6 dB, AS=30^o], N_c=1 (consistent to "Model A, LOS" in [67]).

Each model is characterized by having LOS or NLOS components, by different number of clusters and by different values of AS. These channels have been simulated using the channel model described in Section 3.2 for both NLOS and LOS components. The RLWA has been used only at the receiver of the communication link and at the transmitter an ideal array with two element spatially decorrelated has been employed ($\mathbf{R}_t = \mathbf{I}$). The capacity has been computed according to Eq. (4.5) for the four RLWA pattern configurations

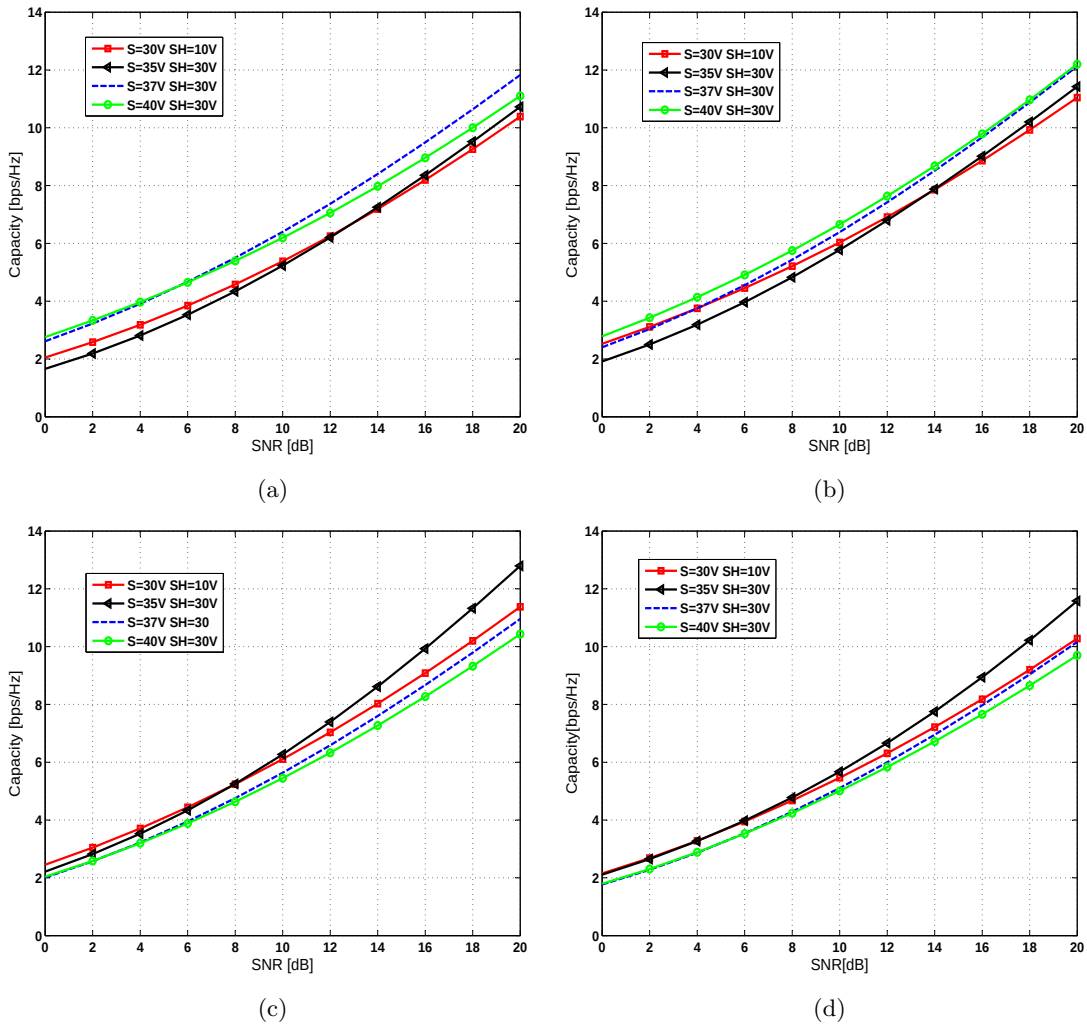

Figure 7.15: Channel capacity achievable with four different configurations of the RLWA when used at one end of the communication link in (a) Model 1, (b) Model 2, (c) Model 3, (d) Model 4.

described in Fig.7.10. The channel matrix, **H**, has been determined according to Eq. (3.2) including the effect of NLOS and LOS components. The measured radiation patterns of the RLWA have been used to conduct this performance analysis in cluster channel models through Monte Carlo simulations.

Fig.7.15 shows the channel capacity as a function of the SNR at the receiver for four different configurations of the RLWA when operating in different channel scenarios. We observe that the configurations characterized by higher gain and lower pattern decorrelation ("S=30V SH=10V" and "S=35V SH=30V") outperforms the configurations with lower gain and higher pattern decorrelation ("S=37V SH=30V" and "S=40V SH=30V") in LOS scenarios (Model 3 and Model 4). The behavior is instead opposite in NLOS scenarios (Model 1 and Model 2). It is clear the importance of having highly decorrelated radiation patterns when operating in NLOS scenarios while it is of prominent importance to employ high gain antennas, well directed towards the transmitter, when operating in LOS environments. We also observe that the number of clusters in NLOS scenarios notably affects the performance of the different RLWA configurations. In Model 1 ($N_c = 6$) the scattering is higher than in Model 2 ($N_c = 2$) and we note that the capacity improvement achievable by configurations "S=37V SH=30V" and "S=40V SH=30V" with respect to configurations "S=30V SH=10V" and "S=35V SH=30V" grows with the number of clusters.

7.7 Summary

The RLWA is a highly pattern reconfigurable multi element antenna characterized by directive radiation patterns excited with a relatively compact design.

According to the results obtained from channel measurements and from stochastic simulations in clustered channel model we can conclude that the RLWA delivers the highest gain in presence of scarce multipath environments (e.g. LOS scenarios) because of the high

array directivity. In NLOS, while the gain achievable with respect to an array of dipoles are lower than in LOS scenarios, the RLWA configurations, which are characterized by lower gain but higher decorrelation between the array elements, are more effective than those characterized by higher gain and lower decorrelation.

The performance improvement achievable with the RLWA with respect to a standard array of dipoles is notable in terms of both channel capacity and power saving. These results were obtained using a subset of all the possible configurations that can be excited with the RLWA and employing the RLWA only at the receiver. Considering that the RLWA is capable of generating a very large set of array configuration further improvements can be expected. In particular greater benefit are also expected using the RLWA at both ends of the communication link.

The high number of array configurations in the RLWA requires development of proper configuration switching schemes that can be used to select the array pattern without conducting an extensive search. An implementation of control algorithms for this antenna can be based on the performance analysis derived from channel measurements and clustered channel model simulations presented in this chapter.

Chapter 8: Reconfigurable antennas in MIMO ad hoc networks

Research in the area of ad-hoc networks has yielded important advances, notably in the field of physical layer techniques. In particular, a lot of effort has been spent in: *i.)* applying smart antennas and antenna diversity techniques to ad-hoc networks (*e.g.,* [125–127]), *ii.)* developing medium access control protocols suitable for Multiple Input Multiple Output (MIMO) ad hoc networks (*e.g.,* [128–130]) and *iii.)* adaptive algorithms for antenna beamforming in ad hoc networks (*e.g.,* [131–133]). Directional antennas, like phased arrays [134, 135] and switchable parasitic elements antennas [136, 137] have been proposed as a solution to reduce the interference of adjacent nodes, maximizing overall network throughput [125,127,138]. In order to further increase the network spectral efficiency, MIMO spatial multiplexing (SM) techniques and diversity techniques have been adopted [128, 129, 139]. However, directional arrays and MIMO SM/diversity techniques cannot be integrated on compact portable devices, where the limited space available makes mounting multiple directional antennas difficult.

In order to overcome practical space limitations and merge the benefits of MIMO SM/diversity techniques with those of directional antennas, we propose to adopt electrically reconfigurable antennas as a key element of MIMO transceivers in ad-hoc networks.

Through this chapter, we aim to quantify the benefits achievable with reconfigurable antennas in MIMO ad-hoc networks, while also investigating antenna configuration selection

schemes at each node. In a network scenario, the antenna configuration selection algorithm for a single link not only seeks the configuration combination (i.e., the configuration at the receiver and the configuration at the transmitter) that will provide a "rich" channel between the receiver and the transmitter, but will also aim to mitigate the interference that the link is suffering from. This configuration selection process is made more complex by the fact that when the antenna configuration at a transmitter is modified, it changes the interference seen by the other links in the network. While directional antennas can perform interference mitigation by estimating the direction of the incoming signals at the receiver, we show that reconfigurable MIMO antennas can achieve a similar result, with lower system complexity, by only estimating the channel matrix.

In order to maximize network sum capacity without a centralized controller, a distributed selection algorithm that can be used to efficiently select the antenna configuration at each node is proposed. The performance of this distributed selection scheme is compared to that of an ideal centralized approach that uses an exhaustive search process to assign the optimal antenna configuration to every node. In this analysis we assume that all transmitters make use of the equal power allocation scheme proposed in [140] which requires no channel feedback from the receiver to the transmitter.

We determine the sum network capacity that can be achieved with MIMO reconfigurable antennas for different network topologies through channel measurements and electromagnetic ray tracing simulations conducted in an indoor environment. We consider two prototype electrically reconfigurable antenna architectures in a 2×2 MIMO system employing

SM: *i.)* the Reconfigurable Printed Dipole Array (RPDA) presented in Chapter 4 and *ii.)* the Reconfigurable Circular Patch Antenna for pattern diversity (RCPA-PD) presented in Chapter 5. We show that parameters like the number of antenna configurations, the spatial orthogonality between the array elements, and the level of antenna radiation efficiency can be used to predict the achievable performance with a particular reconfigurable antenna in an ad-hoc network.

8.1 Comparison of RCPA-PD with RPDA

A comparison between the RPDA and the RCPA-PD shows that, based on the results of Tables 4.2, 4.3, 5.2, and 5.3, in a rich scattered environment, the RCPA-PD provides a higher degree of diversity for all its configurations (and among the different configurations) with respect to the RPDA. In contrast, the RPDA allows for switching between double the number of radiation patterns offered by the RCPA-PD. Thus, the RPDA and RCPA-PD can be viewed as representing two different "philosophies" for using reconfigurable antennas in wireless communications systems: *i.)* substantial changes in radiation pattern (e.g., RCPA-PD), and *ii.)* a large number of radiation pattern states (e.g., RPDA).

From a comparison between the radiation efficiency of the two antennas (see Tables 5.4 and 4.4) we note also that the RCPA-PD is less efficient than the RPDA; thus we expect the RPDA to achieve higher capacity values than the RCPA-PD.

8.2 System model and notation

We assume that the ad-hoc network consists of $\mathcal{L}$ co-located links which interfere with each other. All links are single hop (i.e., no node is used for relaying) and all transmit-receive pairs are pre-determined. For the rest of the chapter, we will be using the following notation. $\mathbf{H}_{i_{rc},j_{tc}}$ denotes the channel between the receiver of link i and the transmitter of link j, which is a function of the receive configuration of link $i(i_{rc})$ and the transmit configuration of link $j(j_{tc})$. In the case of the RPDA, $l_{rc}, l_{tc} \in [1,4]$, and for the RCPA-PD,$l_{rc}, l_{tc} \in [1,2]$. $\mathbf{x}_i$ is the signal vector of link i, which results in the power covariance matrix of link i, $\mathbf{Q}_i$ as $\mathbf{Q}_i = E\{\mathbf{x}_i\mathbf{x}_i^\dagger\}$. Operation $(\cdot)^\dagger$ denotes the conjugate transpose. Using this notation and assuming a flat fading channel, we can write the input-output relationship for link l as:

$$\mathbf{y}_l = \mathbf{H}_{l_{rc},l_{tc}}\mathbf{x}_l + \sum_{i\in\mathcal{L}\backslash l} \mathbf{H}_{l_{rc},i_{tc}}\mathbf{x}_i + \mathbf{n} \tag{8.1}$$

where $\sum_{i\in\mathcal{L}\backslash l} \mathbf{H}_{l_{rc},i_{tc}}\mathbf{x}_i + \mathbf{n}$ is the interference plus noise, which results in an interference plus noise covariance matrix for link l: $\mathbf{W}_l = \sigma_n^2\mathbf{I} + \sum_{i\in\mathcal{L}\backslash l} \mathbf{H}_{l_{rc},i_{tc}}\mathbf{Q}_i\mathbf{H}_{l_{rc},i_{tc}}^\dagger$. For the above equation, the assumption was made that the noise has power σ_n^2 and is independent across receive elements. Vector $\mathbf{c}$ is an $1 \times 2\mathcal{L}$ vector that contains the configurations for all links, (i.e.,$\mathbf{c} = [1_{rc}, 1_{tc}, 2_{rc}, 2_{tc}, \ldots, L_{rc}, L_{tc}]$). Notice also that the interference plus noise covariance matrix is a function of the receive configuration of the link and the transmit configurations used in the network. We also assume that the single type of reconfigurable antenna, RCPA-PD or RPDA, is used by all nodes in the network.

The power allocation strategy that we considered in this analysis is the Equal Power Allocation technique. It is the simplest MIMO transmission strategy, proven to be optimal in the case where there is no channel feedback to the transmitter [140]. This strategy consists of splitting the total available power in a node equally among the transmit antenna elements and assigning each element an independent symbol to transmit. In this case, $\mathbf{x}$ has N_t non-zero elements, while $\mathbf{Q}$ is always a diagonal matrix with diagonal elements equal to $\frac{P_t}{N_t}$ each. For the Equal Power Allocation technique, the capacity of link l becomes

$$C_l = \log_2 \left(\det \left(\mathbf{I} + \frac{P_t}{\sigma_n^2 N_t} \mathbf{H}_{l_{rc},l_{tc}} \mathbf{H}_{l_{rc},l_{tc}}^{\dagger} \mathbf{W}_l^{-1} \right) \right) \tag{8.2}$$

where $\mathbf{W}_l = \mathbf{I} + \sum_{i \in \mathcal{L} \setminus l} \frac{P_t}{\sigma_n^2 N_t} \mathbf{H}_{l_{rc},i_{tc}} \mathbf{H}_{l_{rc},i_{tc}}^{\dagger}$ is the interference plus noise covariance matrix.

To quantify the performance of the different types of reconfigurable antennas in an ad-hoc network, we use the sum capacity of the network:

$$C = \sum_{l \in \mathcal{L}} \log_2 \left(\det \left(\mathbf{I} + \frac{P_t}{\sigma_n^2 N_t} \mathbf{H}_{l_{rc},l_{tc}} \mathbf{H}_{l_{rc},l_{tc}}^{\dagger} \mathbf{W}_l^{-1} \right) \right) \tag{8.3}$$

Closed loop MIMO power allocation algorithms that make use of channel feedback information from the receiver to the transmitter could also be implemented to improve link and network capacity. However these algorithms become more complex when reconfigurable antennas are used. In particular, channel feedback information would have to be provided for all the different antenna configurations used by the transmitter and receiver. Closed loop algorithms become even more challenging in a network using reconfigurable antennas

because knowledge of the interference state of the network would be needed. This interference also depends on the specific antenna configurations used by all the transmitters in the network so it would be difficult to keep all channel and interference estimates current.

8.3 Antenna configuration selection methods

We consider three different cases for using reconfigurable antennas in the network. In the first case, which we call Double-Side Reconfigurable Antennas (DSRA), both the receiver and the transmitter of any given link can adapt its configuration. For the other two cases, either the link receiver or the link transmitter alone is allowed to switch its configuration. We refer to these situations as Receiver-Side Reconfigurable Array (RXRA) and Transmitter-Side Reconfigurable Array (TXRA), respectively. The side of the link that is not allowed to change configuration is restricted to use the most efficient configuration at all times (i.e., the short-short configuration for the RPDA case, and mode 2 for RCPA-PD). For these three different cases, we consider centralized and a distributed configuration selection schemes, discussed below.

8.3.1 Centralized configuration selection technique

To provide an upper bound on the performance of reconfigurable antennas in ad-hoc networks, we consider the use of a powerful centralized controller that has instantaneous knowledge of all communication and interference channels (e.g., $\mathbf{H}_{l_{rc},i_{tc}}, \forall l, i \in \mathcal{L}$). This controller is allowed to control the state of all reconfigurable antennas in the network to optimize the

sum capacity given in Eq. (8.3). Specifically, the central controller solves the following optimization problem:

$$\max_{\mathbf{c}}\Big(\sum_{l\in\mathcal{L}}\log_2(\det(\mathbf{I}+\frac{P_t}{\sigma_n^2 N_t}\mathbf{H}_{l_{rc},l_{tc}}\mathbf{H}^{\dagger}_{l_{rc},l_{tc}}\mathbf{W}_l^{-1}))\Big) \tag{8.4}$$

where $\mathbf{c}$ is an $1\times 2\mathcal{L}$ ia a vector that contains the configurations for each node. To solve this optimization problem, the centralized controller conducts an exhaustive search over all possible antenna configurations in all network nodes.

8.3.2 Distributed configuration selection technique

For a more practical approach to configuration selection in MIMO ad-hoc networks making use of reconfigurable antennas, we also consider a distributed configuration technique. In this technique, each link makes its own configuration selection using only the link channel ($\mathbf{H}_{l_{rc},l_{tc}}$) and interference plus noise covariance matrix $\mathbf{W}_l$. The assumption of such locally available channel information is commonly used in ad-hoc networks (e.g., [131, 141–144]). Since each link does not have information about other channels in the network, the antenna configuration decision cannot be geared towards maximizing network sum capacity. Instead, each transmitter performs configuration selection to optimize individual link capacity. Mathematically, link l solves the following optimization problem:

$$\max_{rc,tc}\Big(\log_2(\det(\mathbf{I}+\frac{P_t}{\sigma_n^2 N_t}\mathbf{H}_{l_{rc},l_{tc}}\mathbf{H}^{\dagger}_{l_{rc},l_{tc}}\mathbf{W}_l^{-1}))\Big) \tag{8.5}$$

where $\mathbf{W}_l$ continues to depend on the transmit configuration of all the other links and the receive configuration of link l. However, a change in transmit configuration for a particular link leads to a different amount of interference encountered by the other links. These other links, in turn, will have to respond to this change in interference levels by choosing their antenna configurations to maximize their own capacity. Thus, the Distributed technique is an iterative procedure where each link continually updates its configuration selection in response to changes in the interference. The procedure is very similar to the Iterative Waterfilling [142,144] algorithm, but instead of using different power allocation matrices to respond to changes in the interference, the nodes will use different antenna configuration combinations.

8.3.3 Single side reconfigurable antennas

We individually consider situations with reconfigurable antennas at both ends of the link (DSRA), at the transmitter only (TXRA), and at the receiver only (RXRA). In the Distributed configuration selection discussed previously, when reconfigurable antennas are used at the transmitter (i.e., DSRA and TXRA), there is a need for channel feedback information to be provided to the transmitter. When the receiver alone is allowed to switch antenna states, the configuration selection in the same for the Centralized and Distributed techniques. However, the selections will not necessarily be the same when the transmitter alone is allowed to switch antenna states. This result occurs because the TXRA Distributed technique will have each transmitter "selfishly" maximize its own capacity, which is not guaranteed to have a positive impact on the overall sum network capacity due to the changes

made in the interference levels seen by the other links. Furthermore, since a change in transmitter antenna configuration will lead to a change in interference seen by the rest of the network, there will be a convergence time before all antenna configurations can be finalized. For these reasons, all other things being equal, use of reconfigurable antennas only at the receiver (i.e., RXRA) in ad-hoc networks would be desirable.

The RXRA technique is also desirable in that the Distributed and Centralized schemes become equivalent; when a link maximizes its own capacity by changing reconfigurable antennas only at the receiver, it also maximizes network sum capacity. Distributed and Centralized schemes are not necessarily equivalent when reconfigurable antennas are used at the transmitters of ad-hoc network links as the "selfish" choice that each node makes to maximize its own capacity, is no longer guaranteed to have a positive impact on the overall network sum capacity.

Configuration adaptation at a single side of the link also provides a smaller search space for the Centralized technique and less channel training for the Distributed technique. For example in the case of RPDAs where there are four configurations available, a link has 16 different configuration combinations to choose from with DSRA. However, this number decreases to four configuration combinations for TXRA and RXRA. This difference in the number of available configurations, while reducing the degrees of freedom the network has, would also require less training. Less channel training may have a positive impact on the performance when the channel estimation errors are taken into account, depending on the total number of configuration combinations that need to be considered.

When assuming configuration adaptation at only one side of the link, we still assume that the other link end uses a reconfigurable antenna, since in an ad-hoc network any node can be either a receiver or a transmitter. However, the side that is not allowed to switch its configuration is restricted to use the most radiation efficient configuration at all times.

8.4 Data collection

The performance that can be achieved, in terms of sum network capacity, combining reconfigurable antennas and the techniques described in Section 8.3, was investigated through field measurements and electromagnetic ray tracing simulations in an indoor environment.

8.4.1 Measurement setup

Our measurement campaign took place in the 3^{rd} floor of the Bossone building on Drexel campus, which is the location of the Drexel Wireless Systems Laboratory (DWSL). The network topology where measurements were made is shown in Fig.8.1. For the measurements we used the HYDRA Software Defined Radio platform, described in Appendix A.

The network measurement topology is shown in Fig.8.1. Three nodes (RX1 to RX3) with two receive elements each acted as receivers and three nodes (TX1 to TX3) with two transmit elements each acted as transmitters, so as to create 6 different network topologies, by perturbing the intended receiver-transmitter pairs. To capture small scale fading effects, the receive elements were placed on a robotic antenna positioner and were moved at 40 different positions at displacements of $\lambda/10$ along the y-axis for RX1 and RX2 and along the

x-axis for RX3. At each position, 100 noisy channel estimates were captured and averaged for each subcarrier, so as to get the channel response between each receiver-transmitter pair. Based on these estimated channels for each of the positions, the sum network capacity was calculated as discussed in Section 8.3. In this way, we acquired 240 samples (6 network topologies with 40 samples each) of sum network capacities per subcarrier for each of the employed antennas and each configuration selection scheme. The response at each subcarrier was treated as an independent narrow band channel and for each location, the sum network capacity was averaged over these 52 subcarriers.

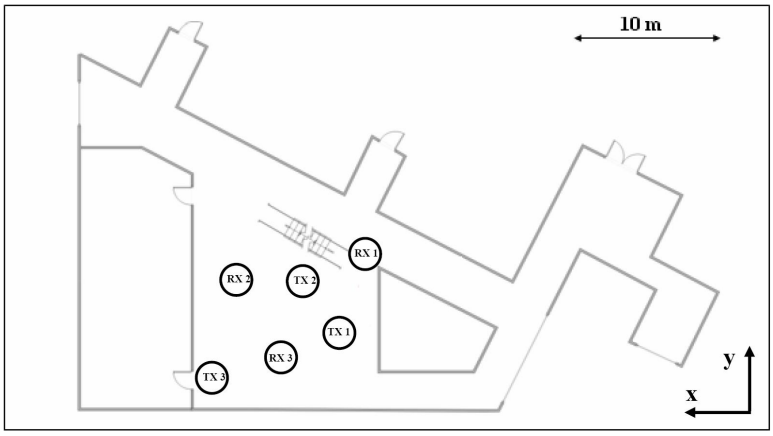

Figure 8.1: Measured Topology

The acquired channels were normalized with a common parameter, so that

$$\max_{l,i\in\mathcal{L},rc,tc} E\Big\{\sum_{s=1}^{52} |\mathbf{H}^{s}_{l_{rc},i_{tc}}||^2_F\Big\} = 4\cdot 52 \tag{8.6}$$

with the expectation over the 40 positions and subcarrier index, s. With this normalization procedure, we are able to remove path loss effects from the strongest channel, while maintaining the relative strength of the channels between the different configurations and between different receiver-transmitter pairs. This normalization was performed on a per reconfigurable antenna basis (i.e., one normalization parameter for the RCPA-PD and one for the RPDA) because of the large difference in radiation efficiency between the two antenna architectures.

8.4.2 Simulation setup

The simulated channels were acquired via numerical computation using an electromagnetic ray tracer, FASANT [95]. A 3D model of the hallway of the 3^{rd} floor of the Bossone Research building on Drexel University campus was simulated as the geometry input of FASANT.

The 3D radiation patterns of the antennas were used in the ray tracing simulation both at the receiver and at the transmitter in a 2×2 MIMO ad-hoc network. These patterns were acquired by measurements in an anechoic chamber. Note that the orientation of the reconfigurable antennas was selected such that the maximum degree of pattern diversity between the patterns of different antenna configurations was in the azimuthal plane.

The simulations were conducted by transmitting a single tone at $2.484\,GHz$ to obtain the values of the entries of the channel matrices, $\mathbf{H}$, for all channel and interference matrices. The extracted channel matrices were then used to calculate the sum network capacity for each of the methods discussed in Section 8.3.

The simulated channels, as in the measurement case, were normalized with a common

parameter, so that $\max_{l,i\in\mathcal{L},rc,tc} E\{|\mathbf{H}^s_{l_{rc},i_{tc}}||^2_F\} = 4$, with the expectation over the 40 positions. Again, like measurements, one normalization factor was used for the RPDA and another normalization factor was used for the RCPA-PD.

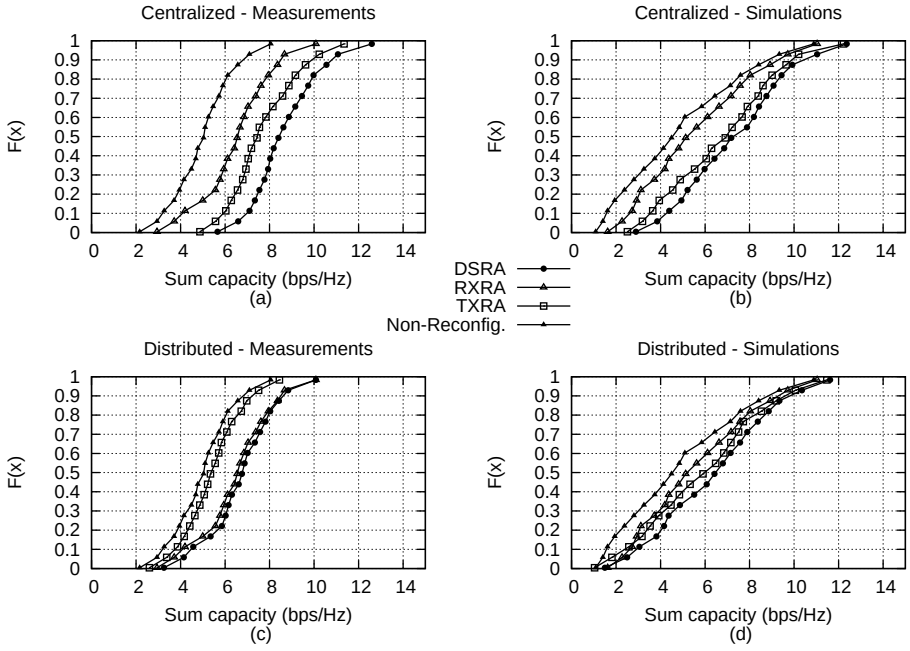

Figure 8.2: CDF of Sum Capacity for RCPA-PD with Equal Power Allocation (a)Measurements of Centralized Selection, (b)Simulations of Centralized Selection, (c)Measurements of Distributed Selection and (d)Simulations of Distributed Selection

8.5 Results

For the following results, we assumed that $\frac{P_t}{\sigma_n^2} = 100$ for all the nodes. The maximum number of iterations allowed for the Distributed TXRA and DSRA techniques was 10. If convergence was still not achieved after 10 iterations, the sum capacity achieved at the 10^{th} iteration was used in forming the CDFs that appear in Sections 8.5.1 and 8.5.2. However,

when the Distributed TXRA and DSRA techniques did not converge, the iteration count was not included in the calculation of the average number of iterations discussed in Section 8.5.1 and 8.5.2.

8.5.1 RCPA-PD

Sum capacity results

In figures 8.2(a) and 8.2(b), the CDFs of the network sum capacity using the Centralized configuration selection methods are plotted for the measured and simulated results respectively. The CDFs of sum capacity resulting from the Distributed configuration selection schemes appear in Figure 8.2(c) for the measurement results and in Figure 8.2(d) for the simulation results. Both the simulation and measurement CDFs show that the increases in sum capacity, as compared to the case where all nodes are equipped with non-reconfigurable Mode 3 circular patch antennas, are considerable. For easier comparison, the expected sum capacity resulting from these CDFs along with the capacity percentage increase of using reconfigurable antennas, are summarized in Table 8.1. From these tables, we can see that the measured sum capacity increases are greater than those predicted from the simulations. In particular, for the Centralized DSRA scheme, simulations show an increase of around 50% when using reconfigurable antennas, whereas for the measurements the percentage increase is around 75%. Not that both simulations and measurements show that relatively large sum capacity increases can be expected - the minimum increase is 8.70% for the measured Distributed TXRA case, while for the more appealing Distributed RXRA

technique (Section 8.3.3), the percentage increase is 14% for the simulations and 31% fro the measurements. The trends in selection technique performance are generally the same for both measured and simulated results. However, in the Distributed RXRA and TXRA techniques, the trends are reversed: in the measurements Distributed RXRA outperforms Distributed TXRA, while in simulations the reverse is true.

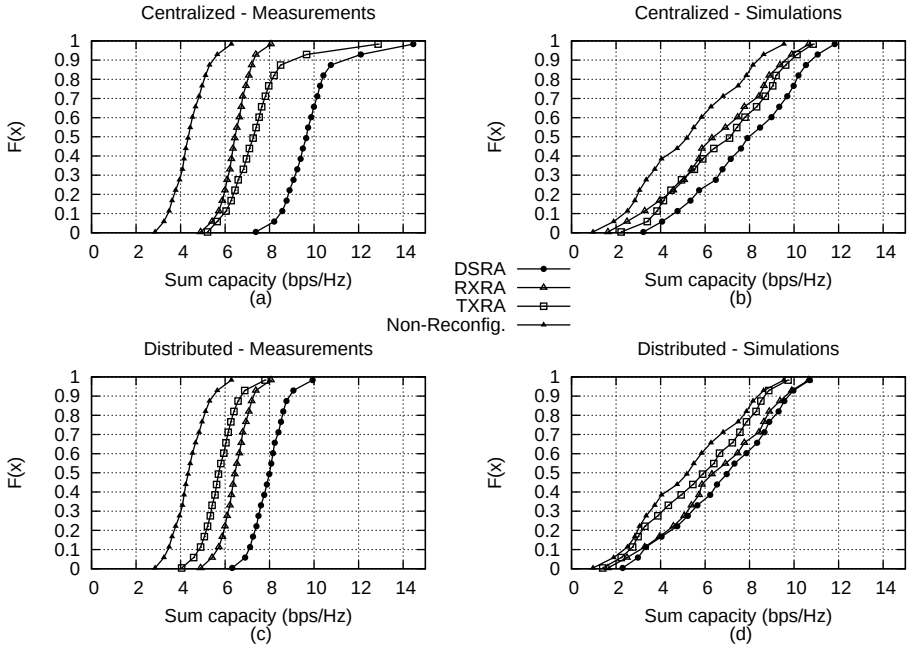

Figure 8.3: CDF of Sum Capacity for RPDA with Equal Power Allocation (a)Measurements of Centralized Selection, (b)Simulations of Centralized Selection, (c)Measurements of Distributed Selection and d)Simulations of Distributed Selection

Convergence properties

Table 8.3 shows the average number of iterations required before convergence for the iterative Distributed DSRA and Distributed TXRA techniques. From the table we can see that convergence is achieved quickly, even in the DSRA case, where both transmitter and receiver were adapting their antenna configurations. Recall that scenarios in which there was no convergence after 10 iterations were not included in the average shown in 8.3. However, in both measurements and simulations more than 99% of the scenarios reached convergence before the 10^{th} iteration.

Table 8.1: RCPA-PD mean sum network capacity.

Simulations		
Selection Technique	Mean Sum Capacity (bps/Hz)	% Increase vs. Non-Reconfigurable
DSRA - Distributed	6.40	30.77
RXRA - Distributed	5.60	14.42
TXRA - Distributed	5.91	20.93
DSRA - Centralized	7.33	49.90
RXRA - Centralized	5.60	14.42
TXRA - Centralized	6.79	38.80
Non-Reconfigurable	4.89	0
Measurements		
DSRA - Distributed	6.84	35.51
RXRA - Distributed	6.60	30.81
TXRA - Distributed	5.49	8.70
DSRA - Centralized	8.87	75.68
RXRA - Centralized	6.60	30.81
TXRA - Centralized	7.83	55.11
Non-Reconfigurable	5.05	0

8.5.2 RPDA

Sum capacity results

The network sum capacity CDFs for the Centralized selection schemes when the nodes are equipped with RPDAs appear in Figure 8.3(a) for measurements and in figure 8.3(b) for simulations. The corresponding sum capacity CDFs when the configuration selection is performed in a Distributed manner appear in Figure 8.3(c) for the measurements and in Figure 8.3(d) for the simulations. In Table 8.2 the expected sum capacities resulting from these CDFs are gathered together with the percentage increase in expected network sum capacity versus the non-reconfigurable case, where all the nodes were equipped with dipoles in the "short-short" configuration. As in the RCPA-PD results, we again see that the simulations underestimated the performance increase that was observed using the measurement results. However for the RPDA results, the relative performance between the configuration selection schemes is maintained between measurements and simulations, with the Centralized DSRA technique performing the best and the Distributed TXRA technique performing the worst of all techniques using reconfigurable antennas. By comparing these results with the RCPA-PD results in the previous Section, we can see that in both simulations and measurements, RPDAs provide a larger percentage increase in capacity than RCPAs. Furthermore, we can see that the worst we can expect as a percentage increase in sum capacity relative to non-reconfigurable antennas is 10% for the simulated TXRA technique and 30% for the measured TXRA technique. For the desirable Distributed RXRA scheme discussed in Section 8.3.3, there is a simulated increase in capacity of 24% and an increase of 31% in

measured capacity relative to non-reconfigurable antennas.

Convergence properties

The two iterative configuration selection schemes using RPDAs needed on average more iterations before convergence than the RCPA-PD case, as shown in Table 8.3. This longer convergence time can be attributed to the fact that RPDAs have more configurations to choose from than the RCPAs. The greater number of configurations to choose from also increased the number of scenarios in which there was no convergence after 10 iterations. In particular, for the measurement data, in the Distributed DSRA case, 26% of the scenarios did not converge before 10 iterations. Similarly, in the Distributed TXRA case, 7% of the scenarios did not converge before 10 iterations. While it would certainly have been possible to continue the iterative process until convergence was achieved, we chose to limit the number of iterations to 10 before stopping the configuration update process because a practical system would not have an indefinite amount of time for configuration selection before network information became outdated.

8.5.3 Comparing RCPA-PD with RPDA

A direct comparison of the performance of the RPDA and the RCPA-PD, when employed in an ad-hoc network shows that the performance of the RPDA is higher - both in percentage increase relative to non-reconfigurable architectures, and in absolute sum network capacity values. The performance of a reconfigurable antenna array should be a function of the following factors: *i.)* the number of configurations available, *ii.)* the pattern diver-

Table 8.2: RPDA mean sum network capacity

Simulations		
Selection Technique	Mean Sum Capacity (bps/Hz)	% Increase vs. Non-Reconfigurable
DSRA - Distributed	6.83	30.40
RXRA - Distributed	6.51	24.38
TXRA - Distributed	5.78	10.31
DSRA - Centralized	7.91	51.04
RXRA - Centralized	6.51	24.38
TXRA - Centralized	6.85	30.79
Non-Reconfigurable	5.23	0
Measurements		
DSRA - Distributed	8.00	81.42
RXRA - Distributed	6.48	46.85
TXRA - Distributed	5.77	30.71
DSRA - Centralized	9.83	122.76
RXRA - Centralized	6.48	46.85
RXRA - Centralized	7.48	69.42
Non-Reconfigurable	4.41	0

sity between different configurations and, *iii.)* the relative efficiency between the different configurations. While the relative radiation efficiency between RPDA and RCPA-PD is important, the normalization process described in Section 8.4, effectively sets the efficiency of RPDA configuration "short-short" equal to RCPA-PD configuration Mode 3. If we had not performed this normalization, a direct comparison between the two architectures would not have been possible, since RPDA efficiency is much higher than that of the RCPA-PD.

The superior performance of the RPDA, as compared to the RCPA-PD, can be explained by the fact that the RPDA has more configurations available (4 configurations per array as opposed to 2 for the RCPA-PD) and that its configurations are closer to each other in terms of efficiency (i.e., RPDA efficiency varies from 84% to 48% as opposed to the RCPA-PD

Table 8.3: Average number of iteration before convergence.

Antenna	Selection Technique	Simulations	Measurements
RCPA-PD	DSRA - Distributed	2.1	1.9
RCPA-PD	TXRA - Distributed	1.7	1.2
RPDA	DSRA - Distributed	2.5	3.0
RPDA	RXRA - Distributed	2.0	2.3

where the efficiency varies from 21% to 5%). On the other hand, the RCPA-PD does have an advantage in that the radiation patterns of all available configurations show very low correlation (Table 6.2).

Table 8.4: Mean sum network capacity - RPDA results using "short-short" and "long-long" configurations.

Simulations		
Selection Technique	Mean Sum Capacity (bps/Hz)	% Increase vs. Non-Reconfigurable
DSRA - Distributed	5.93	13.3
RXRA - Distributed	5.84	11.58
TXRA - Distributed	5.38	2.76
DSRA - Centralized	6.60	26.06
RXRA - Centralized.	5.84	11.58
TXRX - Centralized	6.04	15.31
Non-Reconfigurable	5.23	0
Measurements		
DSRA - Distributed	6.41	45.23
RXRA - Distributed	5.50	24.70
TXRA - Distributed	5.33	20.73
DSRA - Centralized	7.3	65.37
RXRA - Centralized	5.50	24.70
RXRA - Centralized	6.23	41.06
Non-Reconfigurable	4.41	0

8.5.4 Effect of the number of configurations

In order to better analyze the effects of the number of available configurations, we calculated the sum network capacity for the case where the RPDAs were only allowed to switch between the "short-short" and the "long-long" configurations. In this case, we are able to gain insight into the importance of having a large number of array configurations. In this situation, the RPDA has as many configuration settings as the RCPA-PD, but with radiation patterns that are highly correlated (Table 4.3). Comparing Table 8.4 with Table8.2 from Section 8.5.2, we see that the percentage capacity increase relative to the non-reconfigurable case was almost halved for both measurements and simulations when the RPDA was restricted in switching only between the "short-short" and "long-long" configurations. These results highlight the importance of having a large number of antenna configurations to switch between, even if these configurations have radiation patterns that are relatively highly correlated.

We can also observe the RCPA-PD performs better, in absolute numbers, than the RPDA when the RPDA is confined to using only 2 of the available configurations. This result holds true even though the radiation efficiency difference between "short-short" configuration and "long-long" configuration is smaller than the radiation efficiency difference between Modes 3 and 4 of the RCPA-PD. This result is due to the smaller correlation that exists between Mode 3 and 4 patterns in the RCPA-PD, as compared to the correlation between "short-short" and "long-long" patterns in the RPDA. The effect of uncorrelated patterns will be considered in more detail in the next Section.

Table 8.5: Mean sum capacity for patterns normalized separately with RPDA using only "short-short" and "long-long" configurations.

Simulations		
Selection Technique	RPDA Mean Sum Capacity (bps/Hz)	RCPA-PD Mean Sum Capacity (bps/Hz)
DSRA Distributed	6.43	7.13
RXRA Distributed	6.01	6.07
TXRA Distributed	5.54	5.91
DSRA Centralized	6.85	8.05
RXRA Centralized	6.01	6.07
TXRA Centralized	5.97	6.84
Non-Reconfigurable	5.23	4.89
Measurements		
DSRA Distributed	6.42	8.12
RXRA Distributed	5.51	6.80
TXRA Distributed	5.35	6.12
DSRA Centralized	7.31	9.17
RXRA Centralized	5.51	6.80
TXRA Centralized	6.23	7.52
Non-Reconfigurable	4.41	5.05

8.5.5 Effect of correlation between the patterns

In this Section, we introduce a new normalization procedure to isolate the effect of correlation between the radiation patterns in reconfigurable antennas. In particular, we normalized each antenna configuration separately, so that the maximum expected squared Frobenious norm between the channels with the same configuration combination would be the same. Thus, there are four normalization factors for the "reduced" RPDA discussed in the previous Section (i.e., one for when the transmitters use the "short-short" configuration and the receivers the "short-short" configuration, another for the transmitters using "short-short" and the receivers "long-long", etc). Similarly, there are four normalization factors for the

RCPA-PD (i.e., one for when the transmitters are using Mode 3 and the receivers Mode 3,another for the transmitters using Mode 3 and the receivers Mode 4,etc). In this way, we removed the effects of radiation efficiency, forcing all configuration combinations to "receive" the same power, while keeping the relative channel strengths of the different links in the topology. Mathematically, the normalization parameter for the case where the receiver was using configuration rx and the transmitter was using configuration tx was chosen such that $\max_{l,i} E\left\{|\mathbf{H}_{l_{rc},i_{tc}}|_F^2\right\} = 4$ for simulations and $\max_{l,i} E\left\{\sum_{s=1}^{52} |\mathbf{H}_{l_{rc},i_{tc}}|_F^2\right\} = 4 \cdot 52$ for measurements, with the expectation taken along the 40 points.

The RPDA performance was again considered for the case where only the "short-short" and the "long-long" configurations were used. In this way, we can compare the performance of two reconfigurable antenna array structures, with each having 2 configurations available and with all the configurations having the same radiation efficiency. The only difference between the two structures is the correlation between the available configurations. The RCPA-PD structure exhibits almost uncorrelated patterns (Table 5.3), while the RPDA configurations are highly correlated (Table 4.3). The calculated expected sum network capacities appear in Table 8.5.

From this table, we can see that the less correlated patterns that the RCPA-PD offers significantly improves the expected sum capacity. We can also observe that the capacity values for the RPDA do not change much with this new normalization, unlike the RCPA-PD values, whose mean sum capacity values are significantly improved by forcing both modes to receive the same power. These results show that uncorrelated radiation patterns, as well as

the number of configurations and relative radiation efficiency, can be a mechanism through which reconfigurable antennas enhance ad-hoc networks.

8.6 Summary

The achieved results show the effectiveness of using multi element reconfigurable antennas in wireless ad hoc networks. Pattern reconfigurability allows to decrease the co-channel interference with respect to common non reconfigurable antenna systems while taking full advantage of the benefits that derive from using multi element reconfigurable antennas in single link communication systems. In particular, we showed the importance of having a high number of array configurations characterized by low pattern correlation in order to take full advantage of reconfigurable multi element antenna in ad hoc networks.

We proposed two different control schemes that can de used to drive reconfigurable antennas in ad hoc networks. The Distributed technique in which only the receiver is allowed to switch configurations (i.e., RXRA) was shown to strike a good balance between sum network capacity increases and practical channel feedback and network information constraints.

Chapter 9: Conclusions

MIMO communication system has recently emerged as one of the most significant technical breakthroughs in modern communications. The potential benefit of this technology is enhanced channel capacity and improved robustness of the link. In this dissertation the benefits of MIMO communications are dramatically improved through a combination of novel adaptive antenna array structures and algorithms that drive the antenna elements for adaptation to the changing multivariate channel.

Three different novel classes of electrically multi element reconfigurable antennas have been proposed: *i*) reconfigurable printed dipole that exploits the inter element mutual coupling to achieve pattern reconfigurability, *ii*) circular patches capable of exciting higher order modes to achieve pattern and polarization diversity, and *iii*) metamaterial leaky wave array that can be reconfigured in pattern to achieve unprecedented degrees of pattern reconfigurability.

Each antenna structure is capable of achieving high improvement with respect to standard non reconfigurable antennas while being compact in size with respect to standard multi element antennas (see Fig.9.1). We demonstrated the benefits achievable with such multi element reconfigurable antennas through channel measurements and electromagnetic simulations and we provided a complete methodology to analyze the benefit and drawbacks of these antenna systems in MIMO communications. In particular we demonstrated the

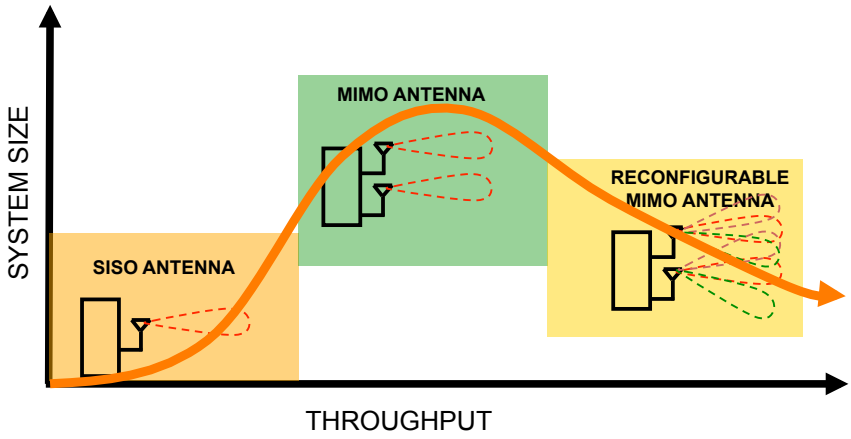

Figure 9.1: Potential of reconfigurable MIMO antenna systems with respect to standard MIMO and SISO systems.

importance of having reconfigurable multi element antennas with a high number of configurations decorrelated from one other, with high decorrelation between the radiation patterns excited at the different array elements and with small differences in radiation efficiency and impedance matching between the different configurations. Each of these antenna parameters can greatly affect the system performance achievable with reconfigurable multi element array and they need to be carefully analyzed when designing such antennas.

According to the results obtained through this work we showed that such antennas can be used to improve the channel capacity with respect to standard antenna systems or to achieve performance comparable to that of standard multi element antenna systems while saving a considerable amount of transmitted power. Great benefit can be achieved with these antennas both in single link communications and in next generation ad hoc networks. Thanks to their capability of dynamically changing the radiation properties these

antennas can be used to "create" an optimal wireless channel between the transmitter and the receiver. The communication channel is optimized for maximum throughput in single link communications, while it needs to be tuned for maximum throughput and minimum co-channel interference in ad hoc networks.

To effectively use such antennas without the need of switching between all the array configurations prior selecting the optimal one, we developed a selection algorithm that can be used with pattern reconfigurable antennas. The nested dependence between the environment that surround the antenna and the antenna radiation characteristics was exploited to propose an efficient selection scheme. Such algorithm has been tailored on the radiation characteristics of a reconfigurable circular patch array and its achievable performance have been studied with electromagnetic simulations. Through this work we demonstrated a first complete reconfigurable antenna system composed of mutli element reconfigurable antennas and a control unit capable of efficiently "drive" the antennas to deliver unprecedented system performance.

Overall the most fascinating result to which this research has led is the use of reconfigurable antennas for MIMO systems as solutions for portable devices to maintain good communication link capacity. Moreover the combined use of reconfigurable antenna systems and selection schemes for driving the antennas showed the possibility of developing a complete smart communication system capable of sensing the channel and providing the optimal solution to achieve the best communication performances. From this point of view this research contributed to the development of cognitive radio systems, which are based

on highly reconfigurable transceivers and constitute one of the main areas of research for future communications.

The promising performance achievable with such reconfigurable MIMO systems have driven a lot of attention in the antenna and wireless communication community and several research groups have also started investigating such technology [42,104,145–147]. From the obtained results, further developments in the direction of conceiving adaptive and cognitive communication systems can be undertaken. In particular future work in this research area may address the following topics:

Miniaturized reconfigurable array for portable devices: the proposed MIMO array design can be further miniaturized to satisfy more stringent size constraints of portable devices. Recent advances in the field of metamaterials can be exploited to notably decrease the size of the printed antenna while maintaing good radiation characteristics. Examples of such miniaturization techniques are the zero order resonator metamaterial antennas [148] and antennas built on substrate with enhanced permeability and permittivity [149, 150].

Configuration selection algorithm: novel selection algorithms that can be used to control multi element reconfigurable antennas when used in single link and ad hoc networks need to be developed. The same selection approach proposed in this thesis can be adopted for other antennas systems and it can be further improved to be used with pattern and polarization reconfigurable antennas.

Integration with adaptive transmission schemes: more complex adaptive algorithm can be conceived capable not only of switching between array radiation patterns,

but also between different transmission techniques, modulation schemes and frequencies of operation in order to dramatically improve the degrees of freedom available in the communication system.

Improvement of the switching system: the proposed antenna design were developed using PIN diode switches. These switches however introduce losses that affect the overall array radiation efficiency and power consumption. MEMS switches should be investigated as a suitable candidate for diminishing the RF and DC power consumption. Though current MEMS switches are still not reliable and have relatively slow switching time compared to PIN diodes, further development in this area could lead to the possibility of having more switches per antenna and consequent higher levels of complexity and capacity improvement.

Appendix A: MIMO channel sounder

For measurements, a multi-node MIMO-OFDM communication network was used. Each node (see Fig.A.1) consists of 802.11a/b/g transceivers to implement the RF front end, and high-speed sampling boards and arbitrary waveform generator boards to implement the baseband. Each node has two RF antenna array elements and transceivers, and the system can be expanded without re-design to 4 array elements and transceivers.

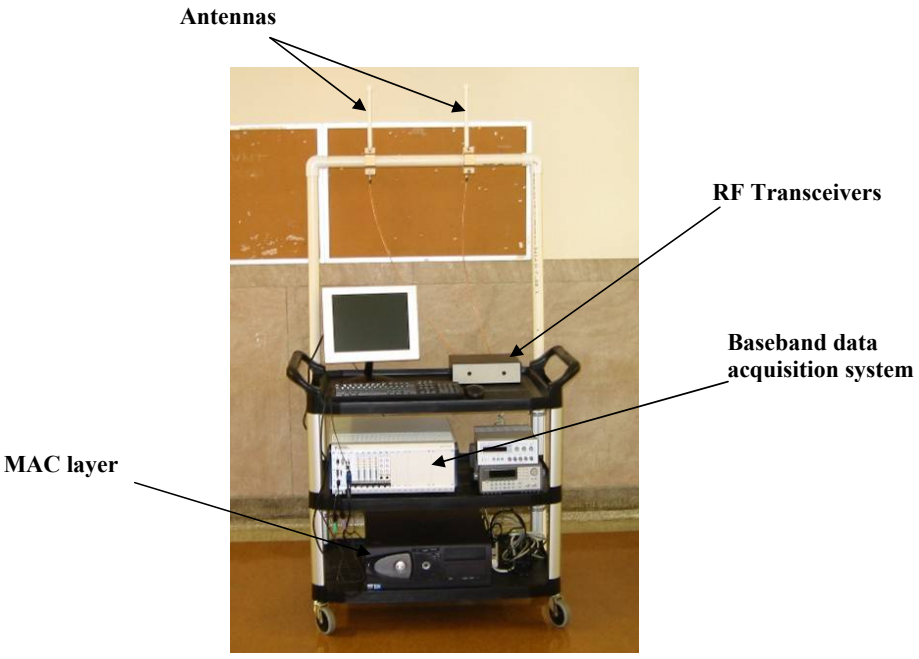

Figure A.1: MIMO channel sounder.

In each node, there are three main components, an analog front end/transceiver that

can include conformal or standalone antenna arrays, a frequency agile RF transceiver (RCS 110), a software defined baseband data acquisition system, and general purpose PCs for the MAC and higher layers. The RF transceiver cards are capable of transmitting at all channels in both the Industrial, Science, and Medicine (ISM) band between 2.4 and 2.5 GHz as well as in the Unlicensed National Information Infrastructure (UNII) band between 4.9 and 5.9 GHz. The cards are designed to operate independently of existing wireless standard, and thus provide maximum flexibility.

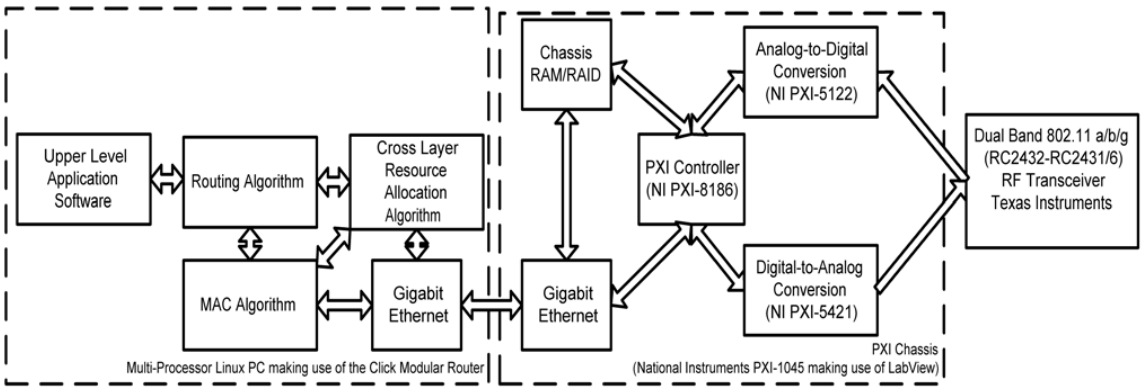

Figure A.2: Schematic of the MAC and physical layer of the channel sounder.

The analog front end and the baseband data acquisition system are all contained in a PXI chassis from National Instruments. Analog signals are converted to and from digital using PXI data acquisition cards from National Instruments and then passed to a dedicated chassis processor (PXI-8186) which implements the physical layer in LabView. This processor then communicates over gigabit ethernet with a general purpose host which runs the MAC, higher layer network protocols, and any application software. A schematic of the MAC layer, the

physical layer and the RF front-end of the node is shown in Fig.A.2.

Each node is capable to support different modulation scheme, from BPSK up to 64 QAM. The generated analog signal is modulated using OFDM with the data being sent on 52 sub-carriers. The spacing between each sub carrier is 312.5 KHz. The baseband data acquisition system is equipped with A/D and D/A converters that operate at 100 MS/s with 14-bit quantization.

Appendix B: Table of symbols

Symbol	Description
$*$	convolution operator
$C^{n\times m}$	operator to denote complex matrix with dimension$n \times m$
$(\cdot)^{\dagger}$	conjugate transpose operator
$\cdot$	inner product operator
$(\cdot)^{*}$	conjugate operator
$(\cdot)^{T}$	transpose operator
$\lvert \cdot \rvert$	absolute value operator
$\otimes$	Kronecker product operator
$\lvert\lvert \cdot \rvert\rvert_F$	Frobenius norm operator
A	amplitude of a transmitted data symbol
A_p	amplitude of a transmitted training symbol
$\mathbf{a}_r$	receive array factor
$\mathbf{a}_t$	transmit array factor
C	channel capacity
$\mathbf{c}$	vector of antenna configurations for all links in an ad hoc network
d	array elements separation
D_λ	reciprocal condition number
$\mathbf{E}$	far field radiation pattern
$\mathbf{E}_{iso}$	far field radiation pattern of an isotropic radiator
E_θ	θ component of the radiated electric field
E_ϕ	ϕ component of the radiated electric field
f	frequency of operation
$\mathbf{G}$	measured channel matrix without normalization
$g_{i,j}$	entries of the measured channel matrix $\mathbf{G}$
$\mathbf{H}$	channel matrix
$\hat{\mathbf{H}}$	estimated channel matrix using MMSE receivers
$\mathbf{H}_{los}$	channel matrix of the LOS components
$\mathbf{H}_{nlos}$	channel matrix of the NLOS components
$\mathbf{H}_w$	matrix of complex Gaussian coefficients
$\mathbf{H_e}$	MMSE estimation error on $\mathbf{H}_w$
h	substrate thickness

Symbol	Description
$\mathbf{I}$	identity matrix
J_n	Bessel function of the first kind and order n
K	Ricena K-factor
k_0	free space wavenumber
L	number of symbols composing a training sequence
$\mathcal{L}$	number of links in an ad hoc networks
m	total number of subcarriers
N	number of rays
N_F	normalization factor
N_r	number of receive antenna elements
N_t	number of transmit antenna elements
$\mathbf{n}$	complex additive white Gaussian noise
P	number of configurations at the receiving reconfigurable array
P_{av}	average transmit power from all antennas of the transmitting array
$P(\Omega)$	power angular spectrum
P_ϕ	power angular spectrum of the ϕ component
P_θ	power angular spectrum of the θ component
P_t	transmitted power at each antenna element
Q	number of configurations at the transmitting reconfigurable array
$\mathbf{Q}$	power covariance matrix
$Q(\Omega)$	power angular spectrum pdf
Q_R	antenna radiation quality factor
Q_T	antenna total quality factor
$\mathbf{R}_H$	channel covariance matrix
R_{max}	maximum throughput
$\mathbf{R}_r$	receive spatial correlation matrix
$\mathbf{R}_t$	transmit spatial correlation matrix
r	entry of the spatial correlation matrices $\mathbf{R}_t$ and $\mathbf{R}_r$
S_{11}	voltage reflection coefficient
SNR	signal to noise ratio
T	number of symbols composing a training period
$tan\delta$	tangent loss
$\mathbf{V}$	unitary polarization matrix
V_0	edge voltage in a circular patch antenna
v	noise at the receiver
$\mathbf{W}$	interference plus noise covariance matrix
$\mathbf{x}$	signal vector at the transmitter
$\mathbf{y}$	signal vector at the receiver
α	attenuation constant
β	phase constant

Symbol	**Description**
γ	complex propagation constant
δ	Dirac delta function
Δf	frequency bandwidth
ΔP_t	difference in transmit power
ϵ_r	dielectric permittivity
ζ	parameter that relates A to A_p
η	antenna radiation efficiency
θ	elevation angle
λ	wavelength
λ_{max}	maximum eigenvalue of the spatial correlation matrix
λ_{min}	minimum eigenvalue of the spatial correlation matrix
ρ	circular patch antenna radius
μ	percentage of power allocated to the training symbols
μ_s	substrate dielectric permeability
σ	material conductivity
$\sigma^2_{H_e}$	variance of the MMSE estimation error
σ^2_n	variance of the additive white Gaussian noise
$\boldsymbol{\Upsilon}$	covariance matrix of the random vector $\mathbf{H_e x}$
ϕ	azimuth angle
ϕ_1, ϕ_2	azimuth displacements of feed point 1 and 2 in a circular patch
ϕ_c	mean angle of arrival
$\chi_n^{'}$	first zero of the derivative of the Bessel function J_n
ψ	complex Raileigh channel coefficient
Ω	solid angle

Appendix C: Table of acronyms

Acronym	Definition
DSRA	Double Side Reconfigurable Antennas
MIMO	Multiple Input Multiple Output
RCN	Reciprocal Condition Number
RCPA	Reconfigurable Circular Patch Antenna
RCPA-PD	Reconfigurable Circular Patch Antenna for Pattern Diversity
RCPA-PPD	Reconfigurable Circular Patch Antenna for Pattern and Polairization Diversity
RPDA	Reconfigurable Printed Dipole Array
RLWA	Reconfigurable Leaky Wave Antenna
RX	Receiver
RXRA	Receiver Side Reconfigurable Array
SNR	Signal to Noise Ratio
TX	Transmitter
TXRA	Transmitter Side Reconfigurable Array

Bibliography

[1] G.J. Foschini and M.J. Gans, "On limits of wireless communications in a fading environment when using multiple antennas," *Wireless Personal Communications*, vol. 6, no. 3, pp. 311 – 335, 1998.

[2] G.J. Foschini, "Layered space-time architecture for wireless communication in a fading environment when using multi-element antennas," *Bell Labs Technical Journal*, vol. 1, no. 2, pp. 41 – 59, 1996.

[3] G.G. Raleigh and J.M. Cioffi, "Spatio-temporal coding for wireless communication," *IEEE Transactions on Communications*, vol. 46, no. 3, pp. 357 – 366, 1998.

[4] H. Boleskei, D. Gesbert, and A.J. Paulraj, "On the capacity of OFDM-based multi-antenna systems," *Proceedings of the IEEE International Conference on Acoustics Speech and Signal Processing*, vol. 5, pp. 2569 – 2572, 2000.

[5] V. Pohl, V. Jungnickel, T. Haustein, and C. Von Helmolt, "Antenna spacing in MIMO indoor channels," *Proceedings of the IEEE Vehicular Technology Conference*, vol. 2, pp. 749 – 753, 2002.

[6] D. Liang, C. Hosung, R. W. Heath Jr., and L. Hao, "Simulation of MIMO channel capacity with antenna polarization diversity," *IEEE Transactions on Wireless Communications*, vol. 4, no. 4, pp. 1869 – 73, 2005.

[7] D. Liang, L. Hao, and R. W. Heath Jr., "Multiple-input multiple-output wireless communication systems using antenna pattern diversity," *Proceedings of the IEEE Global Telecommunications Conference*, vol. 1, pp. 997 – 1001, 2002.

[8] A. Forenza and R. W. Heath Jr., "Benefit of pattern diversity via two-element array of circular patch antennas in indoor clustered MIMO channels," *IEEE Transactions on Communications*, vol. 54, no. 5, pp. 943 – 954, 2006.

[9] M.R. Andrews, P.P. Mitra, and R. DeCarvalho, "Tripling the capacity of wireless communications using electromagnetic polarization," *Nature*, pp. 316 – 318, 2001.

[10] D.D. Stancil, A. Berson, J.P. Van't Hof, R. Negi, S. Sheth, and P. Patel, "Doubling wireless channel capacity using co-polarised, co-located electric and magnetic dipoles," *Electronics Letters*, vol. 38, no. 14, pp. 746 – 747, 2002.

[11] P. Mattheijssen, M.H.A.J. Herben, G. Dolmans, and L. Leyten, "Antenna-pattern diversity versus space diversity for use at handhelds," *IEEE Transactions on Vehicular Technology*, vol. 53, no. 4, pp. 1035 – 1042, 2004.

[12] S. Sanayei and A. Nosratinia, "Antenna selection in MIMO systems," *IEEE Communications Magazine*, vol. 42, no. 10, pp. 68 – 73, 2004.

[13] A.F. Molisch and M.Z. Win, "MIMO systems with antenna selection," *IEEE Microwave Magazine*, vol. 5, no. 1, pp. 46 – 56, 2004.

[14] D.A. Gore, R. W. Heath Jr., and A.J. Paulraj, "Transmit selection in spatial multiplexing systems," *IEEE Communications Letters*, vol. 6, no. 11, pp. 491 – 493, 2002.

[15] A. Gorokhov, "Antenna selection algorithms for MEA transmission systems," *Proceedings of IEEE International Conference on Acoustics, Speech, and Signal Processing*, vol. 3, 2002.

[16] M. Chryssomallis, "Smart antennas," *IEEE Antennas and Propagation Magazine*, vol. 42, no. 3, pp. 129 – 136, 2000.

[17] A. Alexiou and M. Haardt, "Smart antenna technologies for future wireless systems: trends and challenges," *IEEE Communications Magazine*, vol. 42, no. 9, pp. 90 – 97, 2004.

[18] C.A. Balanis, *Antenna theory: analysis and design*, Wiley, 2005.

[19] S. Kozowski, Y. Yashchyshyn, and J. Modelski, "Performance of MIMO system with receiver employing phased array antennas," *Proceedings of the 9th International Conference, CADSM 2007*, pp. 133 – 135, 2007.

[20] L. Bai and P. Yang, "Application of phased array in MIMO system," *Proceedings of International Conference on Wireless Communications, Networking and Mobile Computing*, 2008.

[21] S. Nikolaou, R. Bairavasubramanian, C. Lugo Jr., I. Carrasquillo, D. C. Thompson, G. E. Ponchak, J. Papapolymerou, and M.M. Tentzeris, "Pattern and frequency reconfigurable annular slot antenna using pin diodes," *IEEE Transactions on Antennas and Propagation*, vol. 54, no. 2, pp. 439 – 448, 2006.

[22] R.F. Harrington, "Reactively controlled directive arrays.," *IEEE Transactions on Antennas and Propagation*, vol. 26, no. 3, pp. 390 – 395, 1978.

[23] D. Sievenpiper, J. Schaffner, B. Loo, G. Tangonan, R. Harold, J. Pikulski, and R. Garcia, "Electronic beam steering using a varactor-tuned impedance surface," *Proceedings of International Symposium on Antennas and Propagation*, vol. 1, pp. 174 – 177, 2001.

[24] R. Schlub, D.V. Thiel, J.W. Lu, and S.G. O'Keefe, "Dual-band six-element switched parasitic array for smart antenna cellular communications systems," *Electronics Letters*, vol. 36, no. 16, pp. 1342 – 1343, 2000.

[25] D.V. Thiel, "Switched parasitic antennas and controlled reactance parasitic antennas: A systems comparison," *Proceedings of IEEE International Symposium Antennas and Propagation*, vol. 3, pp. 3211 – 3214, 2004.

[26] D. V. Thiel, "Impedance variations in controlled reactance parasitic antennas," *Proceedings of IEEE International Symposium Antennas and Propagation*, vol. 3, pp. 671 – 674, 2005.

[27] S. Zhang, G.H. Huff, J. Feng, and J.T. Bernhard, "A pattern reconfigurable microstrip parasitic array," *IEEE Transactions on Antennas and Propagation*, vol. 52, no. 10, pp. 2773 – 2776, 2004.

[28] G.H. Huff, J. Feng, S. Zhang, and J.T. Bernhard, "A novel radiation pattern and frequency reconfigurable single turn square spiral microstrip antenna," *IEEE Microwave and Wireless Components Letters*, vol. 13, no. 2, pp. 57 – 59, 2003.

[29] A. Handerson, J.R. James, A. Fray, and G.D. Evans, "New ideas for beam scanning using magnetised ferrite," *Proceedings of the IEE Colloquium on Electronically Scanned Antennas*, vol. 1, 1988.

[30] G. Lovat, P. Burghignoli, and S. Celozzi, "A tunable ferroelectric antenna for fixed-frequency scanning applications," *IEEE Antennas and Wireless Propagation Letters*, 2006.

[31] Y. Yashchyshyn and J. Modelski, "Rigorous analysis and investigations of the scan antenna on ferroelectric substrate," *Proceedings of the 15th International Conference on Microwaves, Radar and Wireless Communications, MIKON - 2004*, vol. 2, pp. 391 – 394, 2004.

[32] V.K. Varadan, V.V. Varadan, K.A. Jose, and J.F. Kelly, "Electronically steerable leaky wave antenna using a tunable ferroelectric material," *Smart Materials and Structures*, vol. 3, no. 4, pp. 470 – 475, 1994.

[33] D. Sievenpiper, J. Schaffner, J.J. Lee, and S. Livingston, "A steerable leaky-wave antenna using a tunable impedance ground plane," *IEEE Antennas and Wireless Propagation Letters*, vol. 1, pp. 179 – 182, 2002.

[34] D. Sievenpiper and J. Schaffner, "Beam steering microwave reflector based on electrically tunable impedance surface," *Electronics Letters*, vol. 38, no. 21, pp. 1237 – 1238, 2002.

[35] J.C. Chiao, Y. Fu, I.M. Chio, M. DeLisio, and L.Y. Lin, "MEMS reconfigurable vee antenna," *Proceedings of the IEEE MTT-S International Microwave Symposium Digest*, vol. 4, pp. 1515 – 1518, 1999.

[36] K. Chang, M.Y. Li, T.Y. Yun, and C.T. Rodenbeck, "Novel low-cost beam-steering techniques," *IEEE Transactions on Antennas and Propagation*, vol. 50, no. 5, pp. 618 – 627, 2002.

[37] M. Boti, L. Dussopt, and J.-M. Laheurte, "Circularly polarized antenna with switchable polarization sense," *Electronics Letters*, vol. 36, no. 18, pp. 1518 – 1519, 2000.

[38] Y.J. Sung, T.U. Jang, and Y.-S. Kim, "A reconfigurable microstrip antenna for switchable polarization," *IEEE Microwave and Wireless Components Letters*, vol. 14, no. 11, pp. 534 – 536, 2004.

[39] M.K. Fries, M. Grani, and R. Vahldieck, "A reconfigurable slot antenna with switchable polarization," *IEEE Microwave and Wireless Components Letters*, vol. 13, no. 11, pp. 490 – 492, 2003.

[40] R.N. Simons, D. Chun, and L.P.B. Katehi, "Polarization reconfigurable patch antenna using microelectromechanical systems (MEMS) actuators," *Proceedings of IEEE International Symposium Antennas and Propagation*, vol. 2, pp. 6 – 9, 2002.

[41] P.J. Rainville and F.J. Harackiewicz, "Magnetic tuning of a microstrip patch antenna fabricated on a ferrite film," *IEEE Microwave and Guided Wave Letters*, vol. 2, no. 12, pp. 483 – 485, 1992.

[42] A. Grau, H. Jafarkhami, and F. De Flaviis, "A reconfigurable multiple-input multiple-output communication system," *IEEE Transactions on Wireless Communications*, vol. 7, no. 5, 2008.

[43] D. Piazza and K.R. Dandekar, "Reconfigurable antenna solution for MIMO-OFDM systems," *Electronics Letters*, vol. 42, no. 8, pp. 15 – 16, 2006.

[44] D. Piazza, N.J. Kirsch, A. Forenza, R.W. Heath Jr., and K.R. Dandekar, "Design and evaluation of a reconfigurable antenna array for MIMO systems," *IEEE Transactions on Antennas and Propagation*, vol. 56, no. 3, 2008.

[45] D. Piazza, P. Mookiah, M. D'Amico, and K.R. Dandekar, "Computational electromagnetic analysis of a reconfigurable multiport circular patch antenna for MIMO communications," *Proceedings of the 2007 URSI Electromagnetic Theory Symposium*, 2007.

[46] D. Piazza, P. Mookiah, M. D'Amico, and K.R. Dandekar, "Two port reconfigurable circular patch antenna for MIMO systems," *Proceedings of the European Conference on Antennas and Propagation, (EuCAP)*, 2007.

[47] D. Piazza, P. Mookiah, M. D'Amico, and K.R. Dandekar, "Pattern and polarization reconfigurable circular patch for MIMO systems," *Proceedings of the 2009 European Conference on Antennas and Propagation (EuCAP)*, 2009.

[48] D. Piazza, M. D'Amico, and K.R. Dandekar, "Two port reconfigurable CRLH leaky wave antenna with improved impedance matching and beam tuning," *Proceedings of the 2009 European Conference on Antennas and Propagation (EuCAP)*, 2009.

[49] D. Piazza, P. Mookiah, M. D'Amico, and K.R. Dandekar, "Experimental analysis of pattern and polarization reconfigurable circular patch antennas for MIMO systems," *Submitted to IEEE Transaction on Antennas and Propagation.*

[50] D. Piazza, M. D'Amico, and K.R. Dandekar, "Two port reconfigurable crlh leaky wave antenna for mimo systems," *Submitted to IEEE Antennas and Wireless Propagation Letters.*

[51] J. Kountouriotis, D. Piazza, P. Mookiah, M. D'Amico, and K.R. Dandekar, "Reconfigurable antennas for MIMO ad-hoc networks," *Proceedings of IEEE Radio and Wireless Symposium*, 2008.

[52] J. Kountouriotis, D. Piazza, P. Mookiah, M. D'Amico, and K.R. Dandekar, "Reconfigurable antennas and configuration selection method for MIMO ad-hoc networks," *Submitted to IEEE Transaction on Wireless Communications.*

[53] D. Piazza, J. Kountouriotis, M. D'Amico, and K.R. Dandekar, "A technique for antenna configuration selection for reconfigurable circular patch arrays," *IEEE Transactions on Wireless Communications*, vol. 3, 2009.

[54] D. Piazza, J. Kountouriotis, M. D'Amico, and K.R. Dandekar, "Selection algorithm for reconfigurable antennas in MIMO systems," *U.S. Provisional Application (US 61/147,365*, 2009.

[55] D. Piazza, M. D'Amico, and K.R. Dandekar, "MIMO communication system with reconfigurable circular patch antennas," *Proceedings of the IEEE Symposium on Antennas and Propagation*, 2008.

[56] D. Piazza, P. Mookiah, M. D'Amico, and K.R. Dandekar, "Pattern reconfigurable circular patch for MIMO systems," *Proceeding of RiNEm Conference*, 2008.

[57] W.C. Jakes, *Microwave mobile communications*, IEEE press, 1994.

[58] J. Perez, J. Ibanez, L. Vielva, and I. Santamaria, "Capacity estimation of polarization-diversity MIMO systems in urban microcellular environments," *Proceedings of the IEEE International Symposium on Personal, Indoor and Mobile Radio Communications, PIMRC*, vol. 4, pp. 2730 – 2734, 2004.

[59] M. Wennstrom and T. Svantesson, "An antenna solution for MIMO channels: The switched parasitic antenna," *Proceedings of the IEEE International Symposium on Personal, Indoor and Mobile Radio Communications, PIMRC*, vol. 1, pp. 159–163, 2001.

[60] C.B. Dietrich Jr., K. Dietze, J.R. Nealy, and W.L. Stutzman, "Spatial, polarization, and pattern diversity for wireless handheld terminals," *IEEE Transactions on Antennas and Propagation*, vol. 49, no. 9, pp. 1271 – 1281, 2001.

[61] T. Svantesson, "An antenna solution for MIMO channels: The multimode antenna," *Proceedings of the Asilomar Conference on Signals, Systems and Computers*, vol. 2, pp. 1617 – 1621, 2000.

[62] F. Yang and Y. Rahmat-Samii, "Patch antennas with switchable slots (PASS) in wireless communications: Concepts, designs, and applications," *IEEE Antennas and Propagation Magazine*, vol. 47, no. 2, pp. 13 – 29, 2005.

[63] F. Yang and Y. Rahmat-Samii, "A reconfigurable patch antenna using switchable slots for circular polarization diversity," *IEEE Microwave and Wireless Components Letters*, vol. 12, no. 3, pp. 96 – 98, 2002.

[64] L.N. Pringle, P.H. Harms, S.P. Blalock, G.N. Kiesel, E.J. Kuster, P.G. Friederich, R.J. Prado, J.M. Morris, and G.S. Smith, "A reconfigurable aperture antenna based on switched links between electrically small metallic patches," *IEEE Transactions on Antennas and Propagation*, vol. 52, no. 6, pp. 1434 – 1445, 2004.

[65] A. E. Fathy, A. Rosen, H. S. Owen, F. McGinty, D.J. McGee, G.C. Taylor, R. Amantea, P.K. Swain, S.M. Perlow, and M. Elsherbiny, "Silicon-based reconfigurable antennas - concepts, analysis, implementation, and feasibility," *IEEE Transactions on Microwave Theory and Techniques*, vol. 51, no. 6, pp. 1650 – 1660, 2003.

[66] M. Jankiraman, *Space time codes and MIMO systems*, Artech House, 2004.

[67] V. Erceg et al., "TGn channel models," *IEEE 802.11-03/940r4*, 2004.

[68] A.A.M. Saleh and R.A. Valenzuela, "A statistical model for indoor multipath propagation," *IEEE Journal on Selected Areas in Communications*, vol. 5, no. 2, pp. 128 – 137, 1987.

[69] J.W. Wallace and M.A. Jensen, "Statistical characteristics of measured MIMO wireless channel data and comparison to conventional models," *Proceedings of the IEEE 54th Vehicular Technology Conference*, vol. 2, pp. 1078 – 1082, 2001.

[70] 3GGP Technical Specification Group., "Spatial channel model, SCM-134 text v6.0," *Spatial channel model AHG*, 2003.

[71] L. M. Correia, *Wireless Flexible Personalized communications*, John Wiley and Sons, Inc., 2001.

[72] M.A. Jensen and Y. Rahmat-Samii, "Performance analysis of antennas for hand-held transceivers using FDTD," *IEEE Transactions on Antennas and Propagation*, vol. 42, no. 8, pp. 1106 – 1112, 1994.

[73] P. Soma, D.S. Baum, V. Erceg, R. Krishnamoorthy, and A.J. Paulraj, "Analysis and modeling of multiple-input multiple-output (MIMO) radio channel based on outdoor measurements conducted at 2.5GHz for fixed BWA applications," *Proceedings of the IEEE International Conference on Communications*, vol. 1, pp. 272 – 276, 2002.

[74] Q.H. Spencer, B.D. Jeffs, M.A. Jensen, and A.L. Swindlehurst, "Modeling the statistical time and angle of arrival characteristics of an indoor multipath channel," *IEEE Journal on Selected Areas in Communications*, vol. 18, no. 3, pp. 347 – 360, 2000.

[75] G. German, Q. Spencer, L. Swindlehurst, and R. Valenzuela, "Wireless indoor channel modeling: statistical agreement of ray tracing simulations and channel sounding measurements," *Proceedings of the 2001 IEEE International Conference on Acoustics, Speech, and Signal Processing*, vol. 4, pp. 2501 – 2504, 2001.

[76] Q. Spencer, M. Rice, B. Jeffs, and M. Jensen, "A statistical model for angle of arrival in indoor multipath propagation," *Proceedings of the IEEE 47th Vehicular Technology Conference. Technology in Motion*, vol. 3, pp. 1415 – 1419, 1997.

[77] A.S.Y. Poon and M. Ho, "Indoor multiple-antenna channel characterization from 2 to 8 ghz," *Proceedings of the IEEE International Conference on Communications*, vol. 5, pp. 3519 – 3523, 2003.

[78] K.I. Pedersen, P.E. Mogensen, and B.H. Fleury, "Power azimuth spectrum in outdoor environments," *Electronics Letters*, vol. 33, no. 18, pp. 1583 – 1584, 1997.

[79] K.I. Pedersen, P.E. Mogensen, and B.H. Fleury, "A stochastic model of the temporal and azimuthal dispersion seen at the base station in outdoor propagation environments," *IEEE Transactions on Vehicular Technology*, vol. 49, no. 2, pp. 437 – 447, 2000.

[80] H. Bolckei, D. Gesbert, and A.J. Paulraj, "On the capacity of OFDM-based spatial multiplexing systems," *IEEE Transactions on Communications*, vol. 50, no. 2, pp. 225 – 234, 2002.

[81] R.B. Ertel, P. Cardieri, K.W. Sowerby, T.S. Rappaport, and J.H. Reed, "Overview of spatial channel models for antenna array communication systems," *IEEE Personal Communications*, vol. 5, no. 1, pp. 10 – 22, 1998.

[82] M. Stege, J. Jelitto, M. Bronzel, and G. Fettweis, "A multiple input-multiple output channel model for simulation of Tx- and Rx-diversity wireless systems," *Proceedings of the IEEE Vehicular Technology Conference*, vol. 2, pp. 833 – 839, 2000.

[83] A.F. Molisch, "A generic model for MIMO wireless propagation channels in macro- and microcells," *IEEE Transactions on Signal Processing*, vol. 52, no. 1, pp. 61 – 71, 2004.

[84] J. P. Kermoal, L. Schumacher, K. I. Pedersen, P. E. Mogensen, and F. Frederiksen, "A stochastic MIMO radio channel model with experimental validation," *IEEE Journal on Selected Areas in Communications*, vol. 20, no. 6, pp. 1211 – 1226, 2002.

[85] D.-S. Shiu, G.J. Foschini, M.J. Gans, and J.M. Kahn, "Fading correlation and its effect on the capacity of multielement antenna systems," *IEEE Transactions on Communications*, vol. 48, no. 3, pp. 502 – 513, 2000.

[86] A. Forenza, G. Wan, and R. W. Heath Jr., "Optimization of 2-element arrays of circular patch antennas in spatially correlated MIMO channels," *Proceedings of IEEE International Waveform Diversity and Design Conf.*, 23-27 January 2006.

[87] R.G. Vaughan and J.B. Andersen, "Antenna diversity in mobile communications," *IEEE Transactions on Vehicular Technology*, vol. T-36, no. 4, pp. 149 – 172, 1987.

[88] H. R. Chuang and L. C. Kuo, "3-D FDTD design analysis of a 2.4-GHz polarization-diversity printed dipole antenna with integrated balun and polarization-switching circuit for WLAN and wireless communication applications," *IEEE Transactions on Microwave Theory and Techniques*, vol. 51, no. 2 I, pp. 374 – 381, 2003.

[89] C. Waldschmidt, J.V. Hagen, and W. Wiesbeck, "Influence and modelling of mutual coupling in MIMO and diversity systems," *Proceedings of IEEE International Symposium Antennas and Propagation*, vol. 3, pp. 190 – 193, 2002.

[90] R.G. Vaughan and J.B. Andersen, "Antenna diversity in mobile communications," *IEEE Transactions on Vehicular Technology*, vol. T-36, no. 4, pp. 149 – 172, 1987.

[91] H. Shin and J. H. Lee, "Capacity of multiple-antenna fading channels: Spatial fading correlation, double scattering, and keyhole," *IEEE Transactions on Information Theory*, vol. 49, no. 10, pp. 2636 – 2647, 2003.

[92] H. Ozcelik, M. Herdin, W. Weichselberger, J. Wallace, and E. Bonek, "Deficiencies of 'Kronecker' MIMO radio channel model," *Electronics Letters*, vol. 39, no. 16, pp. 1209 – 1210, 2003.

[93] S. Wyne, A. F. Molisch, P. Almers, G. Eriksson, J. Karedal, and F. Tufvesson, "Statistical evaluation of outdoor-to-indoor office MIMO measurements at 5.2 GHz," *Proceedings of IEEE Vehicular Technology Conference*, vol. 61, no. 1, pp. 146 – 150, 2005.

[94] C. Oestges and E. Ozcelik, H.and Bonek, "On the prectical use of analytical MIMO channel models," *IEEE Antennas and Propagation Society International Symposium*, vol. 3B, pp. 406 – 409, 2005.

[95] M. F. Catedra, J. Perez, A. Gonzalez, O. Gutierrez, and F. Saez de Adana, "Fast computer tool for the analysis of propagation in urban cells," *Annual Wireless Communications Conference, Proceedings*, pp. 240 – 245, 1997.

[96] M. A. Jensen and J. W. Wallace, "A review of antennas and propagation for MIMO wireless communications," *IEEE Transactions on Antennas and Propagation*, vol. 52, no. 11, pp. 2810 – 2824, 2004.

[97] J. W. Wallace, M. A. Jensen, A. L. Swindlehurst, and B. D. Jeffs, "Experimental characterization of the MIMO wireless channel: Data acquisition and analysis," *IEEE Transactions on Wireless Communications*, vol. 2, no. 2, pp. 335 – 343, 2003.

[98] H. Bolcskei, D. Gesbert, and A. J. Paulraj, "On the capacity of OFDM-based spatial multiplexing systems," *IEEE Transactions on Communications*, vol. 50, no. 2, pp. 225 – 234, 2002.

[99] R.G. Vaughan, "Two-port higher mode circular microstrip antennas," *IEEE Transactions on Antennas and Propagation*, vol. 36, no. 3, pp. 309 – 21, 1988.

[100] Y.J. Sung, T.U. Jang, and Y.-S. Kim, "A reconfigurable microstrip antenna for switchable polarization," *IEEE Microwave and Wireless Components Letters*, vol. 14, no. 11, pp. 534 – 536, 2004.

[101] Y. Fan and Y. Rahmat-Samii, "A reconfigurable patch antenna using switchable slots for circular polarization diversity," *IEEE Microwave and Wireless Components Letters*, vol. 12, no. 3, pp. 96 – 98, 2002.

[102] J. Huang, "Circularly polarized conical patterns from circular microstrip antennas," *IEEE Transactions on Antennas and Propagation*, vol. 32, no. 9, pp. 991 – 994, 1984.

[103] I.J. Bahl and P. Bhartia, *Microstrip Antennas*, Artech House, 1980.

[104] J.D. Boerman and J.T. Bernhard, "Performance study of pattern reconfigurable antennas in MIMO communication systems," *IEEE Transactions on Antennas and Propagation*, vol. 56, no. 1, pp. 231 – 236, 2008.

[105] B. Hassibi and B.M. Hochwald, "How much training is needed in multiple-antenna wireless links?," *IEEE Transactions on Information Theory*, vol. 49, no. 4, pp. 951 – 963, 2003.

[106] G.D. Golden, C.J. Foschini, R.A. Valenzuela, and P.W. Wolniansky, "Detection algorithm and initial laboratory results using V-BLAST space-time communication architecture," *Electronics Letters*, vol. 35, no. 1, pp. 14 – 16, 1999.

[107] D. Samardzija, C. Papadias, and R. Valenzuela, "Experimental evaluation of unsupervised channel deconvolution for wireless multiple-transmitter/multiple-receiver systems," *Electronics Letters*, vol. 38, no. 20, pp. 1214 – 1216, 2002.

[108] A. Adjoudani, E.C. Beck, A.P. Burg, G.M. Djuknic, T.G. Gvoth, D. Haessig, S. Manji, M.A. Milbrodt, M. Rupp, D. Samardzija, A.B. Siegel, II Sizer, T., C. Tran, S. Walker, S.A. Wilkus, and P.W. Wolniansky, "Prototype experience for MIMO BLAST over third-generation wireless system," *IEEE Journal on Selected Areas in Communications*, vol. 21, no. 3, pp. 440 – 51, 2003.

[109] D. Samardzija and N. Mandayam, "Pilot-assisted estimation of MIMO fading channel response and achievable data rates," *IEEE Transactions on Signal Processing*, vol. 51, no. 11, pp. 2882 – 2890, 2003.

[110] L. Musavian, M.R. Nakhai, M. Dohler, and A.H. Aghvami, "Effect of channel uncertainty on the mutual information of MIMO fading channels," *IEEE Transactions on Vehicular Technology*, vol. 56, no. 5, Sept. 2007.

[111] M. Bengtsson, D. Astely, and B. Ottersten, "Measurements of spatial characteristics and polarization with a dual polarized antenna array," *Proceedings of IEEE Vehicular Technology Conference*, vol. 1, pp. 366 – 370, 1999.

[112] A. Forenza, A. Pandharipande, K. Hojin, and R.W. Heath Jr., "Adaptive MIMO transmission scheme: exploiting the spatial selectivity of wireless channels," *Proceedings of IEEE Vehicular Technology Conference.*, vol. 5, pp. 3188 – 92, 2005.

[113] Y. Kai, M. Bengtsson, B. Ottersten, D. McNamara, P. Karlsson, and M. Beach, "Modeling of wide-band MIMO radio channels based on NLoS indoor measurements," *Proceedings of IEEE Transactions on Vehicular Technology*, vol. 53, no. 3, pp. 655 – 65, 2004.

[114] M.T. Ivrlac, T.P. Kurpjuhn, C. Brunner, and W. Utschick, "Efficient use of fading correlations in MIMO systems," *Proceedings of IEEE Vehicular Technology Conference*, vol. 4, pp. 2763 – 7, 2001.

[115] M. Herdin and E. Bonek, "A MIMO correlation matrix based metric for characterizing non-stationarity," *Proceedings of Mobile and Wireless Communications Summit*, 2004.

[116] A. Oliner, *Antenna Engineering Handbook*, Y.T. LO and S.W. Lee Edition, 1988.

[117] C. Caloz and T. Itoh, "Transmission line approach of left-handed (LH) materials and microstrip implementation of an artificial LH transmission line," *IEEE Transactions on Antennas and Propagation*, vol. 52, no. 5, pp. 1159 – 1166, 2004.

[118] A. Lai, C. Caloz, and T. Itoh, "Composite right/left-handed transmission line metamaterials," *IEEE Microwave Magazine*, vol. 5, no. 3, pp. 34 – 50, 2004.

[119] A.A. Oliner and K.S. Lee, "The nature of the leakage from higher modes on microstrip line," *Proceedings of IEEE International Microwave Symposium*, pp. 57 – 60, 1986.

[120] M. Guglielmi and D.R. Jackson, "Broadside radiation from periodic leaky wave antennas," *IEEE Transactions on Antennas and Propagation*, vol. 41, no. 1, pp. 31 – 37, 1993.

[121] A.K. Iyer and G.V. Eleftheriades, "Negative refractive index metamaterials supporting 2-d waves," *Proceedings of the IEEE MTT-S International Microwave Symposium Digest*, vol. 2, pp. 1067 – 1070, 2002.

[122] A. Sanada, C. Caloz, and T. Itoh, "Characteristics of the composite right/left-handed transmission lines," *IEEE Microwave and Wireless Components Letters*, vol. 14, no. 2, pp. 68 – 70, 2004.

[123] C. Caloz, A. Sanada, and T. Itoh, "A novel composite right-/left-handed coupled-line directional coupler with arbitrary coupling level and broad bandwidth," *IEEE Transactions on Microwave Theory and Techniques*, vol. 52, no. 3, pp. 980 – 992, 2004.

[124] L. Sungjoon, C. Caloz, and T. Itoh, "Metamaterial-based electronically controlled transmission-line structure as a novel leaky-wave antenna with tunable radiation angle and beamwidth," *IEEE Transactions on Microwave Theory and Techniques*, vol. 52, 2004.

[125] S. Bellofiore, J. Foutz, R. Govindarajula, I. Bahceci, C.A. Balanis, A.S. Spanias, J.M. Capone, and T.M. Duman, "Smart antenna system analysis, integration and performance for mobile ad-hoc networks (MANETs)," *IEEE Transactions on Antennas and Propagation*, vol. 50, no. 5, pp. 571 – 581, 2002.

[126] R. Ramanathan, J. Redi, C. Santivanez, D. Wiggins, and S. Polit, "Ad hoc networking with directional antennas: a complete system solution," *IEEE Journal on Selected Areas in Communications*, vol. 23, no. 3, pp. 496 – 506, 2005.

[127] T. Ohira, "Emerging adaptive antenna techniques for wireless ad-hoc networks," *Proceedings of IEEE International Symposium on Circuits and Systems*, vol. 4, pp. 858 – 861, 2001.

[128] H. Ming and Z. Junshan, "MIMO ad hoc networks with spatial diversity: medium access control and saturation throughput," *Proceedings of IEEE Conference on Decision and Control*, vol. 3, pp. 3301 – 3306, 2004.

[129] P. Minyoung, R.W. Heath Jr., and S.M. Nettles, "Improving throughput and fairness for MIMO ad hoc networks using antenna selection diversity," *Proceedings of the IEEE Global Telecommunications Conference*, vol. 5, pp. 3363 – 3367, 2004.

[130] A. Nasipuri, S. Ye, J. You, and R.E. Hiromoto, "A MAC protocol for mobile ad hoc networks using directional antennas," *Proceedings of IEEE Wireless Communications and Networking Conference*, vol. 3, pp. 1214 – 1219, 2000.

[131] R.A. Iltis, S.J. Kim, and D.A. Hoang, "Noncooperative iterative MMSE beamforming algorithms for ad hoc networks," *IEEE Transactions on Communications*, vol. 54, no. 4, pp. 748 – 759, 2006.

[132] S. Bellofiore, J. Foutz, C.A. Balanis, and A.S. Spanias, "Smart-antenna system for mobile communication networks part 2: Beamforming and network throughput," *IEEE Antennas and Propagation Magazine*, vol. 44, no. 4, pp. 106 – 114, 2002.

[133] R. Ramanathan, "On the performance of ad hoc networks with beamforming antennas," *Proceedings of the 2001 ACM International Symposium on Mobile Ad Hoc Networking and Computing*, pp. 95 – 105, 2001.

[134] R.J. Mailloux, *Phased array antenna handbook*, Artech House, 1994.

[135] S. Bellofiore, C.A. Balanis, J. Foutz, and A.S. Spanias, "Smart-antenna systems for mobile communication networks. part 1: Overview and antenna design," *IEEE Antennas and Propagation Magazine*, vol. 44, no. 3, pp. 145 – 154, 2002.

[136] J. Cheng, M. Hashiguchi, K. Iigusa, and T. Ohira, "Electronically steerable parasitic array radiator antenna for omni- and sector pattern forming applications to wireless ad hoc networks," *Proceedings of IEE Microwaves, Antennas and Propagation*, vol. 150, no. 4, pp. 203 – 208, 2003.

[137] R. Vaughan, "Switched parasitic elements for antenna diversity," *IEEE Transactions on Antennas and Propagation*, vol. 47, no. 2, pp. 399 – 405, 1999.

[138] C. Jaikaeo and C.C. Shen, "Multicast communication in ad hoc networks with directional antennas," *Proceedings of International Conference on Computer Communications and Networks*, pp. 385 – 390, 2003.

[139] S. D. Blostein and H. Leib, "Multiple antenna systems: Their role and impact in future wireless access," *IEEE Communications Magazine*, vol. 41, no. 7, pp. 94 – 101, 2003.

[140] E. Telatar, "Capacity of multi-antenna gaussian channels," *European Transactions on Telecommunications*, vol. 10, no. 6, pp. 585 – 595, 1999.

[141] F.R. Farrokhi, G.J. Foschini, A. Lozano, and R.A. Valenzuela, "Link-optimal BLAST processing with multiple-access interference," *Proceedings of IEEE Vehicular Technology Conference*, vol. 1, no. 52D, pp. 87 – 91, 2000.

[142] S. Ye and R.S. Blum, "Optimized signaling for MIMO interference systems with feedback," *Proceedings IEEE Transactions on Signal Processing*, vol. 51, no. 11, pp. 2839 – 2848, 2003.

[143] R.S. Blum, "MIMO capacity with interference," *IEEE Journal on Selected Areas in Communications*, vol. 21, no. 5, pp. 793 – 801, 2003.

[144] M.F. Demirkol and M.A. Ingram, "Power-controlled capacity for interfering MIMO links," *Proceedings of IEEE Vehicular Technology Conference*, vol. 1, no. 54D, pp. 187 – 191, 2001.

[145] B.A. Cetiner, E. Akay, E. Sengul, and E. Ayanoglu, "A MIMO system with multifunctional reconfigurable antennas," *IEEE Antennas and Wireless Propagation Letters*, vol. 5, no. 31, pp. 463 – 466, 2006.

[146] A.M. Sayeed and V. Raghavan, "Maximizing MIMO capacity in sparse multipath with reconfigurable antenna arrays," *IEEE Journal of Selected Topics in Signal Processing*, vol. 1, no. 1, pp. 156 – 166, 200.

[147] D. Pinchera, J.W. Wallace, M.D. Migliore, and M.A. Jensen, "Experimental analysis of a wideband adaptive-MIMO antenna," *IEEE Transactions on Antennas and Propagation*, vol. 56, no. 3, pp. 908 – 913, 2008.

[148] A. Sanada, M. Kimura, I. Awai, C. Caloz, and T. Itoh, "A planar zeroth-order resonator antenna using a left-handed transmission line," *Proceedings of the European Microwave Conference*, vol. 3, pp. 1341 – 1344, 2004.

[149] P. Mookiah and K.R. Dandekar, "Performance analysis of metamaterial substrate based MIMO antenna arrays," *Proceedings of the IEEE Global Telecommunications Conference*, 2008.

[150] K. Buell, H. Mosallaei, and K. Sarabandi, "A substrate for small patch antennas providing tunable miniaturization factors," *IEEE Transactions on Microwave Theory and Techniques*, vol. 54, no. 1, pp. 135 – 146, 2006.

Vita

Daniele Piazza received the B.S. degree in telecommunication engineering from Politecnico di Milano, Italy, in 2003. In 2006 he received the Laurea degree with high honors in telecommunication engineering, with specialization in radio frequency communications, from Politecnico di Milano, Italy, and the M.S. degree in electrical and computer engineering from Drexel University in Philadelphia, Pennsylvania, where he conducted research focused on reconfigurable antennas for MIMO communications. In 2006 he joined Politecnico di Milano to work as a researcher. His main focus was on RFId systems, antennas and electromagnetic compatibility.

His research interests concentrate mainly on MIMO antenna design, reconfigurable antennas, smart antenna arrays, MIMO systems, RFId and UWB communications.